# NOVEL CONJUGATES OF PEPTIDES AND CONJUGATED POLYMERS FOR OPTOELECTRONICS AND NEURAL INTERFACES

by

Nandita Bhagwat

A dissertation submitted to the Faculty of the University of Delaware in partial fulfillment of the requirements for the degree of Doctor of Philosophy in Materials Science and Engineering

Summer 2015

**NOVEL CONJUGATES OF PEPTIDES AND CONJUGATED POLYMERS FOR OPTOELECTRONICS AND NEURAL INTERFACES**

by

Nandita Bhagwat

Approved: _____
Darrin J. Pochan, Ph.D.
Chair of the Department of Materials Science and Engineering

Approved: _____
Babatunde Ogunnaike, Ph.D.
Dean of the College of Engineering

Approved: _____
James G. Richards, Ph.D.
Vice Provost for Graduate and Professional Education

I certify that I have read this dissertation and that in my opinion it meets the academic and professional standard required by the University as a dissertation for the degree of Doctor of Philosophy.

Signed: _____

Kristi L. Kiick, Ph.D.
Professor in charge of dissertation

I certify that I have read this dissertation and that in my opinion it meets the academic and professional standard required by the University as a dissertation for the degree of Doctor of Philosophy.

Signed: _____

David C. Martin, Ph.D.
Co-Professor in charge of dissertation

I certify that I have read this dissertation and that in my opinion it meets the academic and professional standard required by the University as a dissertation for the degree of Doctor of Philosophy.

Signed: _____

Xinqiao Jia, Ph.D.
Member of dissertation committee

I certify that I have read this dissertation and that in my opinion it meets the academic and professional standard required by the University as a dissertation for the degree of Doctor of Philosophy.

Signed: _____

Mary P. Watson, Ph.D.
Member of dissertation committee

## ACKNOWLEDGMENTS

There are so many lovely people I would like to acknowledge and thank who have been part of this journey and who have contributed to the completion of my dissertation.

To start with I would like to extend my deepest gratitude to my thesis advisor, Prof. Kristi Kiick, without whom I would not be able to finish this degree. Her guidance, encouragement, in-depth knowledge, and constructive criticism has helped me become a better researcher. She always gave me the freedom to develop my own ideas and projects, which has been a fantastic learning experience. I am thankful to her for giving me the opportunity to work with a wide range of projects. As a successful female academician and administrator, she inspires me to aim high. I would like to thank Prof. David Martin, my co-advisor, for making the world of conducting polymers so exciting and fascinating. I thank him for his help, support, advice, and his deep insight which have been vital for the success of my doctoral degree. I would also like to thank the rest of the committee members, Prof. Xinqiao Jia and Prof. Mary Watson for their time, guidance and invaluable suggestions. I would like to thank Prof. Watson for giving me access to the glove box and her helpful directions to conduct organic reactions.

I would like to extend a shout-out to all the Kiick group members, past and present. It has been an absolute pleasure working with all of them in the lab. I am thankful for extremely helpful and collaborative lab mates who are always willing to troubleshoot problematic experiments. I want to especially thank Dr. Rebecca Scott

who has taught me everything I know regarding cell work and whose guidance and insight have been essential for the fruitful completion of the final part of my thesis. A special thanks to Dr. Onur Kas for synthesizing the complex organic chromophore. I also want to thank the Martin group members, especially Chin-Chen Kuo, for their help and suggestions.

Last but not the least I would like to thank my amazing parents, Madhuwanti and Suhas Bhagwat, who have always believed in me and for all their love and support. I would not have been able to achieve this feat without them by my side. I owe so much to my partner in crime, Rohan who has always been there for me through all the ups and downs and encouraged me to do better. I would also like to thank all my dear friends who have made graduate school such an unforgettable experience. I am super happy and thankful that I met my soul sister (Mayuri) here in Newark, DE.

Finally I would like to thank National Science Foundation, National Institutes of Health, and University of Delaware as funding sources.

## TABLE OF CONTENTS

## LIST OF TABLES

## LIST OF FIGURES

## ABSTRACT

Peptide-polymer conjugates are a novel class of hybrid materials that take advantage of each individual component giving the opportunity to generate materials with unique physical, chemical, mechanical, optical, and electronic properties. In this dissertation peptide-polymer conjugates for two different applications are discussed.

The first set of peptide-polymer conjugates were developed as templates to study the intermolecular interactions between electroactive molecules by manipulating the intermolecular distances at nano-scale level. A PEGylated, α-helical peptide template was employed to effectively display an array of organic chromophores (oxadiazole containing phenylenevinylene oligomers, Oxa-PPV). Three Oxa-PPV chromophores were strategically positioned on each template, at distances ranging from 6 to 17 Å from each other, as dictated by the chemical and structural properties of the peptide. The Oxa-PPV modified PEGylated helical peptides (produced via Heck coupling strategies) were characterized by a variety of spectroscopic methods. Electronic contributions from multiple pairs of chromophores on a scaffold were detectable; the number and relative positioning of the chromophores dictated the absorbance and emission maxima, thus confirming the utility of these polymer–peptide templates for complex presentation of organic chromophores.

The rest of the thesis is focused on using poly(3,4-alkylenedioxythiophene) based conjugated polymers as coatings for neural electrodes. This thiophene derivative is of considerable current interest for functionalizing the surfaces of a wide variety of devices including implantable biomedical electronics, specifically neural bio-

electrodes. Toward these ends, copolymer films of 3,4-ethylenedioxythiophene (EDOT) with a carboxylic acid functional EDOT (EDOTacid) were electrochemically deposited and characterized as a systematic function of the EDOTacid content (0, 25, 50, 75, and 100%). The chemical surface characterization of the films confirmed the presence of both EODT and EDOTacid units. Cyclic voltammetry showed that the films had comparable charge storage capacities regardless of their composition. The morphology of the films varied depending on the monomer feed ratio. Thus we were able to develop a method for synthesizing electrically active carboxylic acid functional poly(3,4-ethylenedioxythiophene) copolymer films with tunable hydrophilicities and surface morphologies.

For longer lifetime devices incorporating a biomolecule via covalent immobilization techniques are preferred over physical adsorption or entrapment. We took advantage of the carboxylic acid group on the PEDOTacid copolymer films to modify the surface of these films with a laminin based peptide, the nonapeptide sequence CDPGYIGSR. XPS and toluidine blue O assay proved the presence of the peptide on the surface and electrochemical analysis demonstrated unaltered properties of the peptide modified films. The bioactivity of the peptide along with the need of a spacer molecule for cell adhesion and differentiation was tested using the rat pheochromocytoma (PC12) cells. Films modified with the longest poly(ethylene glycol) spacer used in this study, a 3 nm long molecule, demonstrated the best attachment and neurite outgrowth compared to films with peptides with no spacer and a 1 nm spacer, $PEG_3$. The films with $PEG_{10}$-CDPGYISGR covalently modified to the surface demonstrated 11.5% neurite expression with the mean neurite length of 90 µm. Along with the acid functionalized PEDOT films, vinyl terminated ProDOT films

were also investigated as coatings for neural electrodes. The vinyl group was successfully modified with a RGD peptide via thiol-ene click chemistry. Both the acid and vinyl functional conducting polymer films provide an effective approach to biofunctionalize conducting polymer films.

# Chapter 1

# INTRODUCTION

## 1.1 Peptide-Polymer Conjugates – Background

Conjugates of peptides/proteins and polymers have drawn attention to create highly advanced materials primarily for biomedical applications such as drug delivery,[1, 2] tissue engineering,[3, 4] and immunology.[5] These hybrid materials offer the advantage of synergistically combining the properties of the individual biologic and synthetic materials to generate superior materials. Peptides possess accurately defined structures, a variety of functionalities, selectivity and specificity, and bioactivity.[6, 7] However, these positives are accompanied by certain drawbacks including short in vivo half-life, immunogenicity, poor stability, low solubility, and sensitivity to temperature and pH.[8, 9] Conjugation to synthetic polymers has shown to potentially overcome these limitations. Polymers exhibit high chemical and thermal stability, processability and increased solubility but lack the structural perfection of peptides.[10, 11] Thus by combining hierarchical structure and bioactivity of the peptides with enhanced stability of the polymers, bioconjugates of peptides and polymers can yield complex and structurally enhanced materials.

There are two main approaches used for synthesizing peptide-polymer hybrid systems. The peptide can be linked to a polymer via a divergent or a convergent method.[9, 12, 13] The divergent approach entails growing a polymer chain from the biomolecule of interest or fabricating a peptide from a polymer substrate. The former is achieved by functionalizing the peptide with polymerization initiators or chain

transfer agents (CTAs) followed by growing the polymer from this macroinitiator or macroCTA. Commonly used polymerization techniques for this approach are atom transfer radical polymerization (ATRP) and reversible addition-fragmentation chain transfer polymerization RAFT. For instance, a grafting through approach was utilized by Ayres et al. to polymerize methacrylate functional elastin pentapeptide VPGVG using ATRP.[14] The thermally responsive conjugates exhibited a well-defined structure with a narrow molecular weight distribution. Self-assembling poly (*n*-butyl acrylate) based peptide-polymer conjugates were created via RAFT polymerization of threonine-valine- chain transfer agent by Hentschel et al.[15] For the second strategy, convergent synthesis, the polymer and peptide are synthesized separately and then coupled together to form the desired product. This methodology allows independent purification and characterization of each component. Having the data and knowledge of the structure and the properties of each component makes the purification and characterization of the subsequent hybrid molecule easier and more accurate. Moreover, the chemically versatile peptides provide the opportunity to choose from multiple conjugation chemistries for this combinatory tactic. Popular chemistries include amide bond formation, typically between carboxylic acid groups on the polymer with the N-terminus amine on the peptide chains/ Ɛ-amino groups in lysine containing sequences, and click reactions including Diels-Alder reaction, copper catalyzed azide-alkyne cycloaddition, and thiol-ene/ thiol-yne coupling.[12] Shu and coworkers developed amphiphilic peptide polymer conjugates by covalently linking hydrophobic polystyrene to the N-terminus of a coiled coil helix bundle-forming peptide.[16]

One of the most commonly used polymers to produce peptide-polymer hybrid systems is poly(ethylene glycol), (PEG) also called as poly(ethylene oxide), (PEO) and is the only Food and Drug Administration approved polymer. PEG is a hydrophilic, biocompatible and neutral molecule and as a result is known as the stealth molecule.[17, 18] Conjugation of PEG to drug molecules or the peptide/protein therapeutics increases the molecular weight which leads to increased circulation times and reduces kidney clearance.[19, 20] Conjugation of PEG to a protein was first reported in 1977 by Abuchowski and Davies when they PEGylated bovine serum albumin (BSA).[21] The subsequent conjugate had reduced immunogenicity due to the shielding effects of the PEG. Since then linear and branched PEG molecules have been explored to develop a variety of PEG-peptide conjugates.[22-24] Conjugation of PEG to peptides has also shown to stabilize the secondary and tertiary peptide structures based on the PEG block length,[25] concentration of PEG,[26] number of peptide residues,[27] and experimental conditions such as temperature and pH.[28] Along with peptides, PEG has been successfully used to couple with drugs,[17] proteins,[18] enzymes[29] and antibodies[30] owing to its biocompatibility, hydrophilicity and low toxicity.

Likewise, a variety of polymers have been experimented with to develop conjugates to study the fundamental science (understanding and manipulating the interactions occurring between the two entities), studying the self-assembly of these novel hybrid systems, and eventually exploit their features for biological and non-biological applications. Stimuli-responsive self-assembled materials have been reported by combining polymers and homopolypeptide blocks. Gebhardt et al. synthesized poly(butadiene)-poly(L-lysine) block copolymers that formed spherical and rod like micelles depending on the composition of the block. Decreasing the pH

led to helix-coil transition and caused the assemblies to swell.[31] Block copolymers of poly (butadiene)-poly (L-glutamic acid) were reported by Checot et al. that self-assembled in aqueous solutions to form well defined vesicles. The hydrodynamic radii of the vesicles was controlled from 100-150 nm by changing the pH of the solution.[32]

Biologically inspired peptides provide structural hierarchy and molecular recognition and thus can govern the secondary structure of the hybrid molecule. It is also possible to regulate inter and intra-molecular interactions of the peptide blocks such ah hydrogen bonding, hydrophobic association to have higher control over the final structure and architecture of the conjugate. β-sheet forming peptides derived from amyloid proteins, KLVFF/ AAKLVFF and FFKLVFF, conjugated with PEG demonstrated varying degrees of fibrillization depending on the hydrophobicity of the peptide sequence.[33] Conjugation of PEG to hydrophobic β-sheet peptides results in conjugates that retain their β-sheet conformation which can assemble into higher order structures. Klok et al. reported conjugates of PEG and amphiphilic peptide (GAALEAALKLAAELAAKG and GAALKAALELAAKLAAEG) which revealed partial α-helical conformation independent of pH and demonstrated extended ribbon-type assemblies.[34] Multiblock polymers were synthesized by reacting alkyne-terminated α-helical peptides $(AKA_3KA)_n$ with azide-terminated PEG to mimic the molecular architecture of the natural protein tropoelastin. The resulting multiblock hybrid could form an elastomeric gel with a compressive modulus of 0.12 MPa, comparable to commercially available polyurethane elastomer.[35] Similar to peptides with β-sheet and α-helical secondary structures, coiled coil motifs have also been investigated for self-assembled hydrogels and nanostructures. For such peptides, the self-assembly is driven by the coiled coil interactions. Marsden et al. employed α-

helical coiled coil peptides G(EIAALEK)$_3$ and (KIAALKE)$_3$G in conjunction with two synthetic polymers, polystyrene and PEG to give rise to a new amphiphilic hybrid ABC triblock copolymer which self-assembled into rod-like micelles. This system was thermally responsive and above 50 °C, the rod-like micelles transitioned into spherical micelles.[36]

## 1.2 Peptide/Protein-Conjugated Oligomer/Polymer Hybrid Systems

Relatively less investigated class of macromolecules for building peptide/protein-polymer hybrid systems are conjugated polymers. Conjugated polymers started gaining popularity in 1970s when polymers possessing high electronic conductivity in the partially oxidized state were discovered. Since then multiple groups have investigated these materials to study their fundamentals and used them in applications ranging from optoelectronics to chemical sensors to actuators to biomedical implants. The main reason behind developing peptide/protein – conducting polymer hybrid systems was for developing biomedical and biotechnological devices with controlled opto-electronic properties.[37-39] Predominantly, conducting polymer-peptide interactions are related to fabrication of platforms for cell adhesion and spreading for tissue engineering applications and biomedical implants.[40-44] The opto-electronic and photophysical properties of conjugated systems can also be manipulated by taking advantage of the well-defined secondary structures of peptides and proteins by using these materials to eventually design two-dimensional and three-dimensional model systems. Here we are focusing on synthesizing novel systems comprising of peptides and conjugated polymers for materials for optoelectronics and neural interfaces.

## 1.3 Building Blocks for Peptide/Protein-Conjugated Oligomer/Polymer Hybrid Systems

### 1.3.1 Peptides/Proteins

Proteins are linear polymers which are made up of nature's building blocks, amino acids. Proteins are large biomolecules consisting of hundreds of amino acids joined together by the amide bond. Peptides are shorter than proteins and are usually short amino acid oligomers. There are a total of 20 natural amino acids which are classified based on their chemical nature of the side chain. Based on their side chain functionality amino acids are generally classified under polar with electrically charged side chains (e.g. arginine, histidine), polar with uncharged side chains (e.g. serine, threonine), and hydrophobic side chains (e.g. alanine, valine). Amino acid sequences which constitutes of the primary structure of the peptide ultimately determines the higher order secondary, tertiary and quaternary structures of the peptide which are key to its functionality. The precisely well-defined structures, molecular monodispersity, and diverse chemical functionality lead to higher order structures such as α-helix, β-sheet, and random coil.

The various functionalities on the amino acid side chains can be utilized to synthesize peptide-peptide or peptide-polymer conjugates via chemoselective conjugation reactions. Though this is a useful tool to design new biomaterials a disadvantage of using natural amino acids is that more than one residue of the targeted amino acid may be present in the peptide/protein. To overcome this, non-natural amino acids can be introduced into the peptide/protein. By bringing in non-natural amino acids in the peptides it is possible to achieve exact control over the site and number of conjugations to a peptide. A vast variety of non-natural amino acids have been developed to provide the flexibility of chemical functionality and site-specific

bio-orthogonal conjugation. *p*-Halo-phenylalanine residues have been incorporated in the helical peptides for reactions with activated alkenes via the Heck coupling reaction,[45] or with terminal alkynes via the Sonogashira coupling,[46] or with boronic esters via Suzuki coupling.[47] Amino acids modified with azides and alkynes have been used to conjugate proteins via the copper catalyzed cycloaddition reaction.[48] *p*-Acetyl-phenylalanine residues have been used to form hydrazone and oxime derivatives.[49]

### 1.3.2 Conjugated Polymers

Conjugated polymers were discovered by Shirakawa, MacDiarmid, and Heeger in the 1970s and since then have been a topic of great interest due to their notable photophysical properties arising from their structures consisting of alternating single and double bonds. Figure 1.1 displays the structures of commonly studied and utilized conjugated polymers. The polymer which is otherwise in an insulating state gets transformed into a conductor when doped with either an electron donor or electron acceptor. These π-conjugated backbones enable the movement of holes when the polymers are oxidized (p-doping) and electrons when the polymers are reduced (n-doping) making them conductive in nature. When doped, a net charge of zero is produced because of the close association of the counter ions with the charged polymer backbone. This method leads to the formation of charge carriers in the polymer chain in the form of charged polarons (radical cations or radical anions) or bipolarons (dications or dianions). This process is presented in Figure 1.2.

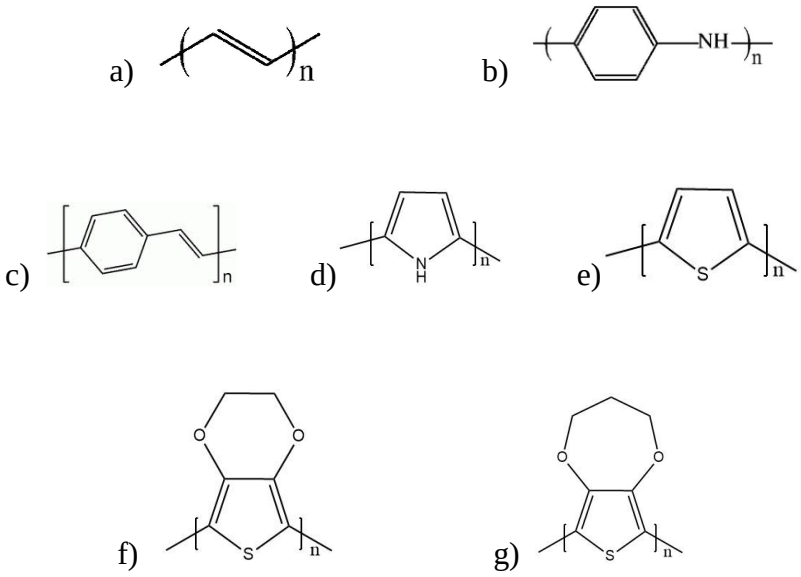


**Figure** 1.1 Structures of conjugated polymers a) polyacetylene, b) polyaniline, c) poly(phyenylenevinylene), d) polypyrrole, e) polythiophene f) poly(3,4-ethylenedioxythiophene), and g) poly (3,4-propylenedioxythiophene)

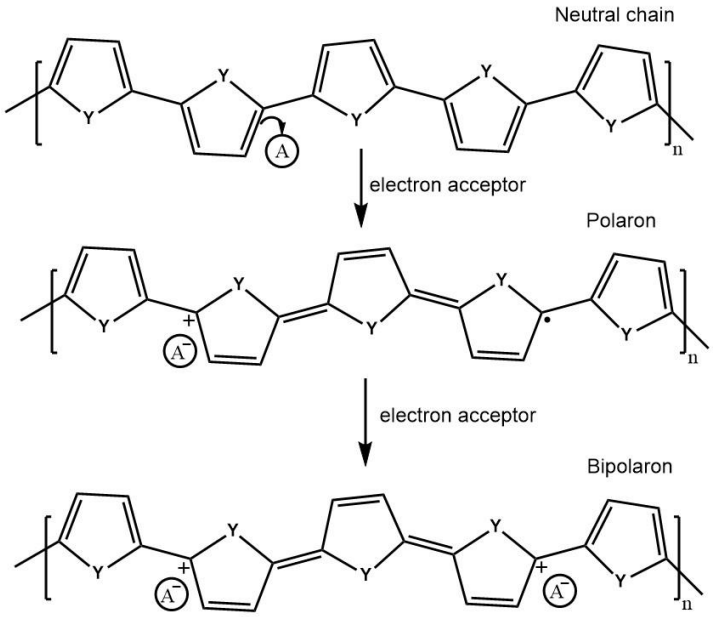


**Figure** 1.2 Introduction of polaron and bipolaron charged species upon oxidation (p-doping) in heterocyclic polymers.

#### 1.3.2.1 Conjugated Polymers for Optoelectronics

Organic electronic devices such as organic light emitting diodes, organic photovoltaics, and organic field effective transistors based on organic active materials are rapidly gaining popularity owing to their low cost manufacturing methods, tunable electronic and processing properties, mechanical flexibility, and reel-to-reel printing methods.[50] To design, optimize and tune the properties of an organic electronic device it is essential to understand the elementary excitations and dynamics in the π-conjugated oligomers or polymers making up the device. Once the polymers have been deposited via vapor or solution deposition they should self-assemble into a direction along the current flow to facilitate charge transport. Conjugated polymers suitable for optoelectronic applications should have high luminescence quantum yields, large apparent Stokes shifts, and broad absorption bands.

Poly(para-phyenylenevinylene) (PPV), and its derivatives such as poly (2-methoxy, 5- (2'-ethyl-hexoxy)-1,4-phenylenevinylene) (MEH-PPV), and its oligomers have been used extensively as the electroluminescent layer in organic light emitting diodes (OLEDs).[51] Photoexcitation of conjugated polymers results in formation of intra-chain singlet excitons. Radiative decay of these excitons is the source of fluorescence for PPV with a quantum yield of about 0.1, the 0-0 transition being localized at 2.37 eV.[52, 53] Excitons are an electron-hole pair on the same polymer chain and the typical lifetime of these species has been reported to be around 300 ps.[54] Long lived excitations, with lifetimes of nanoseconds, from an electron-hole pair present onto adjacent polymer chains are attributed to polaron pairs. Such excited species were reported for MEH-PPV films and cyano-PPV.[55] The kind of excited species generated is directly dependent on the spatial orientation and intermolecular distance between conjugated segments,[45] the π-π stacking between the chains[56] and also the

crystallinity.[57] For improving the performance of organic semiconductor devices understanding the intermolecular interactions is paramount as the formation of excimers, exciplexes, and aggregates have shown to decrease the photoluminescence.

#### 1.3.2.2 Conjugated Polymers for Neural Interfaces

The main objective of using conjugated polymers as coatings for bio-electrodes is improving the electrode-tissue interface by providing a material with low impedance and high surface area more conducive to biological integration. Apart from providing mechanical flexibility and tunability due to their organic nature, conjugated polymers provide mixed electronic/ ionic conductivity, i.e. they can transmit charge both by electron and ionic transport.[58] Monomers with low oxidation potential such as polypyrroles, polyanilines and polythiophenes and its derivatives (Figure 1.1) are used as coatings for bio-electrodes. Out of these polymers the polythiophene derivatives of the class poly (3,4-alkylenedioxythiophene) have attracted the most attention due to their lowered oxidation potential owing to the electron donating ether linkage, moderate bandgap, good stability in the oxidized state, and high conductivity.[59] The blocked β-position of the heterocyclic ring also prevents the formation of α-β linkage during polymerization.

Polymer films for neural electrodes are generally prepared via electrochemical polymerization where the films are directly deposited on the desired electrode surface. The electron rich-monomers undergo electrochemical oxidation when an electric current or potential is applied to form radical cations. Under favorable conditions the radical cations further react to form polymer chains that precipitate onto the electrode surface. This synthesis route is preferred over the traditional chemical oxidative polymerization route as it requires only a small amount of monomer, short

polymerization times, and can produce electrode-supported and self-standing films. The properties of the films can be tailored based on the choice of solvent, deposition parameters, electrode type, and the type of counter ion. Patra et al. reported varying morphologies of poly(3,4-ethylenedioxythiophene) (PEDOT) based on the electrochemical deposition method; low current densities resulted in globular surface morphology, higher current densities and higher potentials led to a more porous morphology whereas the potentiodynamic preparation resulted in a rod-like and fibrous morphology.[60]

Multiple efforts have been made to improve the long-term biological performance of the neural prosthetic implants to make them suitable for implantation. Polypyrroles (Ppy) have been co-deposited with biologically active polyanions including growth factors,[61] hyaluronic acid,[62] and heparin.[63] Different routes have been utilized to biofunctionalize the conducting polymer through various peptide sequences such as RGD,[64] RNIAEIIKDI,[65] CDPGYIGSR[65] and T59 (a binding phage).[66] Ppy films were modified with the cell adhesion promoting sequence RGD through covalent conjugation.[64] The laminin based sequences RNIAEIIKDI, and CDPGYIGSR on the other hand were integrated into the Ppy films via the process of doping.[65] Phage display technique was used to identify the peptide sequence T59 which noncovalently binds to chlorine doped Ppy. The conductivity of T59 modified Ppy surfaces remained unaffected, and these surfaces demonstrated controlled cell attachment and neurite extensions.[66] Polypyrrole films were functionalized with bioactive dipeptides for specific recognition of proteolytic enzymes to create bioselective electroactive materials. By electrochemical control of the pH of the dipeptide enzymatic release could be monitored.[67]

Compared to Ppy, PEDOT is better for devices that need long term implantation and consistent electrical activity. This was proven by Cui and Martin by performing cyclic voltammetry comparisons for Ppy: PSS and PEDOT: PSS where they observed a loss in charge storage capacity for Ppy: PSS while PEDOT: PSS maintained a relatively large charge storage capacity.[68] PEDOT also has superior chemical stability compared to Ppy owing to blocked β-position of the heterocyclic ring which prevents the formation of α-β linkage during polymerization. Similar to Ppy, PEDOT has been co-deposited a wide range of biological polyanions including hyaluronic acid,[69] heparin,[69] collagen,[37] and growth factors.[70] The rat pheochromocytoma (PC12) cells successfully differentiated and resulted in neurite outgrowth when cultured on PEDOT films polymerized with nerve growth factor. Richardson-Burns et al. developed a process to polymerize PEDOT around living neural cells and demonstrated that EDOT monomer was not significantly cytotoxic and that SH-SY5Y neuroblastoma cells could survive the polymerization process.[71] Bioactive peptides such as cell adhesive sequence RGD,[43] neuron promoting sequence YFQRLI,[72] and clot-binding peptide have been integrated with PEDOT films to increase their bioactivity.[73]

## 1.4 Conclusion and Synopsis of Subsequent Chapters

As described in above sections, by combining the advantages of peptides and synthetic polymers it is possible to develop unique and novel hybrid systems. In this dissertation we focus on use of peptide-polymer conjugate systems for two different applications, optoelectronics and neural interfaces. Chapter 2 describes the use of α-helical peptides as templates for display of three oxadiazole containing PPV (Oxa-PPV) oligomers for controlling their electronic interactions. Chapter 3-5 are focused

on poly(3,4-alkylenedioxythiophene) polymer coatings for enhancing neural interfaces. Chapter 3 discusses the electrochemical synthesis and characterization of acid functionalized PEDOT films. Biofunctionalization of these PEDOTacid films is described in Chapter 4. Preliminary results on biofunctionalization of vinyl terminated poly(3,4-propylenedioxythiophene) films are presented in Chapter 5.

# Chapter 2

# POLYMER–PEPTIDE TEMPLATES FOR CONTROLLING ELECTRONIC INTERACTIONS OF ORGANIC CHROMOPHORES

[Portions of this chapter are reproduced by permission of The Royal Society of Chemistry from Nandita Bhagwat, Kristi L. Kiick, *Polymer-peptide templates for controlling electronic interactions of organic chromophores;* J. Mater. Chem. C, 2013, 1, 4836-4845]

## 2.1 Introduction

The carrier mobility and photoluminescence of organic electronic devices, such as light emitting diodes, field effect transistors and photovoltaic cells, are directly dependent on the structure, alignment and orientation of the organic or polymeric molecules that make up the device.[74-76] However, polymer chains in an organic semiconductor device are prone to energetic disorder arising from the polydisperse chain lengths.[77] Manipulation and organization of conjugated polymeric molecules at the nanoscale level can control and reduce disorder through manipulation of intermolecular distance, spatial orientation, and aggregation within organic semiconductor materials and thus, improve electronic properties and device efficiency.[45, 57, 74, 75, 78, 79]

Biological molecules such as peptides,[80, 81] nucleobases,[82-84] and carbohydrates[85] offer a variety of scaffolding options for the bottom-up approach in designing organic semiconductor materials, owing to their utility in controlling chromophore presentation and thus the photophysical properties relevant to the

performance of organic electronic devices. These molecules offer the advantage of atomic precision, flexibility in architecture and design, and side chain functionalization for strategic placement of electroactive side chains to study the optoelectronic properties of conjugated organic molecules. Combinations of peptides and π-conjugated oligomeric systems can lead to well defined two-dimensional and three-dimensional model systems to understand structure–property relationships.[86-88]

The use of biomacromolecular templates has been utilized to investigate electronic interactions between single chromophores including porphyrins,[89-93] stilbenes,[79] phenylenevinylenes,[45, 94] and perylenediimides,[83, 95, 96] as well as electronically active species such as $Cu^{2+}$.[97] For instance, Dunetz et al. covalently modified a helical peptide with a diporphyrin that yielded extended porphyrin arrays – controlled by concentration, temperature, and pH – leading to an increase in long-range electronic communication between the porphyrin moieties.[92] In another report, perylenediimide-linked DNA dumbbells were synthesized which, through control of the number of base pairs separating appended chromophores, demonstrated alteration of observed absorbance and fluorescence in dilute aqueous media.[83] Biological templates have also been utilized to investigate potential electron and energy transfer between organic chromophores.[98-100] For example, Stevens et al. used a DNA template to study energy transfer between multiple naphthalene donors and Cy3.5 acceptor using time-correlated single photon counting, concluding that energy transfer is dependent on temperature and on the length of the DNA template.[98] These examples and others highlight the versatility biopolymeric templates offer to control the organization and properties of electronically active species.

However, few have sought to address how variation in the separation of organic chromophores alters energy transfer using the exquisite spatial control inherent in some bio-macromolecular structures. Those using peptide or protein-based systems have been limited to natural amino acid functionality for chemical modification, and the scaffolds have not been designed in a way to accommodate higher numbers of electroactive species for study of more complex electronic interactions. Non-natural amino acids selected on the basis of their chemical functionality and their ability to participate in selective reactions (used to modify the side chains of the biomolecule) provide flexible chemical functionality and site-specific bio-orthogonal conjugation,[101] and we have thus employed *p*-bromophenylalanine as a chemically reactive group in these approaches.

Kas et al. used alanine-rich helical peptides as templates for grafting two oxadiazole-containing p-phenylenevinylene (Oxa- PPV) oligomers. The inclusion of the oxadiazole moiety in PPV- based oligomers offers advantages relevant to their application in organic electronic devices. The electron-deficient oxadiazole ring helps maintain conjugation, and enhances electron affinity and electron transport, leading to improved emission efficiency of PPV-based devices.[45, 102, 103] By the attachment of the Oxa-PPV oligomers on a helical peptide, Kas et al. demonstrated controlled photoluminescence with variations in the distance between these Oxa-PPV side chains.[45] As a continuation of this work, we use a similar approach to graft three Oxa-PPV based organic chromophores as side chains on similar but longer helical peptide scaffolds to generate a more complex presentation of the chromophores. The organic chromophore, an oxadiazole-containing PPV molecule with a terminal vinyl group, is grafted onto the helical peptide via the palladium- catalyzed Heck coupling with the

halogenated phenylalanine. In this contribution, we also introduce the use of a PEGylated helical peptide scaffold for the display of the electroactive side chains; the PEGylation of the helical peptides imparts both hydrophilicity and structural stability to these hydrophobic residue-rich and Oxa-PPV-modified a-helical peptides. By the deliberate placement of the halogenated *p*-bromophenylalanine (*p*-Br-Phe), two or three chromophores could be appended to the same or opposite faces of the helical template at distances of 6–17 ˚A. Circular dichroic spectroscopy (CD) data indicated the PEGylation of the peptides led to a more stable scaffold which was successfully used for the attachment of Oxa-PPV side chains. The results from exciton-coupled CD, absorbance, and photoluminescence measurements clearly illustrate that the photophysical properties of the side chains are impacted differentially, depending on the number of chromophores in the assembly and their precise orientation with respect to one another. The incorporation of the three side chains with precise molecular separation provides scaffolds that permit better insight into the interaction of organic chromophores and their resulting electronic properties, and thus, introduces a novel biomolecular template for incorporation of an array of structurally similar (or dissimilar) electroactive molecules at prescribed distances and orientations to study the impact of chromophore placement on photophysical properties.

## 2.2 Experimental Procedures

### 2.2.1 Peptide Synthesis and Purification

All the peptides described in this report (Table 2.1) were synthesized via Fmoc-based methods on a Rink amide MBHA resin (Novabiochem, San Diego, CA) using an automated solid-phase peptide synthesizer (PS3, Protein Technologies Inc.,

Tuscon, AZ). The amino acid residues were activated with HBTU and 0.4 M methylmorpholine in DMF as the activator solvent. Deprotection was conducted using 20% (v/v) piperidine in DMF for approximately 30 minutes. Single coupling cycles of 1 hour were used for the first ten residues followed by double coupling of 2 hours for the remainder of the sequence. The N-terminal amine was PEGylated using a 1K PEG-COOH for extended coupling times of 5 hours. Cleavage of the peptide from the resin was performed in a mixture of 95% trifluoroacetic acid (TFA), 2.5% triisopropyl silane (TIPS), and 2.5% water for 3-4 hours. TFA was evaporated and the peptide was precipitated in cold ethyl ether. The water soluble peptides were extracted with water and lyophilized. Purification of peptides was conducted via reverse-phase high performance liquid chromatography (HPLC) (Waters, MA) using a Symmetry C18 semi-preparative scale column. The gradient applied was from 0-100% of solvent B over 45 minutes (Solvent A = 0.1% TFA in 18.2 MΩ water, solvent B = 0.1% TFA in ACN). The identity of each peptide was confirmed via electrospray ionization mass spectrometry (ESI-MS); (**BrF17D**) m/z 3148.8 (M+), calc. 3148.4; (**BrF6,7T**) m/z 3303.6 (M+), calc. 3303.4; (**BrF11,7T**) m/z 3304.8 (M+), calc. 3303.4; (**BrF6,11T**) m/z 3302.4, calc. 3303.4; (**BrF control**) m/z 1067.6, calc. 1068.2; (**PEG-BrF17D**) (all PEG-modified polymers use the reported Mn of the PEG for the estimate of the calculated m/z ratio)) m/z 4103.5, calc. 4088.4; (**PEG-BrF6,7T**) m/z 4301.6, calc. 4243.4 ; (**PEG-BrF11,7T**) m/z 4285.5, calc. 4243.4; (**PEG-BrF6,11T**) m/z 4260.5, calc. 4243.4.

### 2.2.2 General Procedure for Functionalization of the Helical Peptide

The Oxa-PPV oligomer was synthesized via previously reported methods.[104] The peptides were coupled to the Oxa-PPV oligomer using Heck coupling under an

inert atmosphere. The reaction was performed in anhydrous DMF as the solvent, with palladium acetate as the catalyst, tri-*o*-tolylphosphine as the ligand and tributylamine as the base. For a 5 μM peptide template (peptide with two bromophenylalanines), 20 μM of oligomer was added. This was dissolved in 0.6 ml anhydrous DMF and 10 μM of tributylamine, 2 μM of tri-*o*-tolylphosphine and 1 μM of palladium acetate was added. For a 5 μM peptide template (peptide with three bromophenylalanines) 30 μM of oligomer was added. This was dissolved in 0.6 ml anhydrous DMF followed by the addition of 15 μM of tributylamine, 3 μM of tri-*o*-tolylphosphine and 1.5 μM of palladium acetate. This procedure was conducted in a glove box, to ensure an inert atmosphere and lack of contamination. The reaction was carried out at 70 °C for 24-48 hours. The final reaction mixture was precipitated in cold ether. The peptide hybrids were purified *via* reversed phase HPLC using a Delta Pak C4 column using a gradient of 10% to 100% solvent B over 70 minutes (Solvent A = 0.1% formic acid in 18.2 MΩ water, solvent B = 0.1% formic acid in ACN). The identity of each peptide was confirmed *via* ESI-MS; (**Oxa control)** *m/z* 1349.8, calc 1351.5 (**PEG-Oxa17D**) *m/z* 4627.0, calc. 4655.2; (**PEG-Oxa6,7T**) *m/z* 5137.2, calc. 5093.6; (**PEG-Oxa11,7T**) *m/z* 5065.0, calc. 5093.6; (**PEG-Oxa6,11T**) *m/z* 5109.0, calc. 5093.6.

### 2.2.3 Characterization of Peptide Hybrids

#### 2.2.3.1 Molecular Modeling

Molecular modeling of the non-PEGylated Oxa-PPV hybrid peptides was conducted on the Insight II suite of software (Accelyrs Software Inc. San Diego, CA). Energy minimization studies employed CVFF force fields with the peptide in an implicit solvent (methanol) with a dielectric constant set at 33. The steepest descent

and conjugate gradient algorithms were used with 15,000 and 30,000 iterations, respectively, for the minimization studies. These minimized structures were then rendered using PyMol.

#### 2.2.3.2 Circular Dichroic (CD) Spectroscopy

CD spectra were collected on a Jasco J-810 spectropolarimeter (Jasco Inc, Easton, MD), on solutions (140 μM to 15 μM in methanol) in cells with a 0.1 cm pathlength, and at a scan rate of 50 nm/min. All the spectra reported are an average of 2 scans. CD spectra were recorded, at various increasing temperatures, for the wavelength range of 190 nm to 250 nm to determine the thermal stability of the observed secondary structure. Data points for wavelength-dependent measurements were recorded at every 1 nm with a bandwidth of 1 nm. Data points for the thermal denaturation were recorded at 222 nm at increment of every 5 °C with an equilibration time of 1 minute. The mean residue ellipticity, $\theta_{MRE}$ (deg $cm^2$ $dmol^{-1}$) was calculated using the formula, $\theta_{MRE} = \theta_{obs} * 100 / (l * c * n)$ where $\theta_{obs}$ is the measured ellipticity (millidegrees), $l$ is the path length of the cell (cm), $c$ is the concentration (mmolar), and $n$ is the number of residues on the peptide sequence. The fraction folded value for each peptide was calculated using the formula, $FF = (\theta_{MRE})_{T,obs} / (\theta_{MRE})_{5°C}$ where $(\theta_{MRE})_{T,obs}$ is the mean residue ellipticity at 222 nm and at a particular temperature, and $(\theta_{MRE})_{5°C}$ is the mean residue ellipticity at 222nm at 5 °C. Statistical significance was determined by an analysis of variance (ANOVA) followed by the Tukey post-hoc simultaneous testing method. A *p*-value was determined and a maximum value of 0.05 was used to indicate significance. The analysis was conducted on three separate samples of the peptides with *p*-Br-Phe (with and without PEG), and on three separate

samples of PEGylated peptides with and without Oxa-PPV, to verify the impact of the addition of PEG and Oxa-PPV respectively.

#### 2.2.3.3 Exciton Coupled Circular Dichroic (EC-CD) Spectroscopy

EC-CD data were collected from solutions of chromophore-modified peptides in methanol at room temperature in a 2-mm pathlength cell. The wavelength range, 260 nm to 500 nm, represents the absorbance envelope of the Oxa-PPV side chain. Data points were collected every 1 nm at a 1 nm bandwidth. All the solutions used for these experiments were at a concentration of 10 μM.

#### 2.2.3.4 Absorption and Photoluminescence (PL) Spectroscopy

UV-vis absorption spectra were collected on an Agilent 8453 spectrophotometer (Agilent Technologies Inc, Santa Clara, CA). PL measurements were performed on a Horiba Fluoromax 4 spectrofluorometer (Horiba Jobin Yvon Inc, Edison, NJ). All the photophysical experiments were conducted at room temperature on dilute solutions in methanol that exhibited an absorbance value of approximately 0.1 absorbance units. These concentrations were significantly lower than the ones used for CD measurements. Photoluminescent decay dynamics were recorded by exciting the solutions at 405 nm with a picosecond diode laser (Picoquant, GmbH, Germany) and using time-correlated single photon counting electronics (Picoharp, GmbH, Germany) with two avalanche photodiodes.

## 2.3 Results and Discussion

### 2.3.1 Peptide Design and Synthesis

The peptides described in this work were synthesized via standard Fmoc-based solid-phase methods and then modified with Oxa-PPV side chains via Heck coupling (Figure 2.1).

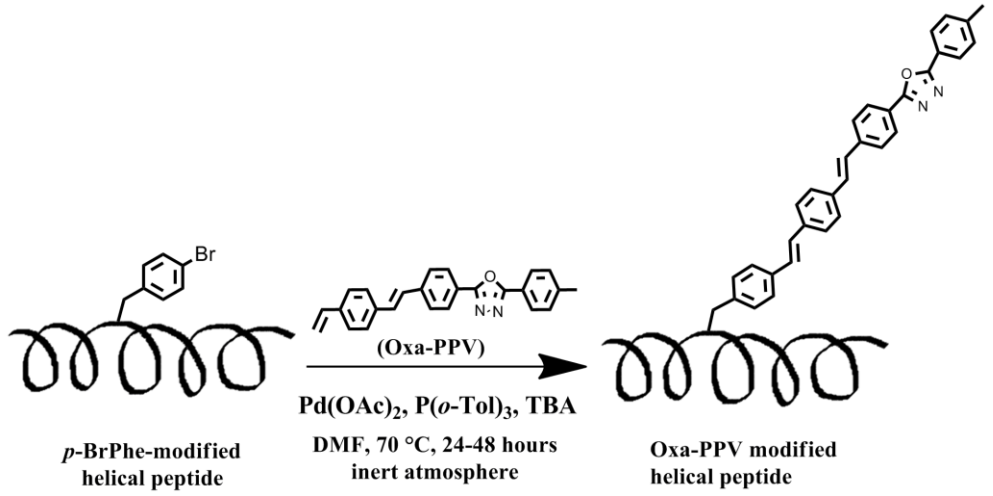


**Figure** 2.1 Schematic of chemical modification of PEGylated helical peptide (a single site modification of a helical domain is shown for simplicity) . J. Mater. Chem. C, 2013, 1, 4836-4845 – Reproduced by permission of The Royal Society of Chemistry.

Oxa-PPV oligomers were produced as previously reported. Given the helical propensity of alanine,[105] all peptides produced in these studies are based on the repeating amino acid sequence AAAX (where A is alanine and X represents another natural or non-natural amino acid). The sequences included lysines for solubility and minimization of aggregation, the non-natural amino acid α-aminoisobutyric acid (Aib) for thermal stability,[106] *p*-Br-Phe to provide the functionality for coupling of the Oxa-

PPV oligomer to the peptide. Based on the a-helix geometry, four templates with two or three Oxa-PPV chromophores at variable distances (6–17 Å) have been designed; Table 2.1 provides details of the peptide sequences, chromophore placement (based on residue placement in an ideal α-helix), and peptide designation. The X in the peptide sequences in Table 2.1 stands for *p*-Br-Phe residues modified with Oxa-PPV chromophores. By strategic placement of the *p*-Br-Phe residues, one to three electroactive side chains can be attached to the peptide, and positioned to lie on the same or the opposite face of the helix in various combinations of pairs at controlled and precise distances. The inclusion of three chromophores will aid in understanding electron coupling and energy transfer, after excitation, between more complicated arrangements of electroactive species than previously studied, with an eye toward understanding more complex photophysical behavior in films.

**Table** 2.1 Peptide sequences. J. Mater. Chem. C, 2013, 1, 4836-4845 – Reproduced by permission of The Royal Society of Chemistry.

| Sequence | Name | Position | Distance (Å) |
|---|---|---|---|
| Ac-KA-Aib-AXA-Aib-AKA-NH2 | Oxa control | - | - |
| PEG-KA-Aib-AKA-Aib-AAX-Aib-AKA-Aib-AAK-Aib-AXA-Aib-AKA-Aib-AKGGY-NH2 | PEG-Oxa17D | i,i+11 | 17 |
| PEG-KA-Aib-KAA-Aib-AAK-Aib-XAA-Aib-XAK-Aib-AXA-Aib-AAK-Aib-AKGGY-NH2 | PEG-Oxa6,7T | i,i+4; i,i+5 | 6,7 |
| PEG-KA-Aib-AKA-Aib-AXA-Aib-AAK-Aib-XAK-Aib-AXA-Aib-AKA-Aib-AKGGY-NH2 | PEG-Oxa11,7T | i,i+7; i,i+5 | 11,7 |
| PEG-KA-Aib-AKA-Aib-AAX-Aib-KAX-Aib-AAK-Aib-AXA-Aib-AAK-Aib-AKGGY-NH2 | PEG-Oxa6,11T | i,i+4; i,i+7 | 6,11 |

The addition of three Oxa-PPV side chains to the original peptide scaffolds resulted in large hydrophobic aggregates that could not be purified. Thus, hydrophilic poly(ethylene glycol) (PEG) was coupled to the N-terminus of the peptides, making characterization possible, while at the same time maintaining the inherent biophysical properties of the helical scaffold. PEG has been used for conjugation to peptides,[27, 107, 108] proteins,[109, 110] enzymes,[111-113] and antibodies,[30] owing to its biocompatibility, hydrophilicity and low toxicity. Conjugates of peptides and polymers take advantage of the structural and functional properties of the peptides and the versatility, composition and architecture of the synthetic polymers. Previous reports on PEG–helical peptide hybrids have shown improvements in the stability of the peptide secondary structure that are dependent on the PEG block length,[25] concentration of PEG,[26] number of peptide residues,[27] and experimental conditions such as temperature and pH.[28]

The purified peptide templates PEG-BrF17D, PEG-BrF6,7T, PEG-BrF11,7T and PEG-BrF6,11T were used for the coupling of Oxa-PPV chromophores via Heck coupling to yield PEG-Oxa17D, PEG-Oxa6,7T, PEG-Oxa11,7T and PEG-Oxa6,11T. (The letters “D” and “T” indicate scaffolds with two or three Oxa-PPV chains, respectively.) Along with the four hybrid peptides, a shorter Oxa control peptide was synthesized, as a control for the photophysical experiments, to provide an isolated Oxa-PPV oligomer with the same length and chemical composition as the conjugated side chains of the modified peptides. Energy minimization studies were performed on the hybrid peptides to predict the probable orientation of the Oxa-PPV side chains in dilute solutions and the average distance between these side chains. According to the energy minimized models, the distances measured between the α-carbon atoms of

adjacent *p*-Br-Phe residues are only slightly different than those indicated in Table 2.1 from theoretical predictions of an ideal α-helix. These differences can be attributed to the lower helicity of the peptide hybrids (discussed in detail in the CD characterization) as a result of incorporation of three bulky side chains (Figure 2.3) shows energy minimized structures of the non-PEGylated modified peptides for improved visualization of the side chains in the absence of the PEG. For the di-substituted 17D hybrid peptide, the Oxa-PPV chains are separated by 17 Å with minimal overlap, reducing the possibility of side-chain interaction. The energy-minimized structures suggest the placement of two of the three chromophores in the tri-substituted peptides 6,7T and 11,7T to be on the same face of the helix, as expected. The placement of the third chromophore on the opposite face of the helix should promote electronic isolation from, but close proximity to, the other two Oxa-PPV side-chains. The side chains in the 6,11T hybrid peptide are all positioned on the same side of the helix.

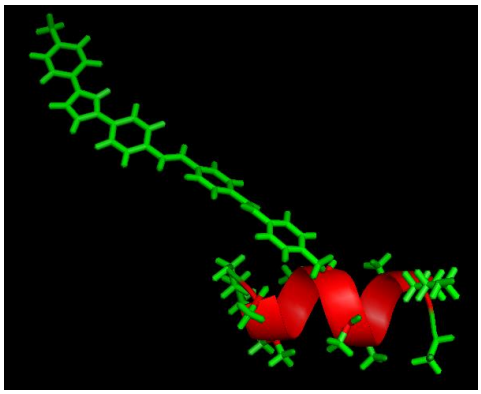

**Figure** 2.2 Energy minimized model of Oxa control peptide. J. Mater. Chem. C, 2013, 1, 4836-4845 – Reproduced by permission of The Royal Society of Chemistry.

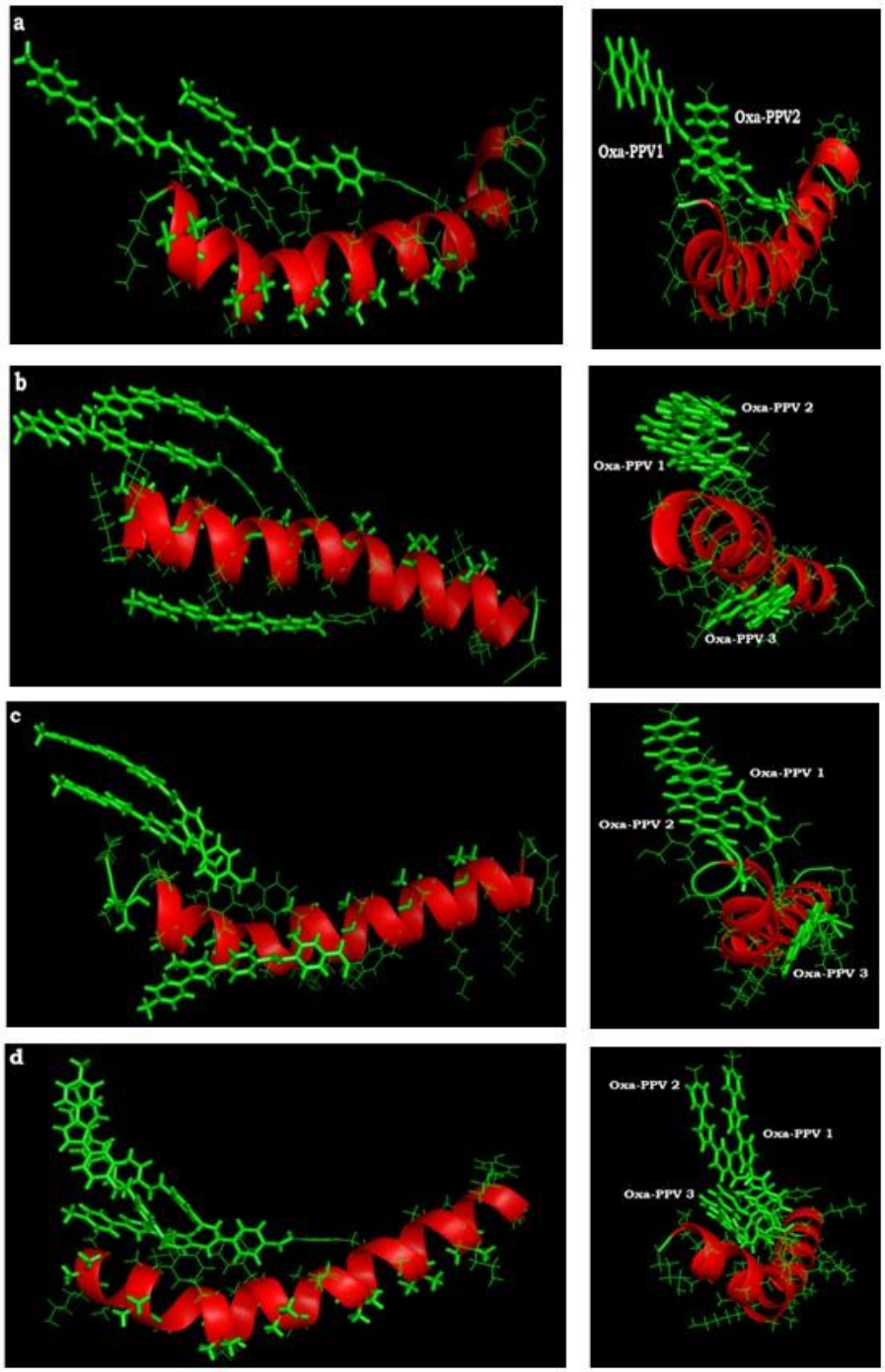


**Figure** 2.3 Energy minimized structures of Oxa-PPV hybrid peptides. a) Oxa17D, b) Oxa6,7T, c) Oxa11,7T, and d) Oxa6,11T. J. Mater. Chem. C, 2013, 1, 4836-4845 – Reproduced by permission of The Royal Society of Chemistry.

### 2.3.2 Determining the Helicity and Stability of the Peptide Scaffolds

All of the characterization experiments were performed in methanol, as characterization of the peptides in this solvent, via DLS, indicated the absence of detectable aggregation for the concentrations (15–140 μM) used for these studies. As mentioned in the introduction, peptide scaffolds with fewer residues (26 residues), which accommodate two Oxa-PPV chromophores, have been previously reported.[45] In addition to our interest in the electronic properties of the side chains, the work reported here also analyzes how the length of the scaffold, PEGylation of the peptide and incorporation of three Oxa-PPV molecules affects the stability and the thermal denaturation of the peptide hybrid molecule in comparison to the previously reported helical peptides. Circular dichroic spectroscopy (CD) experiments were performed, at increasing temperatures, on the non-PEGylated peptides, PEGylated peptides, and also on PEGylated peptides after chemical modification with Oxa-PPV side chains.

CD studies as a function of temperature (5 °C to 80 °C) were conducted to determine the effect of PEGylation on the alanine-rich peptide templates and the effect of Oxa-PPV conjugation on the conformation and thermal stability of the PEGylated peptide. All the peptides showed characteristic α-helical spectra with minima at 208 and 222 nm and a maximum at 192 nm. Figure 2.4, Figure 2.5 and Figure 2.6 show data for BrF6,11T, PEG-BrF11,7T, and PEG-Oxa6,11Twhich is representative for each of the three classes of peptides studied here; non-PEGylated, PEGylated, and Oxa-PPV PEGylated α-helical peptides. As shown in Figure 2.4, Figure 2.5 and Figure 2.6 the intensity of the peak at 222 nm decreases with increasing temperature, suggesting a loss in the helical content of the peptide. The lack of a shift of the spectrum to shorter wavelengths indicates that the reported peptides do not convert to a random coil conformation under the given experimental conditions.

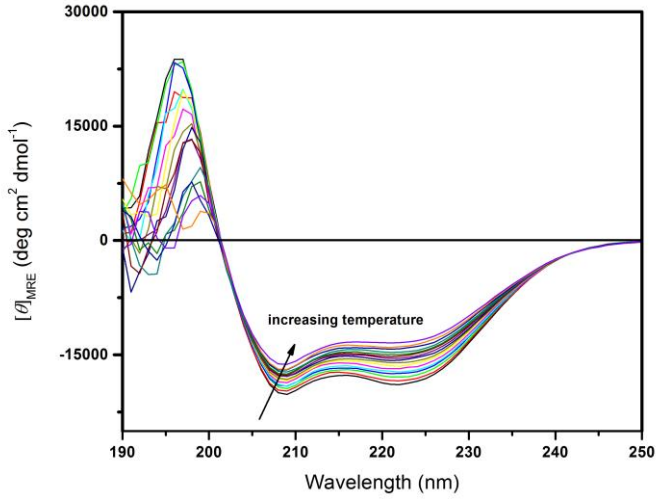


**Figure** 2.4 Full wavelength scan as a function of increasing temperature (5-80 °C) for BrF6,11T in methanol. J. Mater. Chem. C, 2013, 1, 4836-4845 – Reproduced by permission of The Royal Society of Chemistry.

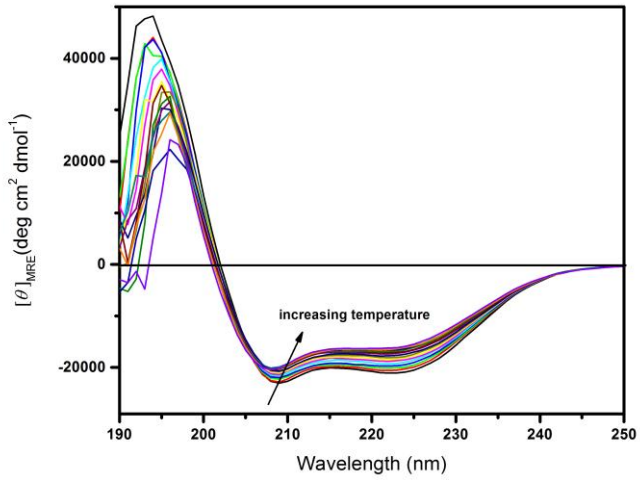


**Figure** 2.5 Full wavelength scan as a function of increasing temperature (5-80 °C) for PEG-BrF11,7T in methanol. J. Mater. Chem. C, 2013, 1, 4836-4845 – Reproduced by permission of The Royal Society of Chemistry.

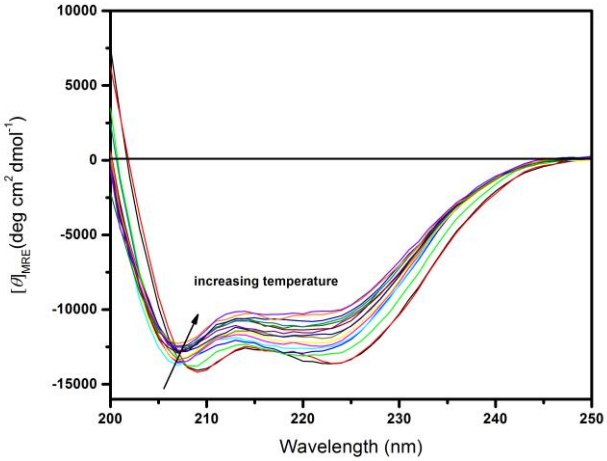


**Figure** 2.6 Full wavelength scan as a function of increasing temperature (5-80 °C) for PEG-Oxa6,11T in methanol. J. Mater. Chem. C, 2013, 1, 4836-4845 – Reproduced by permission of The Royal Society of Chemistry.

The $\theta_{MRE}$ (mean residual ellipticity) values at 222 nm at 5 °C were compared for the peptides with and without PEG and for the PEGylated peptides with and without Oxa-PPV to determine the effect of PEGylation and Oxa-PPV modification respectively. On comparison of the $\theta_{MRE}$ values for all the peptides, it was observed that the $\theta_{MRE}$ values at 222 nm at 5 °C for all the non-PEGylated peptides are approximately -18 000 deg cm$^2$ dmol$^{-1}$ (Figure 2.4), the $\theta_{MRE}$ values for all PEGylated peptides are approximately -21 000 deg cm$^2$ dmol$^{-1}$ (Figure 2.5) and for the Oxa-PPV modified peptides are approximately -15 000 deg cm$^2$ dmol$^{-1}$ (Figure 2.6). Statistical analysis performed on the $\theta_{MRE}$ data for the peptides before and after PEGylation indicates that the results are statistically different ($p \leq 0.05$). However, within each group of peptides (non-PEGylated and PEGylated) any differences in the $\theta_{MRE}$ values were not statistically significant. These results, along with the higher $\theta_{MRE}$ values

observed for the PEGylated peptides, suggest that the addition of PEG stabilizes the secondary structure. The apparent increase in peptide helicity and thermal stability after PEGylation is consistent with previous reports.[25, 114, 115] In addition, the $\theta_{MRE}$ values of the PEGylated, Oxa-PPV-modified peptides are statistically different than those of the PEGylated peptides lacking Oxa-PPV ($p \leq 0.05$), suggesting that the addition of two or three conjugated oligomers to the PEGylated peptides slightly reduces the helicity of the peptides. In spite of this reduction in helicity, the lack of conversion of the secondary structure to random coil (even at elevated temperatures) demonstrates that the addition of the three bulky side chains does not compromise the use of the helical peptide as a scaffold.

Thermal denaturation experiments were performed on the peptide templates before and after PEGylation to estimate the thermal stability of these templates. Similarly, the impact of conjugating the Oxa-PPV oligomer on the stability and secondary structure of the helical scaffold was evaluated by comparing the extent of unfolding of the peptide scaffold before and after conjugation. Spectra were collected in methanol over temperatures ranging from 5 to 80 °C, and normalized values for $\theta_{MRE}$ at 222 nm were plotted as a function of temperature. Normalized, fraction-folded values (FF) for the peptides before and after PEGylation are shown in Figure 2.7 and normalized, fraction-folded values (FF) for the PEGylated peptides before and after Oxa-PPV modification are shown in Figure 2.8. The fraction folded values were calculated by normalizing the $\theta_{MRE}$ values at 222 nm at an observed temperature to those obtained at 5 °C. DLS studies confirmed that the peptides are non-aggregated in the concentrations ranges employed. Consistent with these results, the thermally

induced unfolding behavior was independent of the concentration of the peptide solution.

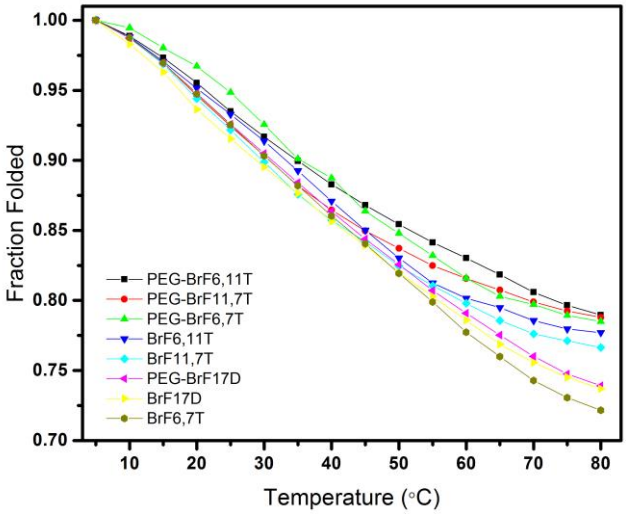


**Figure** 2.7 Thermal unfolding scans for peptides BrF17D, BrF6,7T, BrF11,7T, BrF6,11T, PEG-BrF17D, PEG-BrF6,7T, PEG-BrF11,7T, and PEG-BrF6,11T in methanol. J. Mater. Chem. C, 2013, 1, 4836-4845 – Reproduced by permission of The Royal Society of Chemistry.

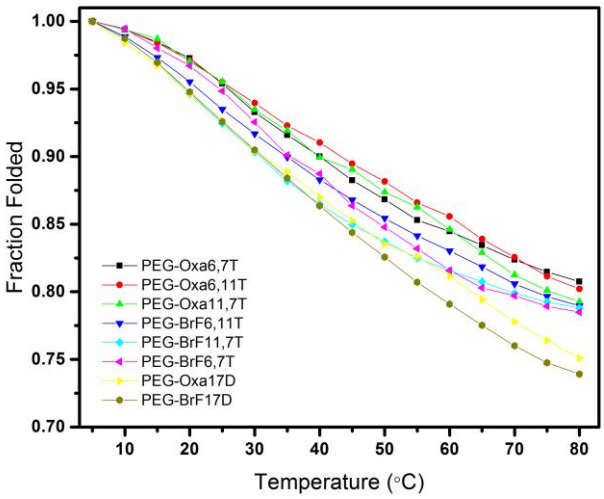


**Figure** 2.8 Thermal unfolding scans for peptides PEG-BrF17D, PEG-BrF6,7T, PEG-BrF11,7T, PEG-BrF6,11T, PEG-Oxa7D, PEG-OxaF6,7T, PEG-Oxa11,7T, PEG-Oxa6,11T, in methanol. J. Mater. Chem. C, 2013, 1, 4836-4845 – Reproduced by permission of The Royal Society of Chemistry.

As is shown in these data (Figure 2.7 and Figure 2.8), all the peptide templates show incomplete loss of helicity (retaining over 70% of their initial helicity) even at the highest temperatures probed in these experiments. The retention of over 70% helicity in these scaffolds, compared to the 40% helicity retained for our previously studied scaffolds, likely results from the increased number of α-aminoisobutyric acid residues which are known to impart thermal stability to peptides,[106] as well from the conjugation of PEG, which has been previously shown to stabilize helical peptides. Consistent with the fact that the PEGylated peptides are more helical at 5 °C than the non-PEGylated peptides (Figure 2.5 and Figure 2.4 respectively), the PEGylated scaffolds also retain a higher percentage of their helical conformation than the non-

PEGylated peptides at elevated temperatures. The increased helicity and stability of the PEGylated peptides may be attributable to the electrostatic and hydrogen-bonding interactions between PEG and the lysine side chains of the peptide.[115]

The peptides equipped with three *p*-Br-Phe residues are inherently more stable than the di-functional ones (Figure 2.7). For all the peptides but the di-functional 17D peptide (which has two *p*-Br-Phe located (17 Å apart), the *p*-Br-Phe residues are placed at shorter inter-residue distances (6 Å and 11 Å), and on the same face of the helix, and are thus in sufficient proximity to stabilize the peptide via the interactions of the aromatic residues.[116] In the di-functional peptide, in contrast, those stabilizing interactions are absent. Along with the aromatic interactions, helix-stabilizing electrostatic cation–π interactions of varying strength exist among all the peptide templates depending on the distance between the lysine and aromatic ring on *p*-Br-Phe; there are multiple such interactions for templates 17D (three), 6,7T (one), 11,7T (three) and 6,11T (two). Amongst the Oxa-PPV-modified, PEGylated peptides, (Figure 2.8) the tri- substituted Oxa-PPV PEGylated peptides (PEG-Oxa6,7T, PEG-Oxa11,7T, and PEG-Oxa6,11T) retain almost 80% of their helicity at elevated temperature, compared to the 75% for the di- substituted Oxa-PPV PEGylated peptide (PEG-Oxa17D), likely, as for the peptides above, as a result of side chain-side chain interactions (i.e. cation–π interactions and aromatic interactions) that stabilize the secondary structure of the helix.[116, 117] The lack of π–π stacking in PEG-Oxa17D, where the electroactive molecules are the furthest apart, results in the lowest thermal stability among the PPV-modified peptides.

### 2.3.3 Photophysical Properties of the Hybrid Peptides

#### 2.3.3.1 Absorbance

Absorbance and photoluminescence measurements were used to evaluate the impact of the varied placement of the Oxa-PPV side chains on their electronic properties. Figure 2.9 shows the absorbance spectra for the peptide hybrid molecules in the ultraviolet-visible wavelength range, along with the spectrum for the Oxa control peptide.

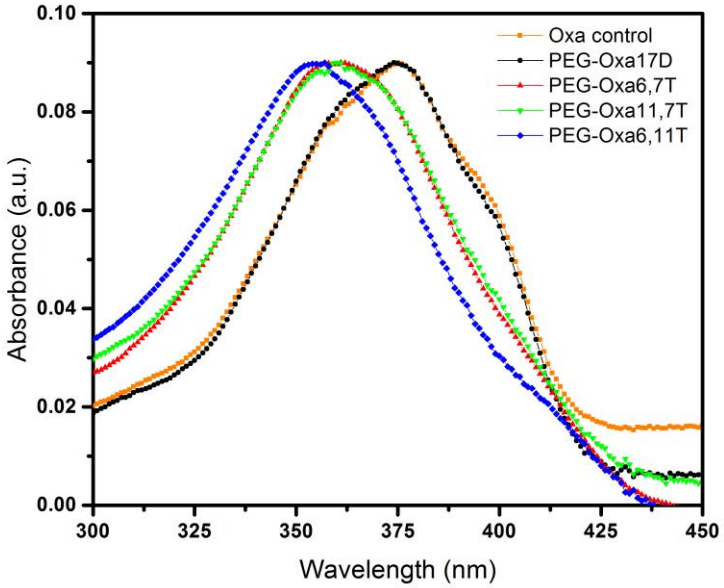


**Figure** 2.9 Absorbance spectra for hybrid peptide templates. Measurements are performed at room temperature on Oxa-PPV modified peptides in methanol. J. Mater. Chem. C, 2013, 1, 4836-4845 – Reproduced by permission of The Royal Society of Chemistry.

As shown in the Figure 2.9, all of the Oxa-PPV-modified peptides have an absorption maxima centered near 365 nm with subtle differences in their maxima and vibrational features that can be attributed to the π-π* and n–π* transition of the PPV and oxadiazole moiety. The wavelength of maximum absorbance for all the peptides is given in Table 2.2. The absorbance spectra for all of the peptides are broad, consistent with the expected spectra of chromophores in solution, as the absorption and emission spectra are not fully resolved given that the electronic states are not well defined.[118] Of relevance for the conjugates, as the size of the molecule increases or the numbers of such molecules increase, obtaining a well-defined spectrum becomes increasingly difficult.[118] The absorbance spectra for the Oxa control, the control peptide with a single Oxa-PPV oligomer side chain, is almost identical to that of PEG-Oxa17D, with both exhibiting vibrational features (the distinct shoulder at 400 nm). The similarity of the two spectra and the presence of the vibrational features suggests that the chromophores at 17 Å separation have minimal interaction with one another and behave as isolated monomeric species.

It is also apparent from the data in Figure 2.9 that the absorption maxima for the Oxa-PPV-coupled helical peptides shift towards shorter wavelengths with an increase in the number of chromophores on the template, with the maxima for the PEG- Oxa6,7T and PEG-Oxa11,7T blue-shifted from those for the Oxa control and PEG-Oxa17D peptides. Likewise, the absorption maximum for PEG-Oxa6,11T (357 nm) is more blue-shifted than the absorption maxima for PEG-Oxa6,7T and PEG-Oxa11,7T given the higher number of PPV oligomers conjugated to the same face of the helix. Kas et al. observed a similar trend in the value of the absorbance maxima for related peptides with one or two Oxa-PPV side chains, with the maxima for the di-

substituted peptide (Oxa6D, Oxa11D) being blue-shifted when compared to those for the peptides where the chromophores behaved as isolated species (Oxa6D mono, Oxa7O).[45] Similar blue shifts in absorption maxima have been observed for aggregates formed in helical peptide–porphyrin complexes[119] and thiophene-based oligomers in the solid state.[120] This shift in the absorbance wavelength maxima can be attributed to the formation of H- aggregates[119-121] in solution, which are observed when the chromophores are arranged in parallel (plane to plane stacking).

**Table** 2.2 Spectra differences among Oxa-PPV peptide hybrids J. Mater. Chem. C, 2013, 1, 4836-4845 – Reproduced by permission of The Royal Society of Chemistry.

| | **Oxa control** | **PEG-Oxa17D** | **PEG-Oxa6,7T** | **PEG-Oxa11,7T** | **PEG-Oxa6,11T** |
|---|---|---|---|---|---|
| **Absorbance maxima (nm)** | 375 | 374 | 361 | 360 | 357 |
| **PL maxima (nm)** | 456 | 458 | 472 | 464 | 469 |

#### 2.3.3.2 Exciton-Coupled (EC-CD) Spectroscopy

EC-CD experiments in the near UV range were performed in neat methanol to examine the differences in chromophore orientation and interaction in the various hybrid peptides. Figure 2.10 shows the exciton-coupled CD spectra for Oxa control, PEG-Oxa17D, PEG-Oxa6,7T, PEG-Oxa11,7T and PEG-Oxa6,11T. In the EC-CD experiment, a bisignate CD signal is observed in the absorption envelope of the chromophore when there is measurable through-space coupling between two or more chromophores.[122] The sign and the intensity of the signal provide information on the

inter-chromophore distance and dihedral angle between the chromophores.[123] The amplitude of the split Cotton effect is known to approach zero when chromophores are non-interacting and/or as the angle between the electronic dipole moments of the interacting chromophores approaches 0 or 180°.[123] Along with the distance and dihedral angle between the chromophores, the splitting of the energy level also varies depending on the chromophore under consideration.

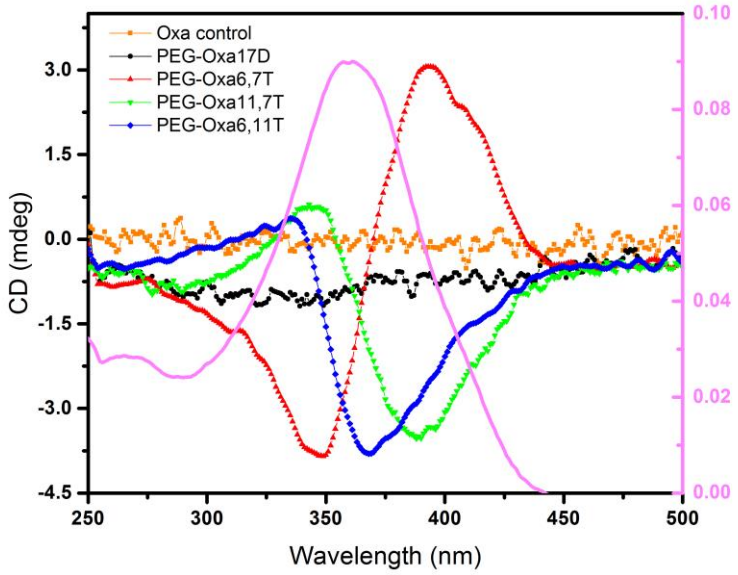


**Figure** 2.10 Exciton coupled circular dichroic spectra for Oxa-PPV modified peptides. The absorption envelope depicted here is of PEG-Oxa6,7T. J. Mater. Chem. C, 2013, 1, 4836-4845 – Reproduced by permission of The Royal Society of Chemistry.

As demonstrated in Figure 2.10, the Oxa control, equipped with a single Oxa-PPV oligomer (Figure 2.2) exhibits no response to the circular polarized light,

demonstrating the lack of a split Cotton effect as expected. Even though EC-CD can detect interactions between chromophores up to 41 Å apart,[124] the di-substituted PEG-Oxa17D also showed a negligible split Cotton effect in the near UV range, similar to the control peptide. While it is possible that the chromophores could be interacting but show no EC-CD owing to their low dihedral angle (Figure 2.3), the EC-CD data coupled with the existence of vibrational features in the absorption spectrum suggests that there is minimal interaction between the two chromophores at a separation of 17 Å and that they behave as isolated species.

Each of the PEGylated tri-substituted Oxa-PPV-modified peptides shows a bisignate signal in the spectral absorbance window of the chromophore, although of different sign. The PEG-Oxa6,7T exhibits a positive Cotton effect whereas PEG-Oxa11,7T and PEG-Oxa6,11T exhibit a negative Cotton effect, suggesting that the side chains of these systems are oriented in opposite chirality. Given that chromophores on opposite sides of a helical scaffold have been previously shown to behave as isolated species with negligible Cotton effects, the bisignate signal for PEG-Oxa6,7T and PEG-Oxa11,7T is likely due to the electronic interaction between the two chromophores separated by 6 Å and 11 Å, respectively, on the same side of the scaffold. It is important to note that in the reports of Kas et al.,[45] only a slight Cotton effect was observed for chromophores separated by 6 Å, implying high degree of overlap of the side chains. The positive Cotton effect of large amplitude, for chromophores separated by 6 Å in the current studies (PEG-Oxa6,7T), suggests that these side chains interact but must be slightly offset from each other. The lower helicity of the PEG-Oxa6,7T, relative to the helical peptide in previous studies, likely contributes to these observations. The sign of the split Cotton effect for PEG-Oxa6,7T

is consistent with that previously observed for Oxa6D (positive, even though slight) while the sign of the split Cotton signal for PEG-Oxa11,7T matches that previously observed for Oxa11D (negative). The EC-CD observations suggesting the opposite orientation of Oxa-PPV chromophores lying on the same face of the helix separated by 6 Å (PEG-Oxa6,7T) and 11 Å (PEG-Oxa11,7T) are also consistent with the difference in the presentation of the Oxa-PPV side chains for Oxa6,7T and Oxa11,7T indicated by the modeling results (Figure 2.3).

The PEG-Oxa6,11T is designed to position all the three Oxa-PPV chromophores on the same side of the helix, with the first two chromophores separated by 6 Å and the following two by 11 Å. As shown in Figure 2.10, this modified peptide exhibits a negative Cotton effect (with a slight blue shift in the absorbance). Previous reports on scaffolds equipped with more than two chromophores indicate that exciton coupling occurred between several chromophores when those chromophores were localized on the same side of the scaffold, although no discussion of chromophore orientation was presented.[79, 81, 125] Based on the energy minimization and exciton coupled CD results from Kas et al. for chromophores with separation of 6 Å (positive) and 11Å (negative), the negative Cotton effect observed for PEG-Oxa6,11T suggests that the chromophores may have a similar orientation as those in the Oxa11D peptide (from Kas et al.). This observed negative Cotton effect for PEG-Oxa6,11T is consistent with the energy minimized models of Oxa6,11T (Figure 2.3). The above results thus demonstrate the use of these scaffolds for desired placement of the organic chromophores to yield desired interaction between the chosen pairs of chromophores.

#### 2.3.3.3 Steady State Photoluminescence

Photoluminescence (PL) experiments were conducted by exciting the chromophores of the hybrid peptides at their observed absorption maxima (Table 2.2). Samples of nearly equal absorbance are used to perform these experiments so that the relative PL intensities can be compared; the data from these experiments are presented in Figure 2.11.

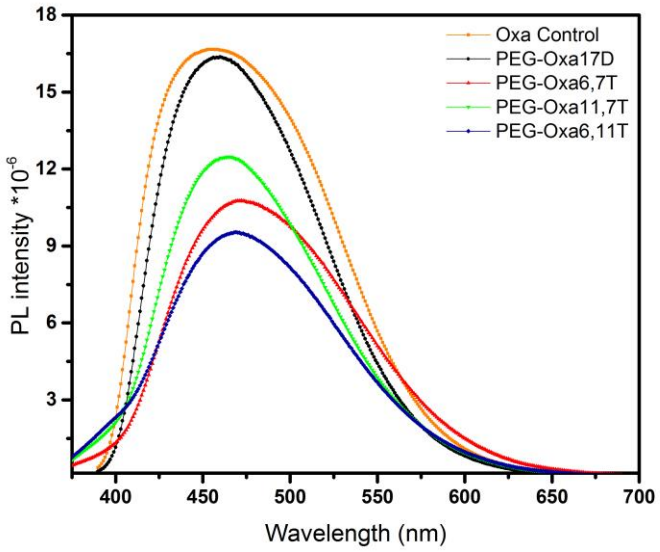


**Figure** 2.11 Photoluminescence spectra of Oxa-PPV peptides. J. Mater. Chem. C, 2013, 1, 4836-4845 – Reproduced by permission of The Royal Society of Chemistry.

The qualitative features of the observed PL spectra suggest differences in the electronic interactions of the Oxa-PPV chromophores attached to the peptide templates. The emission spectrum of the Oxa control is essentially identical to that of the PEG-Oxa17D, confirming that the chromophores separated by 17 Å have an

excitonic emission and thus behave as monomeric species. This observation is consistent with the exciton-coupled CD results for the PEG-Oxa17D peptide (minimal response to circularly polarized light), as well as the absorbance data (red-shifted maxima with vibrational features). For all three tri-substituted peptides, the emission is reduced due to the interchromophore interaction suggested in the EC-CD experiments. Interestingly, the PL maxima for PEG-Oxa6,7T and PEG-Oxa6,11T are slightly red-shifted compared to that of PEG- Oxa11,7T. However, the red shift in the spectra in Figure 2.11 is not as pronounced as that observed previously by Kas et al. (for the peptide Oxa6D).[45] These PL data, coupled with the exciton-coupled CD spectra in Figure 2.10, suggest that the side chains do not have a near perfect face-to-face stacking; as such stacking would result in a significantly red shifted emission. As above, the lack of a dramatic shift of the PL maxima for PEG-Oxa6,7T and PEG-Oxa6,11T most likely can be attributed to the lower helicity of the hybrid peptide at room temperature, which causes incomplete overlap of the Oxa-PPV side chains. The intensity of emission observed for the PEG-Oxa6,11T is the least among the hybrids and is consistent with the increased extent of π–π stacking of the three side chains compared to all of the other peptides, which leads to reduced fluorescence yield. These data are also consistent with the absorbance measurements for PEG- Oxa6,11T, which showed a significantly blue-shifted maximum compared to that observed for the di-substituted peptides. Differences in the UV-Vis absorption spectra for the peptide hybrids are more pronounced than the differences in the PL spectra, likely owing to the fact that the UV-Vis absorption spectrum samples all chain segments and depends only on the number of electroactive species present in the sample and not on their relative positioning.

#### 2.3.3.4 Transient Photoluminescence

Transient photoluminescence spectroscopy was conducted to determine the nature of the excited species. The transient decays for PEGylated Oxa-PPV hybrid peptides are presented in Figure 2.12 and were generally consistent with the steady state luminescence data and expectations. The PEG-Oxa17D clearly behaves as independent chromophores since its dynamics mirror those of the control samples. These observations are in full agreement with the steady state PL unambiguously confirming the behavior of Oxa-PPV chromophores placed 17 Å apart as monomeric species. PEG-Oxa11,7T transient PL dynamics are reminiscent of the photophysics of MEH-PPV polymeric films where the dominant decay reflects that of the monomers but there is a long tail that is presumably associated with polaron pair formation and recombination.[55] As seen from the Figure formation of polaron pairs does not change the emission spectrum or lifetime very much compared to that of the monomer control. In such a case the emission still predominantly comes from the normal excited state but fewer molecules relax to form that state following photoexcitation.

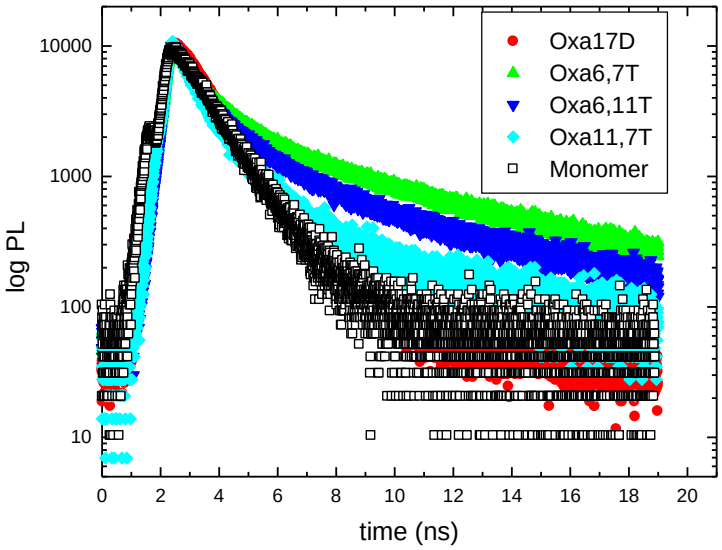


**Figure** 2.12 Transient photoluminescence decay dynamics of Oxa-PPV modified peptides.

Transient decays for peptide hybrid PEG-Oxa6,7T which has chromophores placed at smaller interoligomer distances of 6 Å apart show long tails with extended lifetimes (1/e) of 7.5 ns which are indicative of excimer formation. However, the excimer formation does not dominate the luminescence and most of the luminescence is still from the isolated chain. This is also the case for PEG-Oxa6,11T where the chain is in the polaron pair forming configuration. It would seem that polaron pairs or excitons that form rapidly do not form excimers, a very interesting result. This may explain why even in films dense with chromophores that the availability of many sites that could potentially support excimer formation there remains a reasonable (only reduced by factors of 2-5) luminescence yield from the exciton.

## 2.4 Conclusions

The design and synthesis of an α-helical peptide template capped with a PEG molecule at the N-terminus have been described. The incorporation of PEG to impart hydrophilicity results in a stable helical secondary structure, which allows this molecule to act as a template for effective display of different hydrophobic molecules such as conjugated oligomers, fluorophores, quantum dots, and dyes. The helical peptides reported here were used to graft up to three Oxa-PPV chromophores as side chains in order to study the impact of the side chains on the scaffold as well as the photophysical properties resulting from various chromophore arrangement. The photophysical properties of the molecules varied depending on the position and the orientation of the chromophores. An increased separation of 17 Å resulted in the chromophores behaving as isolated species even though they are positioned on the same face of the helix. For the rest of the scaffolds, chromophores positioned on the same side of the helix interacted with each other whereas the chromophores placed on the opposite face did not have apparent influence on the electronic properties. As the interaction between the chromophores became stronger (indicated by EC-CD) and/or the number of chromophores interacting with each other increased, the absorbance maxima shifted towards shorter wavelengths and the emission spectra shifted correspondingly towards longer wavelengths, thus confirming that these novel peptide templates can reliably position chromophores and yield absorption and emission behavior consistent with theoretical expectations.

# Chapter 3

# ELECTROCHEMICAL DEPOSITION AND CHARACTERIZATION OF CARBOXYLIC ACID FUNCTIONALIZED PEDOT COPOLYMERS

[Portions form this chapter are reprinted from Nandita Bhagwat, Kristi L. Kiick and David C. Martin, *Electrochemical deposition and characterization of carboxylic acid functionalized PEDOT copolymers* with permissions from Journal of Materials Research, 29 (23), 2014, 2835 – 2844; DOI: 10.1557/jmr.2014.314;


## 3.1 Introduction

A wide variety of biomedical devices involve the long-term integration of metallic or semiconducting components with living tissue. Examples include pacemakers,[126] deep brain stimulators,[127] cochlear implants,[128] retinal prosthetics,[129] and microfabricated cortical electrodes.[130] Conjugated polymers are of interest for these devices because they transmit charge by both electron and ionic transport.[58] They also provide an intermediate level of mechanical compliance between the rigid inorganic device substrate and the soft biological tissue. However, to optimize the performance of these devices, there remains an unmet need for developing functionalized conducting polymers that can be modified with biomolecules to improve the interface between the hard electrode and soft tissue.[59]

Conjugated polymers are also of interest for a wide variety of devices, including electrochromic displays, photovoltaics, and chemical sensors.[131] A materials system that has been of particular scientific commercial interest is substituted

polythiophenes, with particular focus on poly(3,4-ethylenedioxythiophene) (PEDOT). PEDOT is of particular interest because of its low oxidation potentials, high conductivity, superior environmental stability, and good chemical and electrochemical properties.[59, 132-135] However, the EDOT side groups are not chemically reactive, making it difficult to create materials with more specific functionality for particular applications.

To generate polymer films with more tailorable surface chemistries, it is possible to modify the chemical structure of the monomer[64, 136] and to copolymerize two or more suitably functionalized monomers to obtain conducting polymers with properties intermediate to those of the individual homopolymers.[137, 138] Substituting the side groups on the backbone of a conducting polymer can change the optical and electrochemical properties of the material and can also be used as a means to introduce functional groups. A wide variety of functional EDOT monomers have been synthesized to date; most of these have been tailored toward applications in electronic and electrochromic devices. Functional groups such as alcohols,[139] carboxylic acids,[140] cyanobiphenyl,[141] and sulfonate[136] have all been incorporated to synthesize functional EDOT molecules. Copolymerization strategies have also been employed to manipulate the properties of the conducting polymers. Copolymers of EDOT with pyrroles,[137, 142] indole,[143] 3-methylthiophene,[144] and pyrenes[138] are examples of few such copolymers. Copolymers of EDOT with functional EDOT molecules provide a means of creating PEDOT coatings with functionalized components and tunable properties, without changing the polymer backbone.[43, 136]

Among these functional groups, carboxylic acids provide a particularly facile means of functionalizing monomers, especially with biological molecules.

Biofunctionalization of conducting polymer coatings has proven to be an attractive method to provide superior interface for polymer-coated neural prosthetic implants. Monomers of EDOT and pyrroles with carboxylic acid functionality have been previously reported.[64, 145] Lee et al. recently reported the synthesis of carboxylic acid functional terthiophene monomers and demonstrated their use as bioactive conductive scaffolds.[42] Luo et al. developed carboxylic acid functional EDOT molecules, linked with ether and ester groups on the ethylene dioxy ring, although the functional group reduced polymerization of the monomer versus rates for unmodified PEDOT, which was attributed to the steric hindrance of the functional group.[145] Povlich et al. thus developed and synthesized an EDOT monomer with the simplest possible COOH modification, as a direct substituent on the ethylene dioxy ring.[43]

In this contribution, we have used this molecule, EDOTacid, to deposit copolymer films of EDOT and EDOTacid, with systematic variations in the monomer feed ratio. Use of this EDOT derivative permits maintenance of the backbone of the conducting polymer but inclusion of a carboxylic acid functional group to generate films with specific properties. Thus, we are able to generate PEDOT coatings with varying number of functional groups on the surface, thereby manipulating the surface concentration of the COOH groups and in turn controlling the hydrophilicity and morphology of the films. EDOT and EDOTacid were successfully copolymerized by electrochemical oxidation of the monomer mixtures from propylene carbonate solutions. The effects of the monomer feed ratio on the resulting copolymer films were characterized via chemical, electrochemical, and spectroscopic methods. The changing morphology of the films was characterized using scanning electron microscopy. These

functional films can be modified with various biomolecules such as peptides and proteins.

## 3.2 Experimental Procedure

### 3.2.1 Materials

All chemicals were used as received from Sigma Aldrich without further purification. The working electrodes used were sputtered gold-palladium barbell-shaped electrodes (6 mm in diameter) on plastic slides. Indium tin oxide (ITO)-coated glass slides (0.7 x 5cm; R, ~4–8 ohms) were used for spectroscopic measurements.

### 3.2.2 Electrochemical Deposition of PEDOTacid Copolymer Films

Electropolymerization was carried out in a two-electrode cell using an AutoLab potentiostat/galvanostat (Utrecht, The Netherlands) with a platinum wire counter electrode. The copolymer films were electrochemically polymerized from a 0.01 M monomer solution in propylene carbonate with 0.1 M lithium perchlorate as the counter ion. All films were polymerized galvanostatically with a current density of ~0.2 $mA/cm^2$ for 10 min and were rinsed with DI water after polymerization.

### 3.2.3 Characterization of PEDOTacid Copolymer Films

#### 3.2.3.1 Chemical Analysis of PEDOTacid Copolymer Films

Chemical analysis of the copolymer films was conducted using Fourier transform infrared (FTIR) spectroscopy (Bruker Tensor 27, Billerica, MA) in the attenuated total reflection (ATR) mode, and x-ray photoelectron spectroscopy (XPS; Omicron EA125, Taunusstein, Germany). To obtain FTIR spectra, each copolymer film was placed on the ATR crystal and scanned for 128 scans from 4000 to 400 $cm^{-1}$.

For XPS, non-monochromatic aluminum (1486.5 eV) x-ray source was employed. Corrections were made by using adventitious carbon peak located at 284.6 eV in C1sregion. 50 and 25 eV pass energies were used for survey scans and high-resolution scans, respectively. To quantify the concentration of carboxylic acid groups on the surface of the copolymer films, a toluidene blue O (TBO) assay was performed. Positively charged TBO has been shown to bind to negatively charged moieties on polymeric surfaces and shows an absorption peak at 630 nm.[146, 147] To construct calibration curves, TBO solutions at various concentrations were prepared by dissolving dry TBO powder in 50% acetic acid solutions, and their light absorbance at 630 nm was measured using an Agilent 8453 spectrophotometer (Agilent Technologies Inc, Santa Clara, CA). For the evaluation of the surface charge concentration of carboxylic acid groups on copolymer films, the films were soaked in an alkaline solution (0.1 mM NaOH) of TBO (0.5 mM) for 2.5 h. After TBO adsorption, the samples were rinsed with 0.1 mM NaOH to ensure removal of any noncomplexed dye. Samples were then soaked in 2 mL of 50% acetic acid solution for 4 h to desorb the complexed dye; a separate set of experiments indicated that this length of time was sufficient for complete desorption. The absorbance of the residual TBO solution was measured at 632 nm. The recorded spectroscopic data were converted into surface concentration (nanomoles per square millimeter) using the calibration curve. Three samples of each copolymer film were used to perform the assay.

#### 3.2.3.2 Contact Angle Measurements

Water contact angles were measured using the drop shape analysis plug-in and DropSnake method using ImageJ software (National Institute of Health). To do so, 1

µL of deionized water was pipetted onto the surface of the copolymer films, and mages were captured using a Canon S5 IS camera attached to a tripod. Three different samples of each copolymer film were measured, and the final value was expressed as mean 6 SD.

#### 3.2.3.3 Electrical Properties of PEDOTacid Copolymer Films

To analyze the electrical activity of the copolymer films, cyclic voltammetry (CV) and electrochemical impedance spectroscopy (EIS) were performed using the Autolab potentiostat/galvanostat (Utrecht, The Netherlands) described above with a platinum counter electrode, a saturated calomel reference electrode, and phosphate-buffered saline electrolyte. For the CV measurements, cycling was performed between +0.8 and -0.6 V with a scan rate of 0.12 V/s. The first stable curve was considered as cycle 1 and used to determine the electroactivity of the film. The charge storage capacity (CSC) was calculated by taking the integral, over time, of the area under the oxidation–reduction curve. For impedance measurements, an alternative current sinusoidal input of 5 mV in amplitude was used as the input signal with the direct current potential set to 0. The magnitude and phase angle for the impedance measurements were determined over six discrete frequencies over the range of $1–10^5$ Hz.

#### 3.2.3.4 Ultraviolet-Visible Spectroscopy

Optical absorption measurements of the films were obtained on a Shimadzu ultraviolet (UV)–visible–near infrared spectrophotometer (Columbia, MD), with scanning from 300 to 800 nm and with an ITO electrode as the reference.

#### 3.2.3.5 Scanning Electron Microscopy

Morphological studies were conducted using a JEOL JSM-7400F field emission scanning electron microscope (Tokyo, Japan) at a 3-kV operating voltage. All the films were sputtered with a thin layer of gold-palladium (45 s) to provide a more conductive surface. The profiles of the copolymer films were imaged via focused ion beam–scanning electron microscopy (FIB-SEM; Zeiss Auriga 60, Oberkochen, Germany). Three separate trenches (of 5 x 5 microns and 5 microns depth on each sample) were milled using an OmniProbe 200 system to determine the thickness of the films. A current of 600 pA was used to do the milling. The thickness of the films was determined by measuring the height at 6 different points for each milled trench for 3 samples (18 measurements for each copolymer film) and reporting the average.

## 3.3 Results and Discussion

### 3.3.1 Synthesis of Copolymer Films

The films of PEDOT, PEDOTacid, and copolymers of PEDOT-PEDOTacid, deposited galvanostatically, with a current density of ~0.2 mA/cm$^2$, exhibited a blue color characteristic of PEDOT films. Various galvanostatic conditions were tested for PEDOTacid by varying current densities to obtain films that adhered to the Au/Pd electrodes and remained intact after washing with DI water. The pure PEDOTacid films deposited with current densities more than 0.3 mA/cm$^2$ were extremely fragile and hence all the copolymer films were deposited with current densities of 0.2 mA/cm$^2$. Copolymer films were obtained from mixtures of the two monomer solutions (in propylene carbonate) at different mole fractions. The total concentration of the monomer solution was maintained at 0.01 M for all depositions. The mole fraction X was calculated as $n_{\text{EDOTacid}}/(n_{\text{EDOT}} + n_{\text{EDOTacid}})$ and films with mole fractions 0, 0.25,

0.5, 0.75, and 1 were deposited; these films are denoted as EA0, EA25, EA50, EA75, and EA100, respectively. The schematic of the copolymer structure is presented in Figure 3.1.

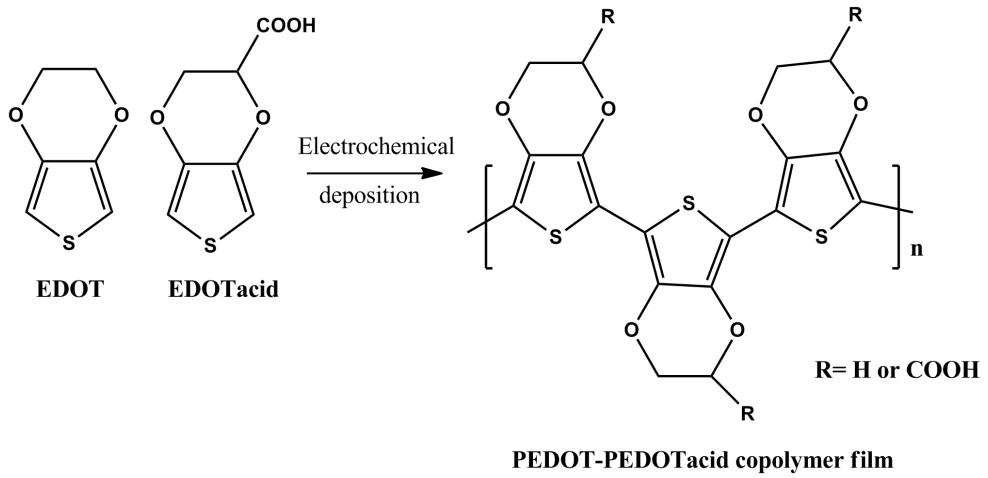


**Figure** 3.1 Schematic of polymerization of PEDOT-PEDOTacid copolymer. Reprinted with permission from J. Mater. Res, 29, 2835-2844. Copyright © 2014 Materials Research Society.

### 3.3.2 Surface Analysis of Copolymer Films

The chemical composition of films was determined via two surface analysis techniques; XPS and FTIR (ATR mode). Figure 3.2 displays the survey spectra for all the different copolymer films EA0, EA25, EA50, EA75, and EA100. For all the various copolymer films the peak at 285 eV was assigned to C1s, the peak at 533 eV was assigned to O1s and the peak at 166 eV was assigned to S 2p. The O 1s and S 2p peaks did not show any significant differences after deconvolution. The C1s peak on

the other hand changed with the copolymer composition. The XPS data presented in Figure 3.3 show the C 1s spectra for EA0 and EA100. The peak at 285 eV corresponds to the C–C bond and that at 289 eV corresponds to the C=O bond, consistent with binding energy values reported in literature.[148]

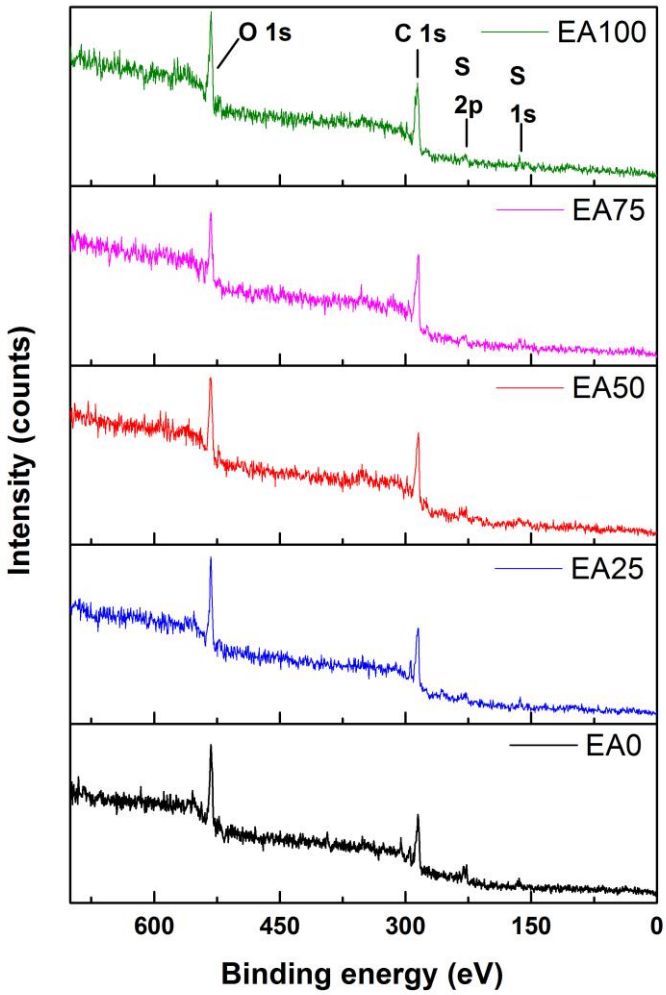


**Figure** 3.2 XPS survey spectra for PEDOT-PEDOTacid copolymer films.

Spectra were analyzed using the peak fitting functions to determine the relative contribution of the two peaks in each spectrum. The slight high-energy shoulder that appears in the EA0 spectra (287.9 eV) contributed 11.6% of the total area under the curve and is likely attributable to oxidation of organic matter on the film. In the EA100 spectrum, the peak at 289 eV (characteristic of the carboxylic acid group) represented 36.5% of the area under the curve, which is consistent with the presence of the carboxylic acid group (approximately 24%) in the EDOTacid monomer. The characteristic C=O peak at 289 eV was also observed in films EA50 and EA75 (data not shown) confirming the presence of EDOTacid in all copolymer films. The O 1s and S 2p spectra, with binding energies at 532 and 164 eV, respectively, were identical in the various copolymer films, as expected.

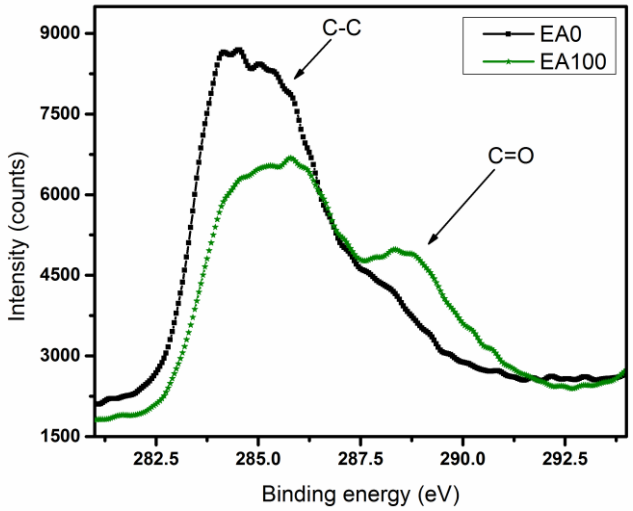


**Figure** 3.3 XPS C 1s spectra for films EA0 and EA100. Reprinted with permission from J. Mater. Res, 29, 2835-2844. Copyright © 2014 Materials Research Society

The presence of the carboxylic acid group, indicative of the incorporation of the EDOTacid into the copolymer film, was also confirmed via FTIR spectroscopy using the ATR mode. Infrared (IR) spectra for the copolymer films are presented in Figure 3.4 and are similar to the spectra that have been reported previously for PEDOT polymers.[142, 149] The peak at 1700–1740 $cm^{-1}$ is characteristic of carbonyl stretching. For the EA0 films, this peak was absent, as expected. However, this peak was also missing from the spectra of EA25, suggesting there was little to no incorporation of EDOTacid in films with lower mole fractions of EDOTacid in the monomer feed solution, in agreement with the XPS observations. There was a distinct peak at 1740 $cm^{-1}$ for films EA50, EA75, and EA100, as expected for copolymer films of PEDOT and PEDOTacid. The following peaks were observed in all of the copolymer films: the peaks at 707, 862, 966, and 997 $cm^{-1}$ originate from the stretching modes of C–S–C in the thiophene rings; the peaks at 1120, 1160, and 1267 $cm^{-1}$ originate from the stretching of the C–O–C group; and the peaks at 1365, 1463, and 1523 $cm^{-1}$ originate from the C–C and C=C stretching in the thiophene ring.[142, 149]

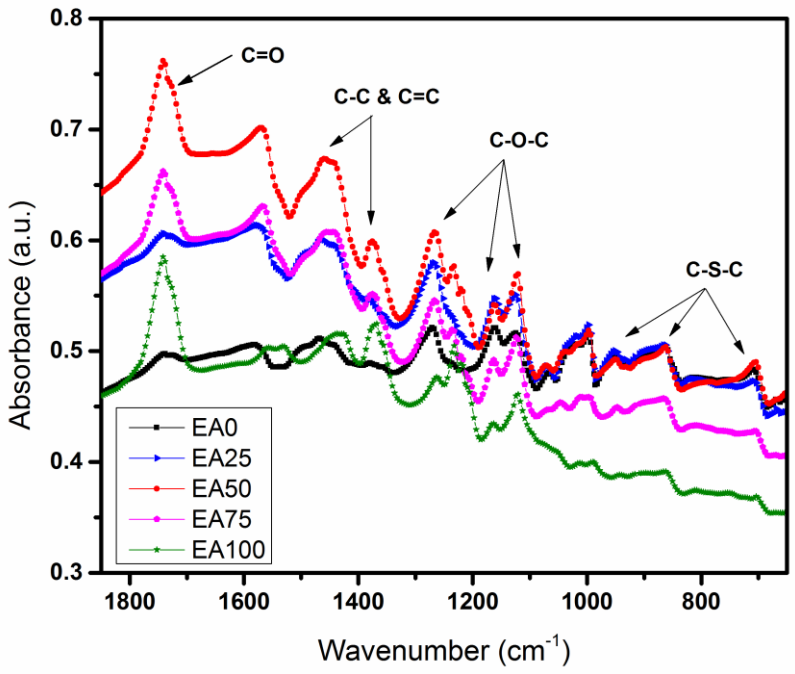


**Figure** 3.4 FTIR spectra for the PEDOT-PEDOTacid copolymer films. Reprinted with permission from J. Mater. Res, 29, 2835-2844. Copyright © 2014 Materials Research Society

To quantify the amounts of surface-available PEDOTacid incorporated in the copolymer film with increasing mole fractions of EDOTacid in the monomer feed solutions, a spectrophotometric assay was employed. Toluidine blue O dye assay is a straight forward method used to analyze the chemical activity of surface moieties.[146, 147] TBO is a salt consisting of an aromatic cation and an associated chloride anion that can bind electrostatically to negatively charged species and that can easily be detected, after desorption, by light absorption in the blue region. The absorbance of the solution of the desorbed TBO can thus be used to calculate the surface concentration of the COOH groups.

The surface concentrations of the COOH groups present in the copolymer films, as determined by the TBO assay, are presented in Figure 3.5. The number of moles of carboxylic acid for EA0, EA25, EA50, EA75, and EA100 were 0.11 6 0.06, 0.14 6 0.05, 0.59 6 0.12, 1.90 6 0.17, and 2.76 6 0.09 nmoles/mm$^2$ respectively. The film EA0 showed a small absorbance for the desorbed TBO solution, which may be due to physical adsorption of the dye to the substrate/film. Consistent with the XPS (Figure 3.3) and FTIR (Figure 3.4) data, the film with 25% EDOTacid in the monomer feed ratio, EA25, showed only a small concentration of carboxylic acid groups on its surface. The remaining films (EA50, EA75, and EA100) exhibited an increasing surface concentration of carboxylic acid groups with the increasing mole fraction of EDOTacid. A possible explanation for the lack of carboxylic acid groups on the EA25 films could be that at low concentrations of EDOTacid, the monomer remains inside the bulk of the film and does not migrate to the surface. Alternatively, given that the increase in surface concentration of the acid groups from 25 to 100% was not linear, it is possible that EDOT acid was not incorporated in the copolymer linearly with increasing mole fraction of EDOTacid. This result is consistent with the IR spectra (Figure 3.4) for the co-polymer films where the C=O stretch appears only for films EA50, EA75, and EA100 and is almost absent for EA25. The data suggest that for lower mole fractions of EDOTacid, the polymer film was mainly comprised of EDOT. At higher concentrations of 75 and 100% of EDOTacid, the films were mainly comprised of EDOTacid.

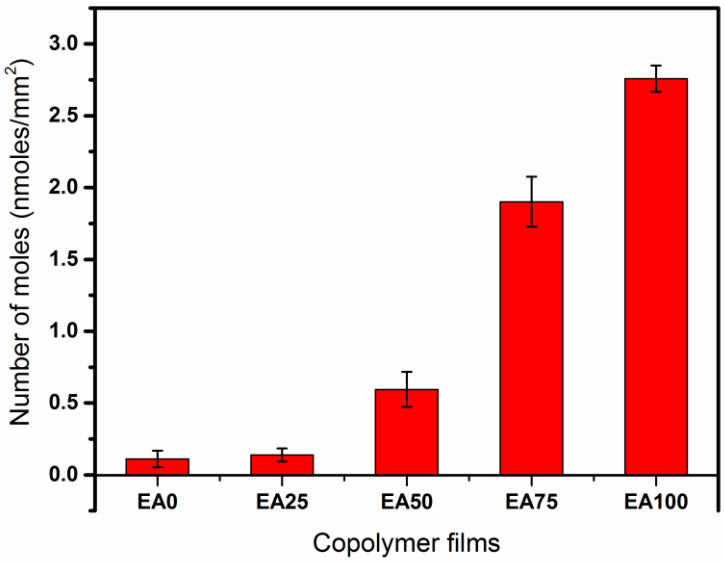


**Figure 3**.5 Surface concentration of the carboxylic acid groups on the PEDOT-PEDOTacid copolymer films (*n*=3). Reprinted with permission from J. Mater. Res, 29, 2835-2844. Copyright © 2014 Materials Research Society

### 3.3.3 Hydrophobicity of Copolymer Films

Static water contact angle measurements were conducted to assess the wettability of the PEDOT-PEDOTacid films. Figure 3.6 shows the water contact angles for the copolymer films, with increasing monomer feed ratio of EDOTacid (EA0 to EA100). The water contact angle for EA0, purely PEDOT films, was measured to be 52.6° 6 0.3°. The contact angle for EA25 was 48.1° 6 1.0°, for EA50 was 42.4° 6 0.3°, for EA75 was 37.9° 6 1.1°, and for EA100 was 32.5° 6 0.6°. The contact angle for PEDOT films (EA0) was consistent with previously reported values for PEDOT.[43, 150] Figure 3.6 demonstrates the decrease in water contact angle with increase in PEDOTacid content in the copolymer films. Consistent with the increasing

concentration of polar COOH groups on the surface of the films from EA0 to EA100, the films become increasingly hydrophilic in nature, resulting in increased wettability. The water contact angles for most of the COOH-functionalized films reported here were lower than those reported for COOH-functional PEDOT films synthesized by Luo et al. (in which the COOH was linked with an ether or an ester linkage); the contact angles reported for the films with ether and ester linkers were 40.2° and 44.6°, respectively. The higher contact angles of the films reported by Luo et al. could be attributed to the alkyl linkers adding to the hydrophobicity of the films.[145] Thus, by manipulating the surface concentration of polar groups, films with varying hydrophilicities were achieved.

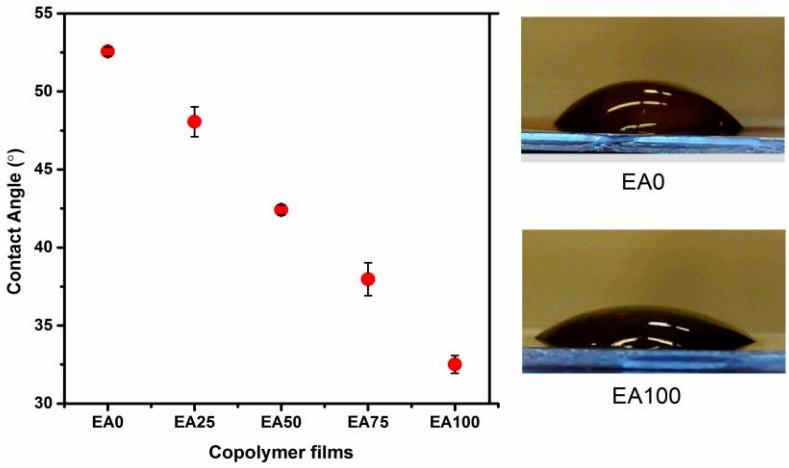


**Figure** 3.6 Water contact angles for PEDOT-PEDOTacid copolymer films. Reprinted with permission from J. Mater. Res, 29, 2835-2844. Copyright © 2014 Materials Research Society

To determine the water contact angle of the PEDOT-PEDOTacid copolymer films theoretically, the Cassie equation was used.[151] Cassie's law is used to determine the effective contact angle for a liquid on a composite surface. For a two-component system, the Cassie equation is given by:

$$\cos(\theta_c) = f_1 * \cos(\theta_1) + f_2 * \cos(\theta_2)$$

where $f_1$ and $f_2$ are the mole fractions and $\theta_1$ and $\theta_2$ are the contact angles for component 1 and component 2, respectively.[151] Using this equation, contact angles for the copolymer films EA25, EA50, and EA75 were calculated. As is illustrated in Table 3.1, the experimental and calculated values are in excellent agreement within 1° of each other.

**Table** 3.1 Experimental and calculated values for water contact angles for PEDOT-PEDOTacid copolymer films. Reprinted with permission from J. Mater. Res, 29, 2835-2844. Copyright © 2014 Materials Research Society

| **Sample** | **Experimental Value (°)** | **Calculated Value (°)** |
|---|---|---|
| EA0 | 52.6 | 52.6 |
| EA25 | 48.1 | 48.2 |
| EA50 | 42.4 | 43.5 |
| EA75 | 37.9 | 38.3 |
| EA100 | 32.5 | 32.5 |

### 3.3.4 Electrical Properties of Copolymer Films

Electrical properties of the PEDOT-PEDOTacid copolymer films were determined via CV and EIS. The electrode sites were swept from +0.8 to -0.6 V at a scan rate of 0.12 V/s versus Ag/AgCl reference electrode. Figure 3.7 shows the first stable CV curve for the copolymer films EA0–EA100. The charge storage capacity (CSC) of the film can be calculated by integration of *I*(t) within the cycled region; the

CSC values for the copolymer films are provided in Table 4.2. As shown in Table 4.2, the CSC values for the films EA0, EA25, EA50, EA75, and EA100 are 3.74, 3.68, 3.81, 3.95, and 3.76 mC/cm$^2$, respectively, indicating that there is no significant difference in the charge storage capacities of the various copolymer films. All the CSC values for the copolymer films were significantly greater than the CSC for Au/Pd electrodes (0.2 mC/cm$^2$). However, the CSC values reported here are lower than previously published results for PEDOT films, where the deposition current density was ~1mA/cm$^2$ and thus resulted in thicker films.[70] The films in this work were polymerized with lower current density, resulting in thinner films and lower charge storage capacities. Nevertheless, our data suggest that differences in the amounts of PEDOT or PEDOTacid in the film do not appear to affect the manner in which charge is transferred from the film. This suggests that charge transfer must mainly happen along the back-bone of the film, and that the carboxylic acid groups, which could generate ions that could contribute to an ionic component of charge transfer, do not seem to participate in the overall CSC of these copolymer films.

**Table** 4.2 CSC values for PEDOT-PEDOTacid copolymer films. (*n*=3) Reprinted with permission from J. Mater. Res, 29, 2835-2844. Copyright © 2014 Materials Research Society

| | **EA0** | **EA25** | **EA50** | **EA75** | **EA100** |
|---|---|---|---|---|---|
| **Charge storage capacity (mC/cm2)** | 3.74 | 3.68 | 3.81 | 3.95 | 3.76 |

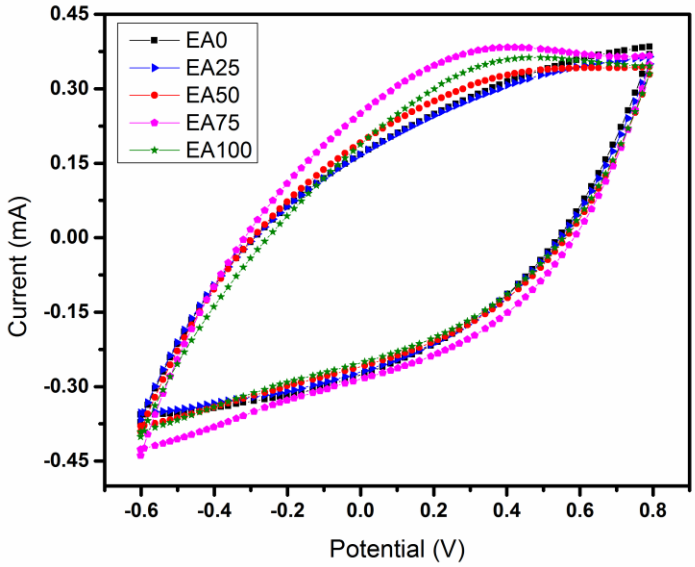


**Figure** 3.7 CV curves for 1st stable cycle for PEDOT-PEDOTacid copolymer films. Reprinted with permission from J. Mater. Res, 29, 2835-2844. Copyright © 2014 Materials Research Society

EIS was conducted to determine how the various amounts of PEDOT and PEDOTacid influenced charge transport in the copolymer films. The magnitude and phase of the impedance are shown in Figure 3.8 and Figure 3.9, respectively. The results for the bare electrode are also included in the same spectrum. The characteristic drop in magnitude of impedance for the polymer-coated electrodes is evident when compared with bare electrodes in the frequency range 1–$10^5$ Hz. However, due to the comparably larger electrode diameter (6 mm) for the films reported here, the bare electrode impedance was lower than other micrometer-sized electrodes investigated elsewhere.[152] The impedance magnitude was monitored in detail at 1 kHz, the frequency most relevant to neural recording and stimulating. The impedance values at

1 kHz for the copolymer films EA0, EA25, EA50, EA75, and EA100 were 952±101 Ω, 1042±65 Ω, 953±42 Ω, 883±145 Ω and 1199±277 Ω, respectively. The magnitude of impedance for all the copolymer films were similar to those of pure PEDOT (EA0) and were consistent with previously reported values for PEDOT.[70, 72, 153] The reduced impedance values were a result of the increase in the effective surface area of the electrode, consistent with previous reports.[71, 154] The phase lag for all the copolymer films in the entire frequency range was less than 10°, indicating that the polymer-coated electrodes function primarily as resistors. For lower frequencies of 1–100 Hz, the phase lag for the Au/Pd electrodes was around 30°. The low phase lag of <10° can also be attributed to the rough morphology of the films which makes them resistive in nature (as illustrated in the phase lag diagram [Figure 3.9]). Even though the phase lag was higher than that of the conducting polymer-coated electrodes, it was not high enough for the bare electrodes to behave as capacitors. The slightly higher magnitude of impedance in case of EA100, when compared with the rest of the films (around 1 kΩ), could be because of the different morphology of the film compared with PEDOT-containing films (see below).

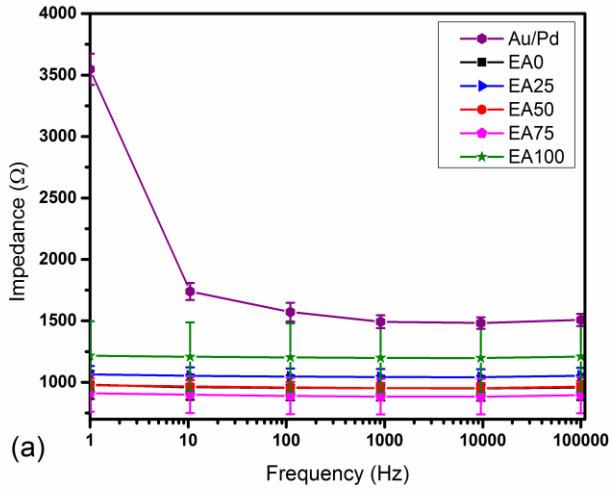


**Figure** 3.8 Impedance magnitude of the PEDOT-PEDOTacid copolymer films. Error bars are marked with one standard deviation (*n*=4). Reprinted with permission from J. Mater. Res, 29, 2835-2844. Copyright © 2014 Materials Research Society

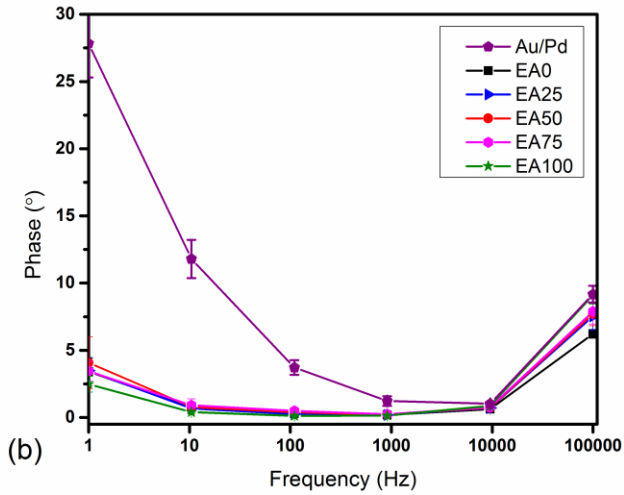


**Figure** 3.9 Phase lag of the PEDOT-PEDOTacid copolymer films. Error bars are marked with one standard deviation. (*n*=4) Reprinted with permission from J. Mater. Res, 29, 2835-2844. Copyright © 2014 Materials Research Society

### 3.3.5 Spectroscopic Properties of Copolymer Films

Optical absorption spectra of the PEDOT-PEDOTacid copolymer films coated on ITO electrodes at different monomer feed ratios in the polymerization solution are shown in Figure 3.10. Normalized spectra of the copolymer films are presented in Figure 3.10 for ease of comparison between the spectroscopic properties of the different PEDOT-PEDOTacid copolymer films. All the copolymer films exhibit a similar spectra consisting of 2 peaks in the UV–visible range. A narrow peak was observed at 360 nm and a broad peak from ~500 to ~675 nm with maxima at 590 nm. EDOT oligomers (dimers, trimers, and tetramers) have been shown to absorb between 300 and 400 nm, indicating that EDOT oligomers are present in the film.[155] PEDOT in its neutral state has a characteristic absorption spectra at 590 nm,[156, 157] attributable to the $\pi$-$\pi^*$ transition and consistent with the peak observed for the PEDOT-PEDOTacid copolymer films. The spectroscopic properties of the copolymer films appear unaltered with increasing amounts of PEDOTacid in the copolymer film, indicating that the incorporation of the acid group in the monomer does not influence the absorbance behavior of the conjugated polymer.

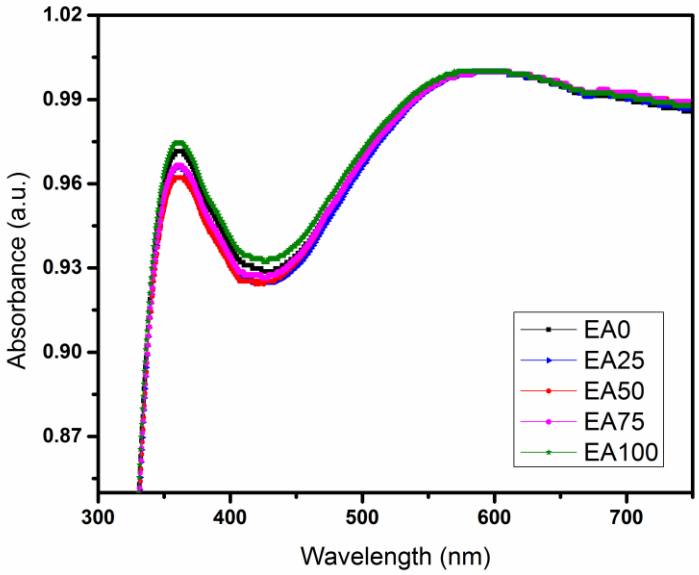


**Figure** 3.10 Ultraviolet-visible spectra for PEDOT-PEDOTacid copolymer films. Reprinted with permission from J. Mater. Res, 29, 2835-2844. Copyright © 2014 Materials Research Society

### 3.3.6 Morphology of Copolymer Films

The structures of the deposited copolymers were studied using SEM and representative images are shown in Figure 3.11. The surface morphology of films EA0, EA50, and EA100 is portrayed in Figure 3.11(a) to 3.11(c), respectively. It is clear from these images that the morphology of the films significantly changes with increasing mole fraction of EDOTacid in the monomer feed solution. The morphology of pure PEDOT films (EA0) was extremely rough in nature; similar to the morphology of PEDOT films deposited from propylene carbonate previously reported.[158, 159] EA0 films were granular in nature with visible aggregation of the grains into clusters. These clusters, which were approximately 1 µm in diameter, were present uniformly over the film surface and were connected by smaller nanofibers (50–100 nm). The granular

nature of the film disappeared with increasing PEDOTacid content in the copolymer films. The EA25 copolymer films had a fewer number of the clusters connected by nanofibers (50–100 nm), and they were smaller in size, ~0.65 µm, when compared with those of the EA0 films. The micrometer-sized clusters disappeared completely for the EA50 films. The rough, granular morphology was almost entirely absent for the EA100 film (pure PEDOTacid), which exhibited a smoother surface decorated with "pleated" features. The EA100 film also lacked a porous morphology, which is consistent with previously reported porous morphologies of PEDOT deposited from organic solvents.[59] The changing morphology of the films with increasing PEDOTacid con- tent further supports the conclusion that the films deposited were indeed copolymers of EDOT and EDOTacid.

Along with characterization of the morphology of the films, FIB-SEM [Figure 3.11(d)-3.11(f)] was conducted on the films to determine the thickness and view the profile of the copolymer films. The film thickness and the maximum peak height varied with the copolymer composition as is shown in Figure 3.11(d)–3.11(f). EA0, with a rough, porous and granulated morphology comprising aggregated clusters, had a film thickness of 535±230 nm. The rough nature of the film resulted in a large standard deviation within the film thickness for EA0. The film thickness reduced for EA50 and EA100 films and was measured to be 355±96 nm and 282±46 nm, respectively. Owing to the absence of clusters on EA50 and EA100 surfaces, the average film thickness reduced with smaller standard deviations suggesting the films became smoother with increasing PEDOTacid content.

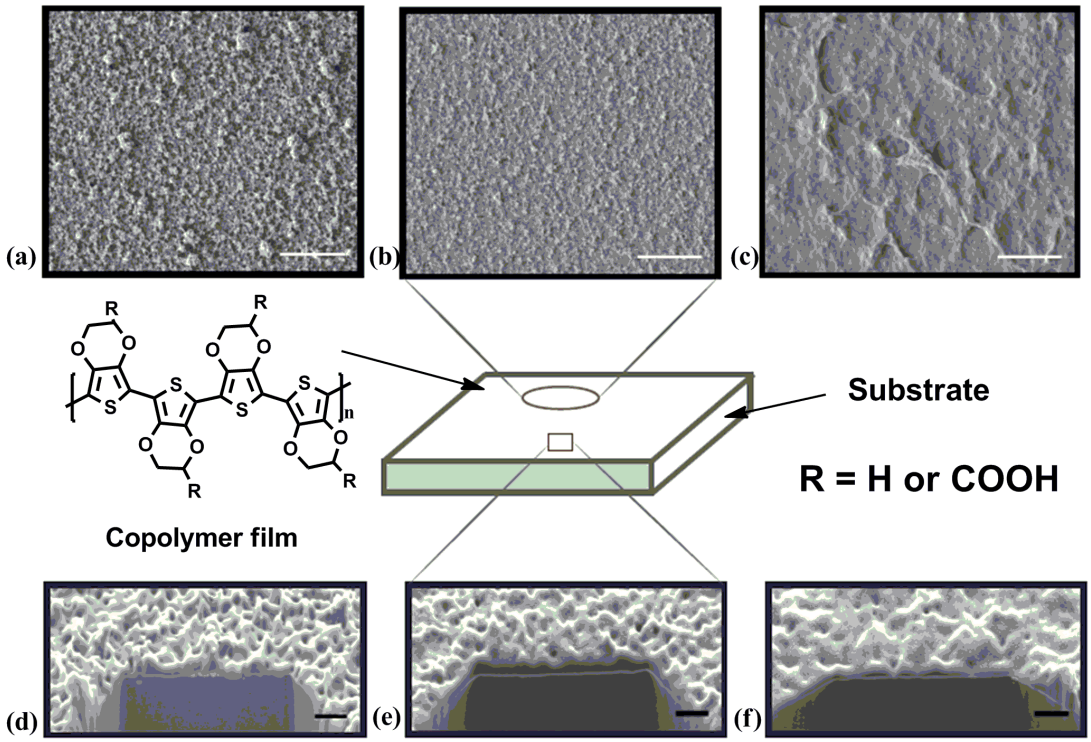


**Figure** 3.11 SEM images of the copolymer films containing different ratios of EDOT to EDOTacid. The top row of SEM images portray the surface of the morphology of the films containing 0, 50, and 100% EDOTacid; (a), (b), and (c), respectively (the scale bar represents 5 µm). The bottom images depict the films in profile, presenting the thickness of the deposited polymer. (d), (e), and (f) illustrate the profile of the films composed of 0, 50, and 100% EDOTacid respectively (the scale bar represents 1 µm). Reprinted with permission from J. Mater. Res, 29, 2835-2844. Copyright © 2014 Materials Research Society

EA0 films, which were comprised of only PEDOT, were the most hydrophobic in nature and had a rough and porous morphology, similar to previously reported PEDOT films.[158-160] Related previous reports suggest pure PEDOT films were rougher and more hydrophobic with a high water contact angle compared with functionalized PEDOT films (with polar side groups), which were smoother and hydrophilic with a

low water contact angle.[145, 154, 161] In particular, Luo et al. have also reported similar observations for the morphologies of PEDOT films with a hydroxyl and a carboxylic acid functionality. Pure PEDOT films were rough and porous, with nanofiber-like structures, whereas PEDOT with polar functional groups (–OH and –COOH) formed smoother films with "nanodots".[154] The changes in morphology of the reported films with changes in the hydrophilicity of the monomers are also in agreement with other reports in the literature that have shown that hydrophobic surfaces in polymer films are associated with rougher morphologies.[162-164] The smoother surfaces of hydrophilic films have been attributed to high surface free energies and high work of adhesion.[162]

The precise copolymer composition of the various PEDOT-PEDOTacid films is difficult to establish unambiguously because of their limited solubility. However, when considering that the measured contact angles show outstanding agreement with theoretical predictions and that clear and nonorganized morphology changes uniformly and systematically with increasing PEDOTacid content, the data suggest that EDOTacid is incorporated randomly in the copolymer chains rather than in an organized or blocky manner. This is also in agreement with conclusions presented by Doherty et al. for a copolymer system of EDOT and EDOT-methanol.[165] Interestingly, from the TBO assay data for EA50 films, it is apparent that equimolar feed concentrations results in a film rich in PEDOT. This is also consistent with Doherty et al. in which calculated reactivity ratios for the EDOT and EDOT-methanol system indicated that $r > 1$ for EDOT and $r < 1$ for EDOT-methanol.[165] Given the similarity in chemical compositions of the polymers here and in the Doherty report, coupled with the results of the contact angle and SEM experiments, it is likely that a similar conclusion applies to the polymers reported here.

## 3.4 Conclusions

Functional copolymer films with various compositions of PEDOT and PEDOTacid were successfully synthesized via electrochemical deposition. FTIR, XPS, and TBO assays confirmed the formation of copolymer films with increasing PEDOTacid content with increasing monomer feed ratios of EDOTacid. The contact angle measurements clearly demonstrate the increasing hydrophilicity of the film as the surface concentration of the carboxylic acid groups increased. Electrical properties of the films were not compromised by the addition of PEDOTacid in copolymer films and were similar to pure PEDOT films. The morphology of the films, however, significantly changed with increasing PEDOTacid content, transitioning from a rough to a smoother morphology. These approaches thus represent a facile method for the synthesis of functional PEDOT films with comparable electrical properties, tunable surface morphologies, and selected hydrophilicities. Myriad opportunities exist for functionalizing these copolymer films to provide an enhanced neural interface.

# Chapter 4

# BIOFUNCTIONALIZATION OF PEDOT FILMS WITH LAMININ BASED PEPTIDES

## 4.1 Introduction

Conducting polymers (CP) have been studied in depth over the past 2 decades and are now commercially used as hole injection layers,[166] active layers,[167] and transparent conductive electrodes[168] in organic electronic devices. Along with their applications in organic light emitting diodes,[131, 169] organic photovoltaics,[170] and electrochromic devices,[171] conducting polymers also have numerous biomedical applications, ranging from coatings for neural prosthetic implants,[172, 173] hydrogels for tissue engineering,[39, 174] guidance channels for nerve regeneration,[175] and materials for biosensing.[176]

Currently, a majority of bio-electrodes are predominantly made from stable metals such as platinum, gold, iridium, and titanium which while inert cannot provide and maintain intimate contact between the neural cells and electrodes. As a result such neural electrodes cannot enable long term stimulation and recording. To overcome this conducting polymers such as polypyrroles and polythiophenes have been used by many research groups to improve the long term performance of neural electrodes.[177-179] Inherently conducting property of conjugated polymers and their ability to transmit charge by both electron and ionic transport makes them attractive for stimulating cells that respond to electrical signals. Also, coating the electrodes with a layer of rough and porous material can increase the effective surface area resulting in superior charge

transfer.[180] Multiple studies performed on polypyrrole (PPy) and poly (3,4-ethylenedioxythiophene) (PEDOT) based CPs have demonstrated effective muscle and nerve regeneration.[181-183]

An ideal neural prosthetic implant would have a surface that has the properties to attract target cells, possesses cell attachment characteristics and provides biological cues and electrical stimulation for cell growth. For instance, Gomez et al. reported a micropatterned PPy surface to create topographical cues for cells that affected axon orientation.[184] In another report, Wang et al. manipulated the nanoscale topography on polyaniline films to induce attachment and proliferation of PC12 cells.[185] The most common and obvious strategy to improve the integration of the device with the tissue is to develop bioactive conducting polymers. The biological functionality imparted to the films can potentially bridge the gap through intimate contact between the tissue and the electrode. This approach has been explored by many groups, however most of the reports discuss incorporating bioactivity via either physically adsorbing the biological molecule or entrapping it as dopants. Stewart et al. studied the effect of adsorbed fibronectin on PEDOT/glycol composites and reported these surfaces to provide good support for cell adhesion and proliferation.[186] In one study, Green et al. used peptides derived from laminin as dopants for PEDOT films and were able to demonstrate higher PC12 cell attachment and longer neurite extension for polymers doped with peptide compared to pTS doped PEDOT.[72] A similar approach has been demonstrated with polypyrroles too, where Cui et al. doped polypyrroles with peptide sequences isolated from laminin and a similar conclusion was presented.[178] Additional biological molecules used with conducting polymers range from proteins to growth factors[61, 70] and proteoglycans such as hyaluronic acid.[62, 187]

Physical adsorption and entrapping the molecule inside the polymer are straightforward methods, however both methods come with certain drawbacks. The adsorbed molecule can dissociate while only a relatively small amount of the biomolecule can be entrapped.[188] The entrapped molecules also tend to disrupt the morphology of the CP compromising the electrical properties of the CP.[68, 70, 189] Covalent modification of the CP surface, albeit more complex, is a more permanent method to functionalize the polymers. It provides a tighter control over immobilization, minimal biomolecule loss over time, and control over biomolecule orientation.[188]

Here we use a laminin derived peptide sequence to covalently modify the surface of carboxylic acid functional PEDOT films. Peptide sequences have been isolated from laminin, a major cell adhesive glycoprotein of the basement membrane matrix, which promote cell adhesion, spreading and migration and enhanced neurite extension.[190-192] We utilize EDOTacid as the functional monomer in this contribution for generating conducting polymer films for surface modification with the peptide CDPGYIGSR. The nonapeptide CDPGYIGSR from the β1 chain of laminin has been proven to promote cell attachment, receptor binding, migration, and enhanced neurite extension.[193-195] The COOH functional PEDOT films are modified with the peptide CDPGYIGSR or a PEGylated CDPGYIGSR through the N-terminus of the peptide. The key to ensure efficient peptide grafting is to present the peptide sequence away from the surface so as to make it available for cellular interaction.[196] This is usually made possible by introducing a spacer or a linker molecule between the polymer surface and the peptide molecule. Spacer molecules also tend to decrease the crowding effect and can reduce the steric hindrance and thus providing multiple binding sites.[17]

Previous reports dealing with the influence of a spacer molecule on cell interactions reported the minimum spacer arm length to be 1 nm to 3.5 nm long.[196-198] A spacer molecule such as PEG can enable the immobilized peptide to move freely and flexibly in the biological environment which is critical for efficient cell spreading.[199] Based on previous literature, peptides with a short PEG spacer of 3 ethylene glycol units (1 nm long) and a long PEG spacer of 10 ethylene glycol units (3 nm long) are utilized in this contribution to investigate the effect of a spacer molecule on cell attachment and differentiation on such rough conducting polymer films. The peptide functional films were characterized using XPS to confirm the successful incorporation of the laminin based peptide. Electrical characterization was performed to determine the effect of covalently conjugating a biomolecule on the charge storage capacity and the impedance of the films. Finally, the bioactivity of the peptide was assessed using neural-like PC-12 cell line.

## 4.2 Experimental Procedures

### 4.2.1 Electrochemical Deposition of PEDOTacid Films

Electropolymerization was carried out in a two-electrode cell using an AutoLab potentiostat/ galvanostat (Utrecht, The Netherlands) with a platinum wire counter electrode. The PEDOTacid copolymer films were electrochemically polymerized from a 0.01 M monomer solution in propylene carbonate with 0.1 M lithium perchlorate as the counter ion. The mole fraction of the EDOTacid and EDOT in the monomer feed solution were maintained at 0.75 and 0.25 respectively and the subsequent films are denoted as EA75. All films reported here were polymerized

galvanostatically with a current density of ~0.2 mA/cm$^2$ for 5 minutes and were rinsed with DI water after polymerization.

### 4.2.2 Peptide Synthesis

All the peptides described in this report (Table 4.1) were synthesized via Fmoc-based methods on a Rink amide resin (AAPPTec, Louisville, KY) using an automated solid-phase peptide synthesizer (PS3, Protein Technologies Inc., Tuscon, AZ). The amino acid residues were activated with HBTU and 0.4 M methylmorpholine in DMF as the activator solvent. Deprotection was conducted using 20% (v/v) piperidine in DMF for approximately 30 minutes. Coupling reactions were carried out for 1 hour. For the peptides with PEGylated N-terminus, the N-terminal amine was PEGylated using a Fmoc-NH-PEG$_3$-COOH or a Fmoc-NH-PEG$_{10}$-COOH for extended coupling times of 10 hours with HBTU as the coupling reagent. The Fmoc group was then removed using a 20% (v/v) piperidine in DMF solution to yield a molecule with a free amine on the N-terminus. Cleavage of the all the described peptides from the resin was performed in a mixture of 94% trifluoroacetic acid (TFA), 1% triisopropyl silane (TIPS), 2.5% ethanedithiol and 2.5% water for 3-4 hours. TFA was evaporated and the peptide was precipitated in cold ethyl ether. The water soluble peptides were extracted with water and lyophilized. Purification of peptides was conducted via reverse-phase high performance liquid chromatography (HPLC) (Waters, MA) using a Symmetry C18 semi-preparative scale column. The gradient applied was from 0-100% of solvent B over 40 minutes (Solvent A = 0.1% TFA in 18.2 MΩ water, solvent B = 0.1% TFA in ACN). The identity of each peptide was confirmed via electrospray ionization mass spectrometry (ESI-MS). (**CDPGYIGSR)**

*m/z* 966.6, calc 966.09 (**$PEG_3$-CDPGYIGSR**) *m/z* 1169.6, calc. 1169.59; (**$PEG_{10}$-CDPGYIGSR**) *m/z* 1477.8, calc. 1477.89

### 4.2.3 Modification of PEDOTacid Films with YIGSR Based Peptides

PEDOTacid copolymer films (EA75) were coupled with CDPGYIGSR, or $PEG_3$-CDPGYIGSR or $PEG_{10}$-CDPGYIGSR. The COOH groups on the surface of the films were activated using 3.5 mg of HATU (AAPPTec, Louisville, KY) and 4.5 µl of N,N-diisopropylethylamine (DIPEA, Acros Organics) in 1 ml DMF for one hour. After activation the films were treated with the 3 µmoles of the desired peptide in 1 ml of 1:1 DMF and DMSO with 1 µl DIPEA for 16–20 h. To remove unbound peptide and unreacted HATU, the films were thoroughly washed with 0.05% Tween 20 in PBS, phosphate buffered saline (PBS, Fisher BioReagents) and finally deionized water. Each washing step was performed multiple times to ensure maximum removal of unbound peptide.

### 4.2.4 Characterization of Peptide Modified Films

XPS: Chemical analysis of the CP films was conducted using X-ray photoelectron spectroscopy (XPS). (Omicron EA125 X-ray photoelectron spectroscope (Taunusstein, Germany)). A non-monochromatic aluminum (1486.5 eV) X-ray source was employed. Corrections were made by using adventitious carbon peak located at 284.6 eV in C 1 s region. 50 eV and 25 eV pass energies were used for survey scans and high resolution scans, respectively.

Quantification of COOH groups on the surface: In order to quantify the concentration of carboxylic acid groups on the surface of the copolymer films before

and after peptide coupling, a toluidene blue O (TBO) assay was performed. To construct calibration curves, TBO solutions at various concentrations were prepared by dissolving dry TBO powder in 50% acetic acid solutions, and their light absorbance at 630 nm was measured using an Agilent 8453 spectrophotometer (Agilent Technologies Inc, Santa Clara, CA). For the evaluation of the surface charge concentration of carboxylic acid groups on copolymer films, the films were soaked in an alkaline solution (0.1 mM NaOH) of TBO (0.5 mM) for 2.5 hours. After the TBO adsorption, the samples were rinsed with 0.1 mM NaOH to ensure removal of any non-complexed dye. Samples were then soaked in 2 mL of 50% acetic acid solution for 4 hours in order to desorb the complexed dye; a separate set of experiments indicated that this length of time was sufficient for complete desorption. The absorbance of the residual TBO solution was measured at 632 nm. The recorded spectroscopic data was converted into surface concentration (nmoles/mm$^2$) using the calibration curve. Three samples of each film were used to perform the assay.

Electrical properties: To analyze the electrical activity of the CP films before and after peptide coupling, cyclic voltammetry (CV) and electrochemical impedance spectroscopy (EIS) were performed using the Autolab potentiostat/ galvanostat (Utrecht, The Netherlands) described above with a platinum counter electrode, a saturated calomel reference electrode, and phosphate-buffered saline electrolyte (PBS). For the CV measurements, cycling was performed between +0.8V and -0.6V with a scan rate of 0.12 V/s. The first stable curve was considered as cycle 1 and used to determine the electroactivity of the film. The charge storage capacity (CSC) was calculated by taking the integral, over time, of the area under the oxidation-reduction

curve. For impedance measurements, an AC sinusoidal input of 5mV in amplitude was used as the input signal with the DC potential set to 0. The magnitude and phase angle for the impedance measurements were determined over six discrete frequencies over the range of 1-$10^5$ Hz.

Scanning electron microscopy was conducted using a JEOL JSM-7400F field emission scanning electron microscope (Tokyo, Japan) at a 3-KV operating voltage to determine the effect of peptide modification on film surface morphology. All the films were sputtered with a thin layer of gold-palladium to provide a more conductive surface. Images were captures at 5,000 X mag.

### 4.2.5 In vitro Cell Culture

PC12 cell cultures were used to determine the bioactivity of the laminin peptides present on the surface of the PEDOTacid copolymer films. The samples were sterilized by soaking the polymer coated electrodes in 70% ethanol for 8-10 hours. The samples were then rinsed with sterile DPBS solution prior to experiments. The bioactivity of CDPGYIGSR, $PEG_3$-CDPGYIGSR and $PEG_{10}$-CDPGYIGSR peptides was assessed through comparison to EA75 and laminin coated EA75 which acted like negative and positive controls respectively. Along with these controls, one set of EA75 with physically adsorbed and chemically conjugate peptides were coated with laminin protein to determine the combined effect of the peptide and protein on the cell attachment and differentiation. The polymer films were coated with 5 µg/ml solution of whole laminin sourced from Engelbreth murine sarcoma (Sigma-Aldrich) in sterile DPBS for 10-12 hours at 37 °C. Fluorescent PC12 cells (GFP-PC12) were cultured in RPMI supplemented with 10% horse serum, 5% fetal bovine serum and 1%

antibiotics. All cells were cultured under sterile conditions in a humidified 5% $CO_2$ atmosphere at 37 °C. The GFP-PC12 cells were plated on all the polymer films at 30,000 cells/cm$^2$ and cultured for 24 hours in low serum media supplemented with 150 ng/ml NGF. After 24 hours of seeding the media was replaced to add fresh media (low serum) supplemented with 150 ng/ml of NGF. The cells were then incubated for a total of 48 hours before imaging.

## 4.3 Results and Discussion

### 4.3.1 Surface Modification of PEDOTacid Films with YIGSR Based Peptides

Copolymer films of EDOTacid and EDOT were deposited galvanostatically with a monomer feed ratio of 0.75 and denoted as EA75. All the peptides described in this work were synthesized via standard Fmoc-based solid phase methods. EA75 films were modified with peptides CDPGYIGSR (YIGSR), $PEG_3$-CDPGYIGSR ($PEG_3$-YIGSR), and $PEG_{10}$-CDPGYIGSR ($PEG_{10}$-YIGSR). The PEDOTacid films were modified with the desired peptide by either physical adsorption (PA) or chemical conjugation (CC). The peptide was coupled to the carboxylic acid functional EA75 films through the N-terminus of the peptide using HATU coupling chemistry. Table 4.1 provides the list of the polymers modified with the peptides with their corresponding denotations. The reaction schematic for surface modification of PEDOTacid films with a representative peptide is presented in Figure 4.1.

**Table** 4.1 Polymer films modified with YIGSR-based peptides.

| **Polymer films** | **Name** |
|---|---|
| EA75 | EA75 |
| | |
| EA75+CDPGYIGSR | PA YIGSR |
| EA75+$PEG_3$-CDPGYIGSR | PA $PEG_3$-YIGSR |
| EA75+$PEG_{10}$-CDPGYIGSR | PA $PEG_{10}$-YIGSR |
| | |
| EA75+hatu+CDPGYIGSR | CC YIGSR |
| EA75+hatu+$PEG_3$-CDPGYIGSR | CC $PEG_3$-YIGSR |
| EA75+hatu+$PEG_{10}$-CDPGYIGSR | CC $PEG_{10}$-YIGSR |

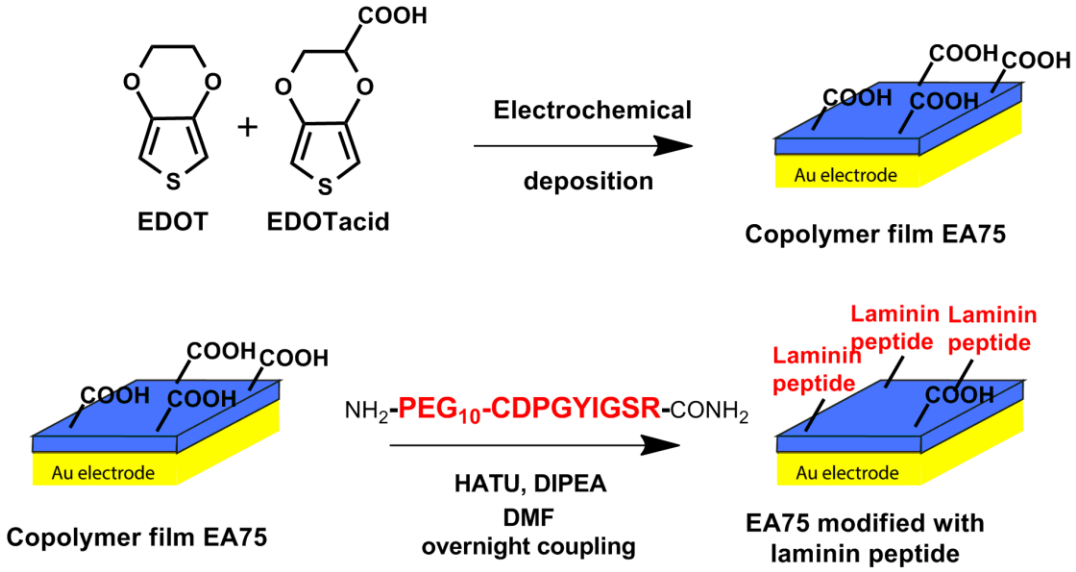


**Figure** 4.1 Schematic of surface modification of COOH functionalized PEDOT films with YIGSR -based peptides.

### 4.3.2 Chemical Analysis of Peptide Modified Films

#### 4.3.2.1 XPS Analysis

XPS was performed on the films before and after peptide modification to determine the chemical composition of the films with and without YIGSR based peptides. The XPS analysis on all the different films modified with YIGSR based peptides confirmed the presence of the peptides on the polymer film surfaces.

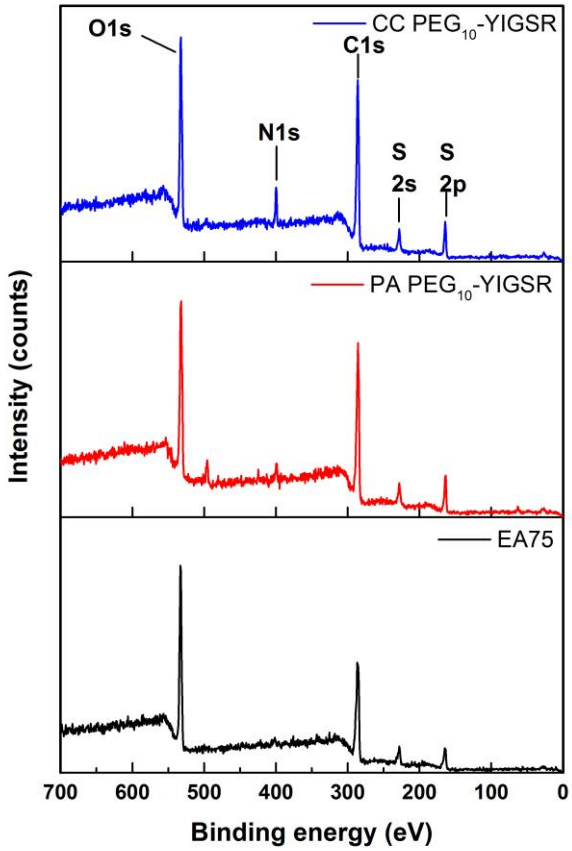


**Figure** 4.2 XPS spectra of chemically modified carboxylic acid PEDOT films with YIGSR based peptide compared to PEDOTacid films and physically adsorbed peptide on PEDOTacid films.

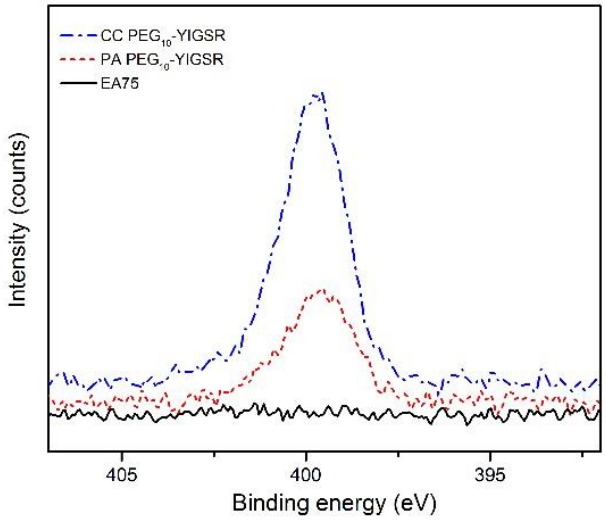


**Figure** 4.3 N 1s spectra comparison for films with and without peptides.

C 1s and O 1s peaks observed at 285.4 eV and 532.2 eV respectively for all the films with and without peptide were deconvoluted however the resulting spectra were not significantly different to draw any conclusions. Figure 4.2 displays an example XPS spectra for PEDOTacid films modified with one of the peptides used in this study, $PEG_{10}$-CDPGYIGSR ($PEG_{10}$-YIGSR) and Figure 4.3 displays the N 1s spectra for the polymer before and after peptide modification. The XPS scans for the PEDOTacid films with physically adsorbed and chemically conjugated peptide demonstrated an N 1s peak at 399.3 eV which was otherwise absent in the accompanying EA75 films. The films with physically adsorbed peptide (PA $PEG_{10}$-YIGSR) showed a weak nitrogen signal even after extensive washing with Tween 20 solution. This suggests there is non-specific binding of the peptides to these PEDOT. However the nitrogen to sulfur ratio (N/S) as presented in Table 4.2 (which shows the

percentage contribution of all the major elements (oxygen, carbon, nitrogen and sulfur)) for the films with chemically conjugated $PEG_{10}$-YIGSR (1.53) is higher than that for films with physically adsorbed $PEG_{10}$-YICGSR (1.36). This observation of higher N/S for chemically conjugated peptides when compared to their physically adsorbed counterparts was valid for the other two peptides (YIGSR and $PEG_3$-YIGSR) used to modify the films too. Based on the higher N/S ratio and also the percent contribution of all the major elements for films treated with the coupling agent hatu alone the data suggest successful covalent modification of the films.

**Table** 4.2 Elemental analysis of PEDOTacid films modified with YIGSR based peptides (*n*=3).

| **POLYMERS** | **ELEMENTAL COMPOSITION** | | | | **N/S ratio** |
|---|---|---|---|---|---|
| | Carbon (%) | Oxygen (%) | Nitrogen (%) | Sulfur (%) | |
| EA75 | 58.5 | 33.2 | 0 | 8.3 | 0 |
| PA YIGSR | 62.4 | 27.1 | 4.0 | 6.5 | 0.61 |
| PA $PEG_3$-YIGSR | 58.0 | 29.3 | 4.5 | 8.2 | 0.55 |
| PA $PEG_{10}$-YIGSR | 59.6 | 28.4 | 5.4 | 6.6 | 0.90 |
| CC YIGSR | 61.3 | 25.0 | 7.5 | 6.2 | 1.21 |
| CC $PEG_3$-YIGSR | 61.9 | 23.9 | 8.2 | 6.0 | 1.36 |
| CC $PEG_{10}$-YIGSR | 62.9 | 23.7 | 8.1 | 5.3 | 1.53 |
| EA75+hatu | 62 | 27.4 | 3.6 | 7 | 0.51 |

#### 4.3.2.2 TBO Assay

A calorimetric toluidine blue O (TBO) assay was performed on the chemically modified PEDOTacid copolymer films to determine the surface concentration of the peptide (physically adsorbed or chemically conjugated) on the surface of the films. TBO is a salt consisting of an aromatic cation and an associated chloride anion that electrostatically binds to negatively charged species and can easily be detected by light absorbance at 632 nm. The surface concentration of the negatively charged species can thus be determined using the absorbance of the desorbed dye in solution and these data are shown in Figure 4.4.

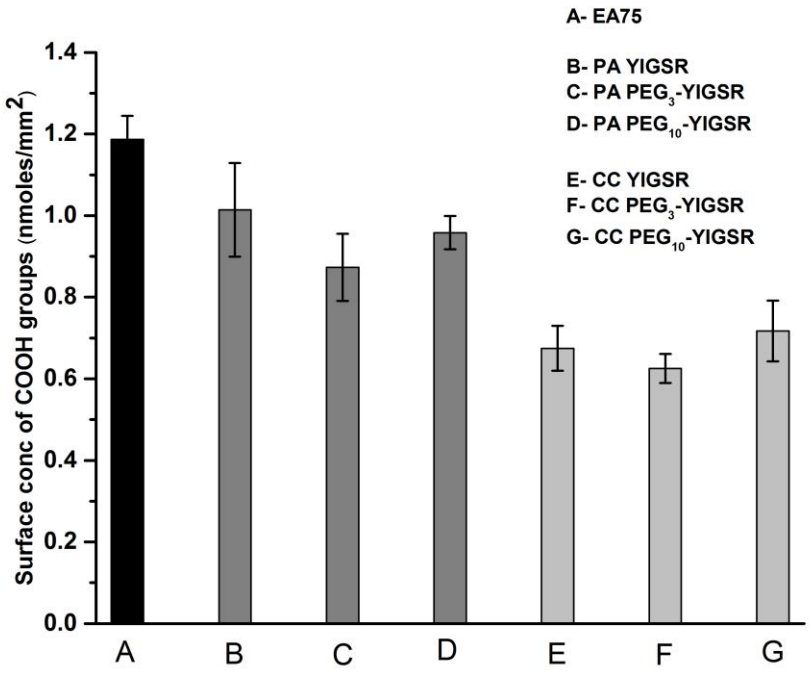


**Figure** 4.4 Surface concentration of carboxylic acid groups on the surface of the PEDOTacid films after peptide modification. (*n*=3)

The carboxylic acid functionalized conducting polymer films have a surface concentration of 1.19±0.06 nmoles/mm$^2$. Post peptide modification the number of carboxylic acid groups available to bind to the TBO dye should theoretically decrease and the difference between the carboxylic acid concentration before and after modification will thus correspond to the amount of peptide on the surface of the films. Similar trends were observed for the TBO assay performed on the films. The carboxylic acid concentration and the corresponding peptide concentration for films with the different YIGSR based peptides physically adsorbed or chemically conjugated is presented in the Table 4.3. The carboxylic acid group concentration for the films with physically adsorbed peptides is ~0.95 nmoles/mm$^2$ and the corresponding peptide concentration is ~0.24 nmoles/mm$^2$. The carboxylic acid group concentration for the films with chemically conjugated peptides is ~0.65 nmoles/mm$^2$ and thus the corresponding peptide concentration is ~0.54 nmoles/ mm$^2$. This clearly demonstrates increased presence of the peptide on the films when chemically conjugated using hatu. This is in agreement with the XPS analysis on the films which reveals presence of peptide on the films when physically adsorbed or chemically conjugated, however the % nitrogen contribution (from XPS analysis, Table 4.2) clearly suggests higher amounts of peptide present when it is chemically conjugated to the carboxylic acid groups on the surface. Previously published values for different peptide and protein concentration on bioactive films and surfaces is in the range of $10^{-6}$ to 100 pmol/cm$^2$.[200-203] Since the apparent peptide concentration is the difference between the carboxylic acid groups on the surface before and after surface modification the peptide concentrations reported in this contribution are higher than that reported in literature possibly because of lack of accessibility of the unreacted

carboxylic acid groups on the surface of the films which may be shielded by the large peptide molecules on the surface. However, this is consistent with all the different peptides tested in this study and the observation of fewer carboxylic acid groups detected for chemically modified polymers compared to the physically adsorbed films is as expected.

**Table** 4.3 Carboxylic acid groups on the surface of PEDOTacid films before and after peptide modification. (*n*=3)

| **Sample** | **Carboxylic acid group concentration (nmoles/mm2)** | **Apparent Peptide concentration (nmoles/mm2)** |
|---|---|---|
| EA75 | 1.19±0.06 | - |
| | | |
| PA YIGSR | 1.01±0.12 | 0.18 |
| PA $PEG_3$- YIGSR | 0.87±0.08 | 0.32 |
| PA $PEG_{10}$- YIGSR | 0.96±0.04 | 0.23 |
| | | |
| CC YIGSR | 0.67±0.05 | 0.52 |
| CC $PEG_3$- YIGSR | 0.62±0.03 | 0.57 |
| CC $PEG_{10}$- YIGSR | 0.72±0.07 | 0.47 |

### 4.3.3 Electrical Properties of Peptide Modified Films

The electrochemical properties of the PEDOTacid copolymer films before and after modification were determined by performing cyclic voltammetry (CV) and electrical impedance spectroscopy (EIS). The electrode sites were swept from +0.8 V to -0.6 V at a scan rate of 0.12 V/s versus Ag/AgCl reference electrode. Figure 4.5 displays the CV curved for EA75, PA $PEG_{10}$-YIGSR and CC $PEG_{10}$-YIGSR. Oxidation and reduction peaks for EA75 polymer films were observed at -0.3 V and -0.2 V respectively. The CV curve for all the films with physically adsorbed peptides

remained identical to those of EA75 films. However, for all the films chemically modified with YIGSR based peptides, irrespective of the peptide chosen, the oxidation peak shifted slightly to ~0.05V with the reduction peak maintaining its value.

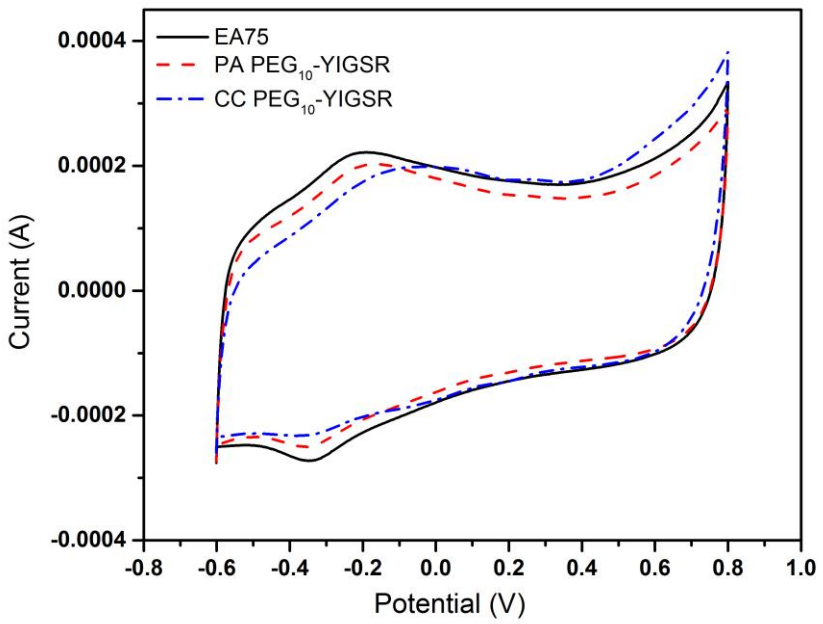


**Figure** 4.5 CV curves for 1st stable cycle for PEDOTacid films before and after peptide modification.

The CSC values for the films before and after peptide modification are provided in Table 4.4. The CSC for EA75 films was 3.85 mC/cm$^2$. As shown in the table the CSC for the peptide modified films are only somewhat lower than that of the unmodified films. In spite of a slight change in the characteristic of the CV curve, the charge storage capacities (calculated by integrating the current versus time within the

cycled region) for all the films with the peptides, either physically adsorbed or chemically conjugated, are comparable to that of EA75. This demonstrates that the modification of the conducting polymer film does not have any significant negative impact on the redox capabilities of these PEDOT based films. The charge storage capacity of a conducting polymer depends on the number of mobile charges moving in and out of the film which are determined by the doping level or the interfacial area between the conducting polymer and the electrolyte in the solution. The presence of the chemically or physically bound peptide molecules which could potentially reduce the interfacial area between the conducting polymer film and the electrolyte leading to poor CSC do not seem to be hampering the films' redox capabilities. The small perchlorate anion used as the dopant for these films is easily able to migrate in and out of the films, without and with the peptides, when they are oxidized and reduced preserving their redox behavior. Large biomolecules used as dopants tend to disrupt the electroactivity of conducting polymer films when incorporated via the entrapment method this compromising their use as a conducting layer.[68, 70, 72, 189] This can be overcome by chemically modifying the film, as is displayed here.

**Table** 4.4 Charge storage capacities for EA75 films before and after peptide modification (*n*=3).

| **Sample** | **Charge storage capacity ($mC/cm^2$)** |
|---|---|
| EA75 | 3.85 |
| PA YIGSR | 3.78 |
| PA $PEG_3$- YIGSR | 3.25 |
| PA $PEG_{10}$- YIGSR | 3.48 |
| CC YIGSR | 3.64 |
| CC $PEG_3$- YIGSR | 3.62 |
| CC $PEG_{10}$- YIGSR | 3.48 |

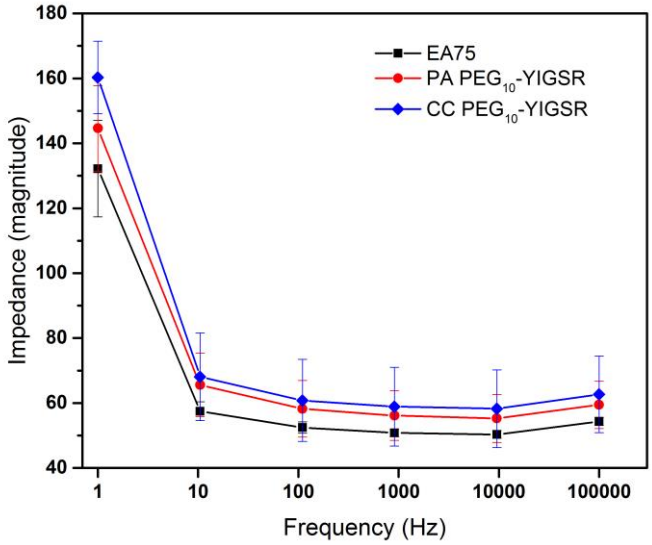


**Figure** 4.6 Impedance magnitude of PEDOTacid films before and after peptide modification. (*n*=3) Error bars are marked with one standard deviation.

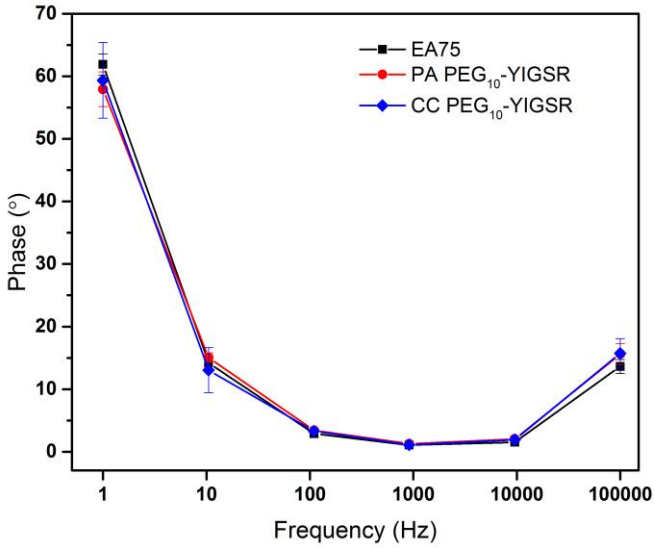


**Figure** 4.7 Phase lag of PEDOTacid films before and after peptide modification. (*n*=3) Error bars are marked with one standard deviation.

Impedance spectroscopy was used to determine the effect of peptide modification on the charge transport properties of the PEDOTacid copolymer films. Figure 4.6 and Figure 4.7 display the magnitude and phase of the impedance. The magnitude of impedance for all the different films with physically adsorbed or chemically conjugated peptide was approximately 60 Ω at 1000 Hz (the frequency used for neural recording and stimulation), with all the polymers reducing the impedance magnitude value by approximately 75% (impedance of the Au electrode before coating with the conducting polymer films was 250 Ω at 1000 Hz, Figure A-3) This value was not significantly different from that of PEDOTacid films thus confirming the lack of impact of the biomolecule on the electrical properties of the films. Similar values for PEDOT films deposited on metal electrodes such as gold and platinum have been reported previously.[72, 204] The phase lag was also reduced across all the different peptide modified PEDOTacid films in the biological focal regime when compared to the bare gold electrode. Impedance spectroscopy results thus demonstrated that the films with peptide performed similarly to PEDOTacid by reducing the magnitude of impedance and phase lag when compared to the bare gold electrode.

### 4.3.4 Morphology of Peptide Modified Films

Scanning electron microscopy was conducted to determine the morphological changes to the polymer after peptide modification. Figure 4.8 illustrates the representative SEM of the PEDOTacid film before and after peptide modification (PA or CC) with the peptide $PEG_{10}$-YIGSR. As demonstrated by Figure 4.8, the morphological features of the films remain unaltered after surface modification; be it physical adsorption or chemical conjugation. All the films were rough and granular in

nature with small nanofibers (50-100 nm). These features are identical to the ones as observed for PEDOT-PEDOTacid films deposited on Au/Pd electrodes (Figure 3.11). The morphological features for conducting polymer films with biological molecules co-deposited with the polymer tend to get disrupted subsequently compromising the electrical properties of the films. This has been observed for PEDOT films co-deposited with growth factors,[70] peptides[72] and also proteins.[189] By using chemical conjugation as the means of surface modification the changes in the morphology can be avoided. The unaltered surface morphology of the peptide modified PEDOTacid films is in agreement with the CV curves (Figure 4.5) and impedance values (Figure 4.6) for the different films which also remain unaffected by surface modification.

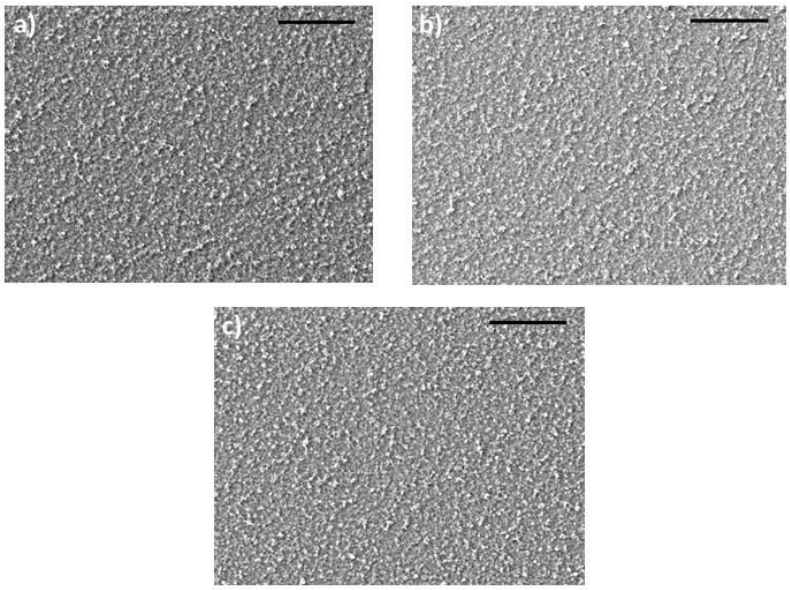


**Figure** 4.8 Morphology of PEDOTacid films before and after surface modification. a) EA75, b) PA $PEG_{10}$-YIGSR, c) CC $PEG_{10}$-YIGSR. (the scale bar represents 5 µm)

### 4.3.5 In vitro Cell Studies

GFP modified PC12 cells were used to perform in vitro cell studies on YIGSR based peptide-modified PEDOTacid copolymer films. 30,000 cells/cm$^2$ were seeded on peptide modified films and dosed with NGF supplemented media. The bioactivity of the peptides YIGSR, $PEG_3$-YIGSR and $PEG_{10}$-YIGSR was assessed through comparison to negative and positive controls EA75 and laminin-coated EA75 polymer films respectively. Chemically conjugating the peptides to the PEDOTacid films led to increased cell attachment (significant attachment was observed for $PEG_{10}$-YIGSR, Appendix A.4 - Figure A-4, and Figure A-5) however neither of the peptide modified (physically adsorbed or chemically conjugate) led to appreciable neurite extension (Figure A-4). The observation that the CDPGYIGSR sequence promotes cell attachment but not significant neurite extension is comparable to reports by Matsuzawa et al.[205] and Asplund et al.[206]

Since the peptide-modified films did not lead to significant neurite extensions, films with physically adsorbed and chemically conjugate peptides were coated with whole laminin protein to determine the effect of the PEG spacer molecules (1 nm and 3 nm long) on the neurite outgrowth and test the synergistic effect of the peptide and the whole protein on the PC12 cell differentiation. The peptide modified films that did not show neurite outgrowth when cultured with PC12 cells without whole laminin protein demonstrated successful neurite outgrowth when coated with whole laminin protein. Sample images of laminin-coated peptide modified (physically adsorbed and chemically conjugated) PEDOTacid films with YIGSR, $PEG_3$-YIGSR, and $PEG_{10}$-YIGSR are presented in Figure 4.9. Figure 4.10, Figure 4.11 and Figure 4.12 illustrate the number of cells attached, percent cells expressing neurites, and mean neurite length respectively.

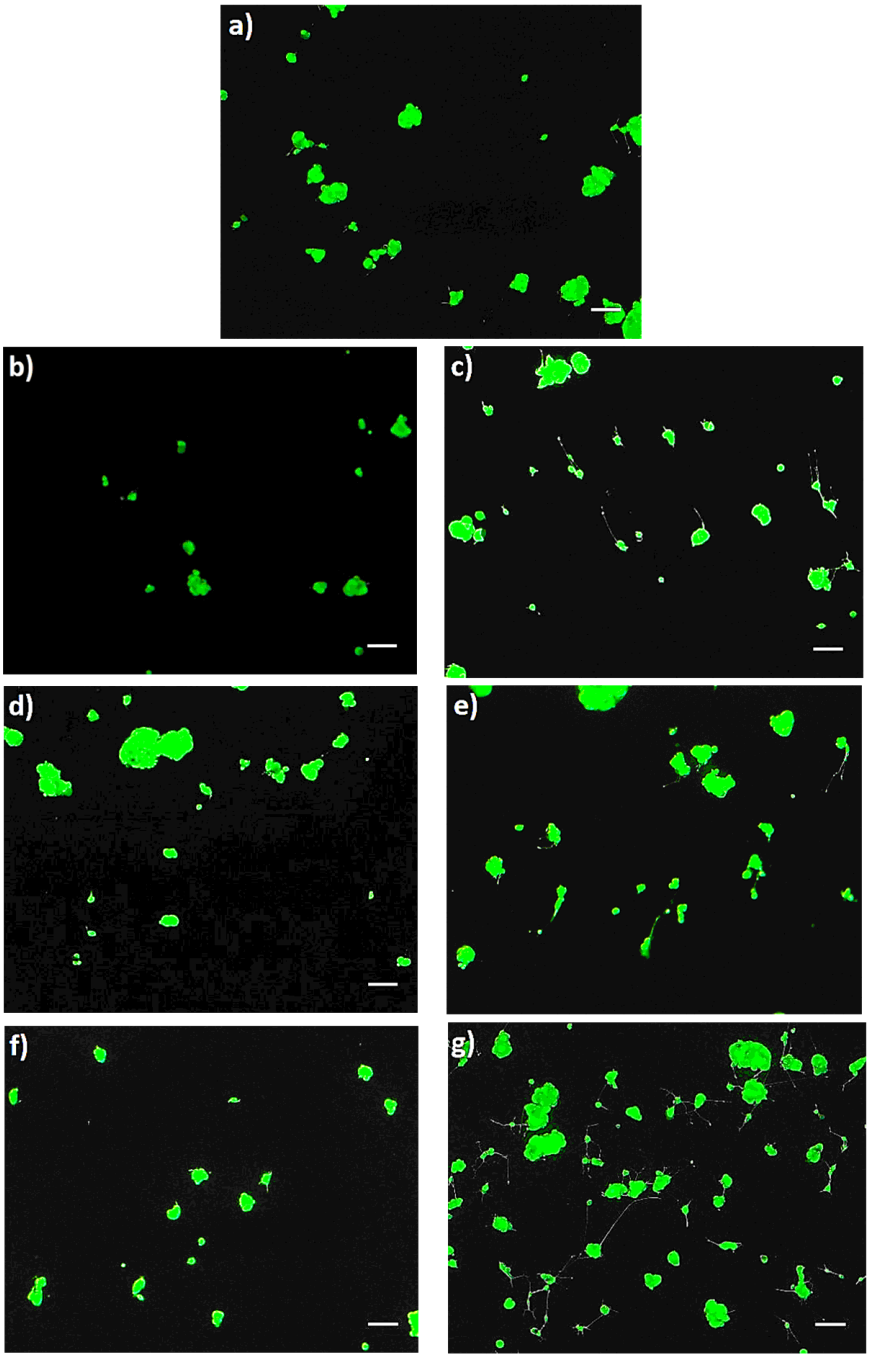


**Figure** 4.9 Sample images of PC12 cell attachment on laminin-coated peptide modified PEDOTacid polymer films at 72 h post-plating a) EA75, b) PA YIGSR, c) CC YIGSR, d) PA $PEG_3$-YIGSR, e) CC $PEG_3$-YIGSR, f) PA $PEG_{10}$-YIGSR, and g) CC $PEG_{10}$-YIGSR (the scale bar represents 100 µm).

The number of cells attached on the surface, the percentage of cells that express neurites (11.5%) and the resulting mean neurite length (90 µm) of laminin-coated CC $PEG_{10}$-YIGSR significantly increased ($p \leq 0.05$) when compared to all the other laminin-coated peptide modified polymer films. When considering all the peptides, it appears that this trend of laminin protein increasing the inherent property of the CDPGYIGSR ligand is valid for all the three peptides studied. This observation is similar to what Green et al. observed for PEDOT/CDPGYIGSR and PEDOT/DEDEDYFQRYLI coatings that demonstrated longer neurite outgrowth for laminin-coated polymer films compared to PEDOT/peptide coatings without laminin protein coating.[72] However this result is the most prominent for $PEG_{10}$-YIGSR suggesting the 3 nm spacer molecule is having a positive effect on the cell attachment.

The whole laminin protein adsorption on the peptide-modified films was confirmed via XPS which demonstrated increased percentage of nitrogen on the surface compared to the peptide alone modified films (Figure A-1). Coating the surface of the films with whole laminin protein is clearly amplifying the ability of $PEG_{10}$-YIGSR peptide to improve cell binding to the surface and led to increased percentage expression and also resulted in longer neurite outgrowth. The whole laminin protein consists of other active peptide sequences such as RGD (proven to be a cell adhesive sequence), IKVAV (shown to promote cell adhesion, spreading and migration), and RNIAEIIKDI (shown to promote neurite outgrowth). The data suggest that the YIGSR ligand in conjunction with the active sequences from the whole laminin protein make the surface conducive for cell attachment and neurite outgrowth. It is also possible that other biomolecules such as growth factors and proteins from the media are better adsorbed when the whole laminin protein and peptide are present

together. Along with the presence of the cell adhesive and neurite promoting sequences, the laminin coating increased the hydrophobicity of the films (contact angle for laminin coated PEDOTacid peptide modified films was measured to be ~50 °). This may also have had an impact on the cell adhesion on the surface. Since cell differentiation is directly dependent on how the cells attach to the substrate the presence of the protein and increase in hydrophobic character has an impact on how many cells express neurites and also how long the neurites grow.

For peptides that are chemically conjugated to the surface of the films, the attachment, % cells expressing neurites and neurite length are greater than those films with peptides physically adsorbed to the surface. The percentage of cells expressing neurite was calculated by the following formula

% cells expressing neurites = Number of cells OR clusters of cells that extended neurites/ total number of cells

Only cells bearing at least one neurite with a length more than 1.5 times the diameter of the cell body were counted for calculating the percentage cells expressing neurites. The laminin-coated CC $PEG_{10}$-YIGSR (3 nm PEG spacer) films result in around 11.5% neurite expression whereas the peptides with no PEG spacer and 1 nm short PEG spacer result in around 5% neurite expression. Minimum length of a spacer molecule to influence cell attachment has been shown to be 1.1 nm-3.5 nm. Based on the results demonstrated in Figure 4.10, Figure 4.11 and, Figure 4.12 it is clear that at least a 3 nm spacer molecule is necessary for cell attachment and differentiation for PEDOT based conducting polymer films. Laminin-coated YIGSR and $PEG_3$-YIGSR do not have an apparent difference in the number of cells attached to the surface or the percentage of the cells that express neurites. Similar to increased percentage of cells

expressing neurites for laminin-coated CC $PEG_{10}$-YIGSR films, the mean neurite length for laminin-coated CC $PEG_{10}$-YIGSR films also is significantly higher than all the other films. The mean neurite length was measured to be around 90 µm for laminin coated CC $PEG_{10}$-YIGSR films. These results indicate that the peptide is indeed accessible to the cells and is bioactive which results in cell attachment however the cells do not differentiate into neuron like cells unless the peptide and protein is present in unison.

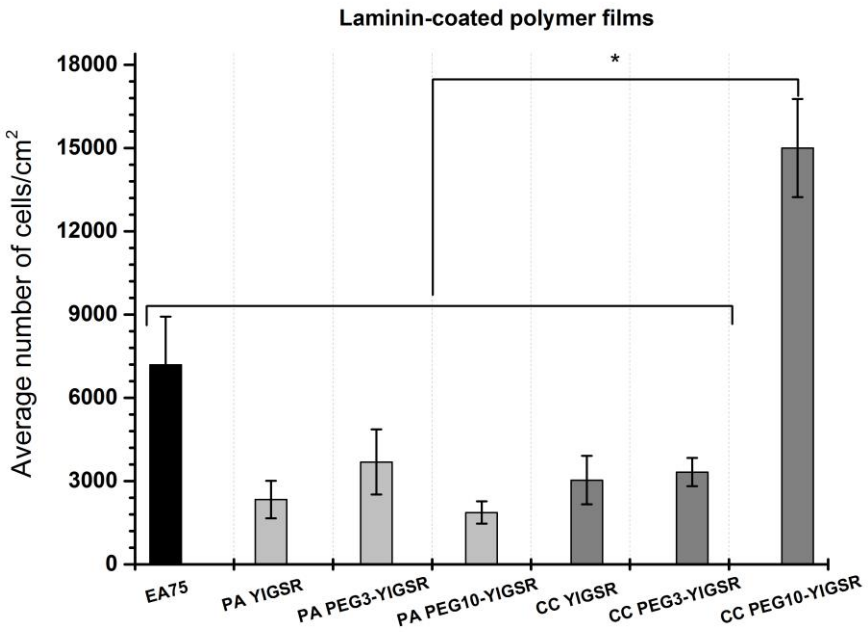


**Figure** 4.10 Average number of PC12 cells/cm$^2$ on the surface of the laminin-coated peptide modified PEDOTacid films. ($n$=3)

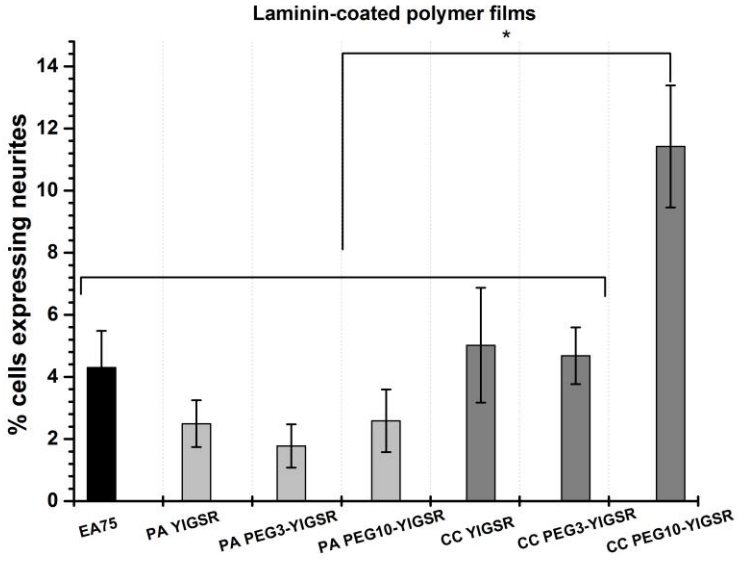


**Figure** 4.11 Percentage cells expressing neurites on laminin-coated peptide modified PEDOTacid films. (*n*=3)

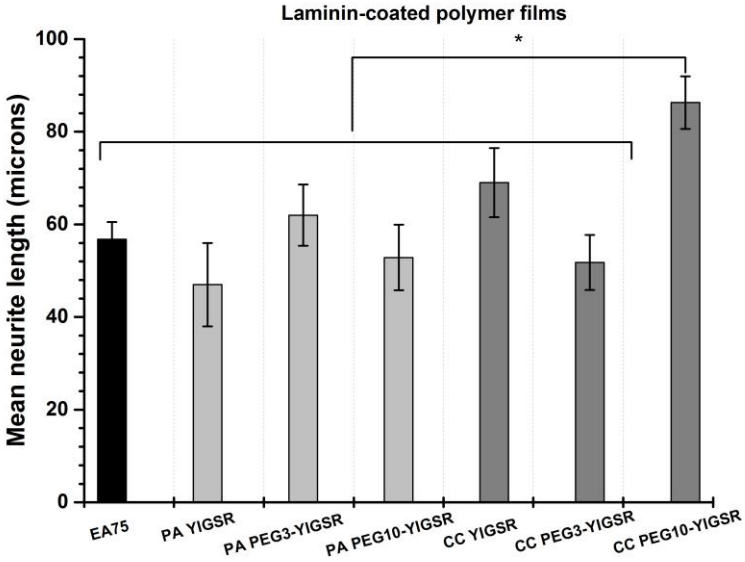


**Figure** 4.12 Mean neurite length on laminin-coated peptide modified PEDOTacid films. (*n*=3)

The goal of this study was to develop a platform for surface modification of carboxylic acid functional conducting polymer films. Amongst the different peptides probed in this study, the aim was to determine the best peptide and also the optimal conditions that would elicit appreciable cell attachment and differentiation in GFP modified PC12 cells. The difference in the bioactivity of the three different peptides and their method of immobilization (physical adsorption or chemical conjugation) was highlighted by coating the surface of the films with whole laminin protein. Amongst all the peptides investigated here chemically conjugated $PEG_{10}$-CDPGYIGSR proved to be the best. Similar to this, other laminin derived peptides (IKVAV, RNIAEIIKDI) or other relevant peptides could be studied in this format. The ultimate objective is to identify a peptide that will result in substantial cell attachment and neurite differentiaion without the aid of coating the surface with a protein. It is important to develop just peptide-modified films given the need to maintain the electrical conductivity of the bio-electrodes.

## 4.4 Conclusions

Carboxylic acid functionalized PEDOTacid films were successfully modified with YIGSR based peptides by covalently immobilizing them on the surface of the conducting polymer films. Peptides without and with spacer molecules were utilized in this study to investigate the bioactivity of the CDPGYIGSR ligand and the impact of a linker molecule on cell attachment and differentiation of a GFP modified PC12 cell line. Peptides were incorporated on PEDOCTacid films via chemical conjugation and physical adsorption and their presence on the surface of the films was confirmed via XPS and a colorimetric toluidine blue O assay. The peptide modified films had comparable electrical properties to the unmodified films indicating that chemically

modifying the films did not compromise the electrochemical characteristics of the films. The PEDOTacid films modified with the peptide $PEG_{10}$-CDPGYIGSR (3 nm spacer molecule) resulted in the highest cell attachment when compared to the peptides linked to the surface without a spacer molecule (CDPGYIGSR) and with a 1 nm long spacer molecule ($PEG_3$-CDPGYIGSR). The peptide modified films were coated with whole laminin protein to test the impact of the spacer molecule on percent neurite expression and neurite outgrowth. Again, the films with chemically conjugated $PEG_{10}$-CDPGYIGSR peptide resulted in the highest neurite expression (11.5%) and the longest mean neurite length (90 µm). These studies demonstrate the use of a carboxylic acid functionality to tether biomolecules on surface of conducting polymer films without compromising their electrochemical properties. From the in vitro cell studies it is apparent that a minimum distance of ~3 nm is required for cell attachment and differentiation for conducting polymer films from the poly(3,4-ethylenedioxythiophene) group.

# Chapter 5

# BIOFUNCTIONALIZATION OF ProDOT FILMS WITH RGD PEPTIDES VIA THIOL-ENE CLICK CHEMISTRY

## 5.1 Introduction

Since their inception in 2001 by Sharpless and coworkers, click reactions have gained a lot of popularity owing to multiple attributes such as being simple, highly efficient, selective, bioorthogonal, result in limited or no byproduct, and can be conveniently performed in biologically benign conditions (aqueous solution, ambient temperature, and near physiological pH).[207] As a result these reactions are being executed as tools to build a variety of products by biologists, chemists, and engineers for a variety of applications including labeling of biomolecules and imaging, protein engineering, drug development, cell surface modifications.[208] Reactions that fall under this envelope of "click reactions" include the Cu(I)-catalyzed azide-alkyne cycloaddition, thiol-ene/ yne reaction, Michael addition, and Diels Alder reaction.

Click reactions are specifically attractive for building materials for biomedical applications as these reactions can be easily conducted in a complex biological milieu at physiological conditions. Robust and biocompatible 3D material scaffolds such as hydrogels have been fabricated successfully via click reactions. Anseth and coworkers have published extensively on poly (ethylene glycol) hydrogels prepared *via* a radically mediated thiol-norbornene photopolymerization as promising synthetic extracellular matrices (ECM) for culturing cells in both 2D and 3D environments.[209, 210] Peptide-polymer conjugates have been developed using click chemistries too for

use in tissue engineering and drug delivery applications. For instance, azide functionalized dendron surfaces were reacted with alkyne bearing hydroxyapatite binding peptides to obtain peptide functionalized dendrons useful in drugs for bone healing.[211] Fluorescent labeling of polymer and proteins was efficiently performed by Robin et al. via bridging reaction of dithiomaleimides with free thiols on the cysteine residues.[212]

However, not much has been reported for clicking molecules with conjugated polymers. Few examples exist for Cu(I)-catalyzed azide-alkyne cycloaddition for PEDOT and Ppy based polymers. Daugaard et al. reported the synthesis of azide functionalized EDOT and demonstrated its utility by attaching a fluorophore.[213] Lind et al. also used the azide modified EDOT to attach a PEGylated RGD peptide (the cell binding domain found in extracellular matrix protein fibronectin) for improved fibroblast attachment.[214] Feldman et al. established the use of 3,4-propylenedioxythiophene with a vinyl termination to generate a family of functional propylenedioxythiophene monomers which were them electrochemically deposited to generate polymer films.[215] These polymer films demonstrated varying electrochemical properties and morphologies depending on the functionality provided to the monomer.

After successfully utilizing the carboxylic acid functionality to modify the PEDOT based conducting polymer surfaces with peptides, we wanted to explore other functionalities that could be used to decorate the surfaces of such conducting polymeric materials. With this aim the 3,4-propylenedioxythiophene with the vinyl termination, referred to as ProDOTene, was electrochemically deposited as films and the ene functionality was used to modify the surface, in this case with a RGD based peptide. Preliminary results demonstrated a promising route for surface modification.

## 5.2 Experimental Procedures

### 5.2.1 Electrochemical Deposition of vinyl terminated ProDOT films

ProDOTene was synthesized as previously described. Vinyl terminated ProDOT films were deposited from a 0.01 M solution of ProDOTene with a 0.1 M tetrabutylammonium perchlorate as the counter ion from acetonitrile. For these sets of films, a potentiodynamic method was applied by sweeping the polymerization potential between -0.6 V to +1.6 V for 4 cycles and the resulting films were rinsed with DI water. The films were denoted as Pene.

### 5.2.2 Trityl Protection of 3-Mercaptopropionic Acid

In an air dried round bottom flask, 430µl (5 mmole) of 3-mercaptopropionic acid was dissolved in 10 ml of DCM. 1.39 g (5 mmole) of trityl chloride dissolved in 5 ml of THF was added drop wise to the reaction mixture at room temperature. After 30-45 minutes a white solid started forming and the resultant reaction mixture was stirred overnight. The reaction mixture was filtered and washed multiple times with DCM. The filtrate was dried in a vacuum oven to yield a white solid. H-NMR spectra on the product confirmed that the obtained was almost 95% pure. The vacuum dried product was used for the next step without purification. H-NMR (CDCl3, 600 MHz) δ (ppm) 2.24 (t, 2H), 2.46 (t, 2H). 7.21-7.23 (m, 2H), 7.26-7.3 (m, 8H), 7.41-7.43 (m, 5H).

### 5.2.3 Peptide Synthesis

Thiol terminated RGD peptide, SH-$CH_2$-$CH_2$-GGGGRGDS (denoted as RGD), was synthesized via Fmoc-based methods on a Rink amide MBHA resin (Novabiochem, San Diego, CA) using an automated solid-phase peptide synthesizer (PS3, Protein Technologies Inc., Tuscon, AZ). The amino acid residues were activated

with HBTU and 0.4 M methylmorpholine in DMF as the activator solvent. Deprotection was conducted using 20% (v/v) piperidine in DMF for approximately 30 minutes. Coupling reactions were carried out for 1 hour. The N-terminal amine of the GGGGRGDS peptide was reacted with trityl protected 3-mercaptopropioninc acid for extended coupling times of 10 hours with HBTU as the coupling reagent. Cleavage of the peptide from the resin was performed in a mixture of 94% trifluoroacetic acid (TFA), 1% triisopropyl silane (TIPS), 2.5% ethanedithiol and 2.5% water for 3-4 hours. TFA was evaporated and the peptide was precipitated in cold ethyl ether. The water soluble peptide were extracted with water and lyophilized. The peptide was purified via reverse-phase high performance liquid chromatography (HPLC) (Waters, MA) using a Symmetry C18 preparative scale column. The gradient applied was from 0-100% of solvent B over 40 minutes (Solvent A = 0.1% TFA in 18.2 MΩ water, solvent B = 0.1% TFA in ACN). The identity of each peptide was confirmed via electrospray ionization mass spectrometry (ESI-MS). (**SH-$CH_2$-$CH_2$-GGGGRGDS**) *m/z* 749.5, calc. 748.79

### 5.2.4 Modification of ProDOTene Films with RGD Peptide

ProDOTene films were coupled with peptide SH-$CH_2$-$CH_2$-GGGGRGDS (RGD) via the thiol-ene click chemistry. 1.5 mg of the peptide was dissolved in 300 µl of a 0.15 wt% solution of LAP photoinitiator in deionized water. The peptide-LAP solution was pipetted on the CP films and exposed to collimated light at 365 nm @ 5mW/$cm^2$ for 10 minutes. To remove unbound peptide, the films were thoroughly washed with 0.05% Tween 20 (company) in PBS, phosphate buffered saline (PBS, Fisher BioReagents) and finally deionized water. Each washing step was performed multiple times to ensure maximum removal of unbound peptide.

### 5.2.5 Characterization of RGD Modified ProDOTene Films

XPS: Chemical analysis of the CP films was conducted using X-ray photoelectron spectroscopy (XPS). (Omicron EA125 X-ray photoelectron spectroscope (Taunusstein, Germany)). A Non-monochromatic aluminum (1486.5 eV) X-ray source was employed. Corrections were made by using adventitious carbon peak located at 284.6 eV in C 1 s region. 50 eV and 25 eV pass energies were used for survey scans and high resolution scans, respectively.

Electrical properties: To analyze the electrical activity of the CP films before and after peptide coupling, cyclic voltammetry (CV) and electrochemical impedance spectroscopy (EIS) were performed using the Autolab potentiostat/ galvanostat (Utrecht, The Netherlands) described above with a platinum counter electrode, a saturated calomel reference electrode, and phosphate-buffered saline electrolyte (PBS). For the CV measurements, cycling was performed between +0.8V and -0.6V with a scan rate of 0.12 V/s. The first stable curve was considered as cycle 1 and used to determine the electroactivity of the film. The charge storage capacity (CSC) was calculated by taking the integral, over time, of the area under the oxidation-reduction curve. For impedance measurements, an AC sinusoidal input of 5mV in amplitude was used as the input signal with the DC potential set to 0. The magnitude and phase angle for the impedance measurements were determined over six discrete frequencies over the range of $1\text{-}10^5$ Hz.

Scanning electron microscopy was conducted using a JEOL JSM-7400F field emission scanning electron microscope (Tokyo, Japan) at a 3-KV operating voltage to determine the effect of peptide modification on film surface morphology. All the films

were sputtered with a thin layer of gold-palladium to provide a more conductive surface. Images were captures at 5,000 X magnification.

### 5.2.6 In vitro Cell Studies

PC12 cell cultures were used to determine the bioactivity of the RGD peptides present on the surface of the ProDOTene films. The samples were sterilized by soaking in 70% ethanol for 8-10 hours. The samples were then rinsed with sterile DPBS solution prior to experiments. The bioactivity of RGD peptide was assessed through comparison to ProDOTene and fibronectin coated ProDOTene which acted like negative and positive controls respectively. Along with these controls, one set of ProDOTene with physically adsorbed and chemically conjugate peptides were coated with fibronectin protein to determine the combined effect of the peptide and protein on the cell attachment. The polymer films were coated with 10 µg/ml solution of fibronectin (Sigma-Aldrich) in sterile DPBS for 10-12 hours at 37 °C. Fluorescent PC12 cells (GFP-PC12) were cultured in RPMI supplemented with 10% horse serum, 5% fetal bovine serum and 1% antibiotics. All cells were cultured under sterile conditions in a humidified 5% $CO_2$ atmosphere at 37 °C. The GFP-PC12 cells were plated on all the polymer films at 30,000 cells/cm$^2$ and cultured for 24 hours in low serum media supplemented with 150 ng/ml NGF. After 24 hours of seeding the media was replaced to add fresh media (low serum) supplemented with 150 ng/ml of NGF. The cells were then incubated for a total of 48 hours before imaging.

## 5.3 Results and Discussion

### 5.3.1 Surface Modification of ProDOTene Films with RGD Peptide

The conducting polymer films based on 3,4-propylenedioxythiophene, ProDOTene, were deposited using the potentiodynamic method. The films were subsequently modified with the RGD peptide, SH-$CH_2$-$CH_2$-GGGGRGDS, using photoinitiated thiol-ene reaction. Multiple photoinitiators such as DMPA, LAP, and Irgacure 184 were tested with different solvents such as methanol, water and DMSO. Out of these the reaction initiated by photocleavage of water soluble visible light photoinitiator LAP (lithium phenyl-2,4,6-trimethylbenzoylphosphonate) led to successful attachment of RGD peptide (tested using XPS). The photocleaved fragment of LAP abstracts a proton from the thiol terminated RGD peptide to generate a thiyl radical, which then reacts rapidly and selectively with the vinyl groups on the conducting polymer films, forming a thioether bond. Figure 5.1 displays the schematic of synthesis of ProDOTene films followed by their surface modification. As a control, ProDOTene films were treated with the same LAP-RGD solution in the absence of UV light. Table 5.1 shows the different films with their denoted names.

**Table** 5.1 Polymer films modified with RGD peptide

| **Polymer films** | **Name** |
|---|---|
| ProDOTene | Pene |
| ProDOTene+lap+RGD | Pene+RGD |
| ProDOTene+lap+RGD @ 365 nm | Pene+RGD @ 365 nm |

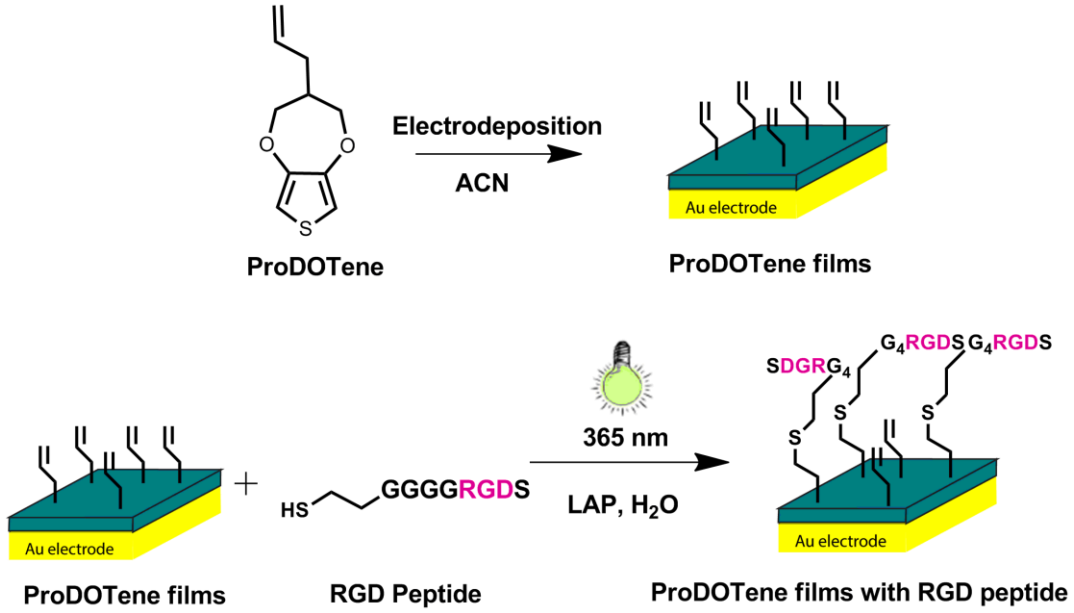


**Figure** 5.1 Schematic of synthesis of ProDOTene films followed by surface modification with RGD peptide.

### 5.3.2 XPS Analysis of RGD Modified ProDOTene Films

XPS was conducted on the ProDOTene films before and after surface modification to confirm the presence of the RGD peptide on the surface. Figure 5.2 displays a sample survey spectra for the films and Figure 5.3 displays the N 1s spectra of the same films. The XPS scan for pure ProDOTene films does not show a nitrogen peak, as expected. The XPS scans for ProDOTene films treated with the LAP-RGD solution in the absence and presence of UV light demonstrated an N 1s peak at 399.3 eV indicating the presence of the RGD peptide on the surface. The presence of the peptide for the films synthesized in the absence of the UV light suggests some level of non-specific binding to the films which unfortunately could not be eliminated in spite of multiple washes with Tween 20 solution. The elemental analysis with the percentage contribution from all the major elements (oxygen, carbon, nitrogen, and

sulfur) is presented in Table 5.2. The N/S ratio as calculated in Table 5.2 increases from Pene (0) to Pene+RGD (0.35) to Pene+RGD @ 365 nm (0.85) suggesting highest amount of peptide is present when the films are exposed to UV light indicating successful covalent modification of the films via thiol-ene click chemistry.

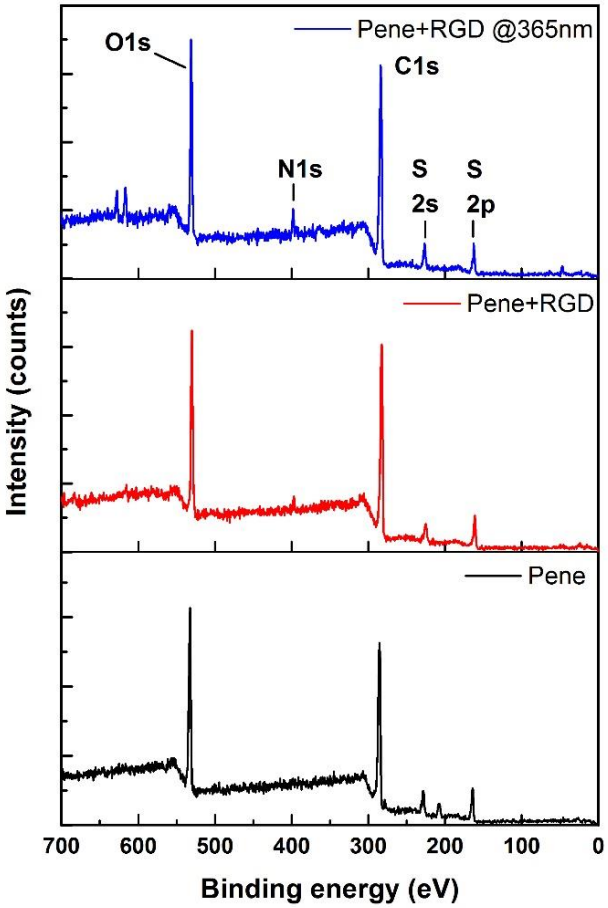


**Figure** 5.2 XPS spectra of ProDOTene films modified with a RGD peptide in the absence and presence of UV light compared to pure ProDOTene films.

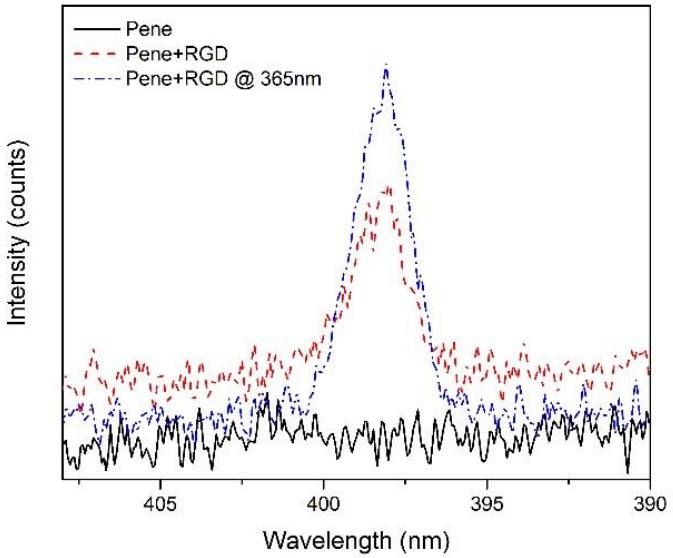


**Figure** 5.3 N 1s spectra of ProDOTene films modified with a RGD peptide in the absence and presence of UV light compared to pure ProDOTene films.

**Table** 5.2 Elemental analysis of ProDOTene films modified with RGD peptide.

| **POLYMERS** | **ELEMENTAL COMPOSITION** | | | | **N/S ratio** |
|---|---|---|---|---|---|
| | Carbon (%) | Oxygen (%) | Nitrogen (%) | Sulfur (%) | |
| Pene | 67.4 | 25.8 | 0 | 5.8 | 0 |
| Pene+RGD | 68.5 | 22.2 | 2.4 | 6.9 | 0.35 |
| Pene+RGD @365nm | 65.1 | 22.3 | 5.8 | 6.8 | 0.85 |

### 5.3.3 Electrical Properties of ProDOTene Films Modified with RGD Peptide

The electrochemical properties of ProDOTene films before and after RGD peptide modification were determined by performing cyclic voltammetry (CV) and electrical impedance spectroscopy (EIS). The electrode sites were swept from +0.8 V

to -0.6 V at a scan rate of 0.12 V/s versus Ag/AgCl reference electrode. Figure 5.4 displays the 1st stable CV curve for Pene, Pene+RGD and Pene+RGD @ 365 nm. The characteristics of the CV curve and the charge storage capacities before and after exposure to the LAP-RGD solution (in the absence or presence of UV light) remain almost identical. The charge storage capacities of Pene, Pen+RGD and Pene+RGD @ 365 nm were 2.89 $mC/cm^2$, 2.52 $mC/cm^2$, and 2.44 $mC/cm^2$ respectively indicating that the peptide modification does not compromise the electrical properties of the films. Just as the CV curves, the impedance magnitude of the peptide modified films remains relatively unaffected compared to the untreated ProDOTene films. The impedance magnitude at 1000 Hz, the frequency relevant to neural recording and stimulation for all the films, with and without peptides, is ~ 70 Ω proving the films before and after modification transport charge in a similar fashion and that the presence of the peptide is not proving detrimental to charge transport.

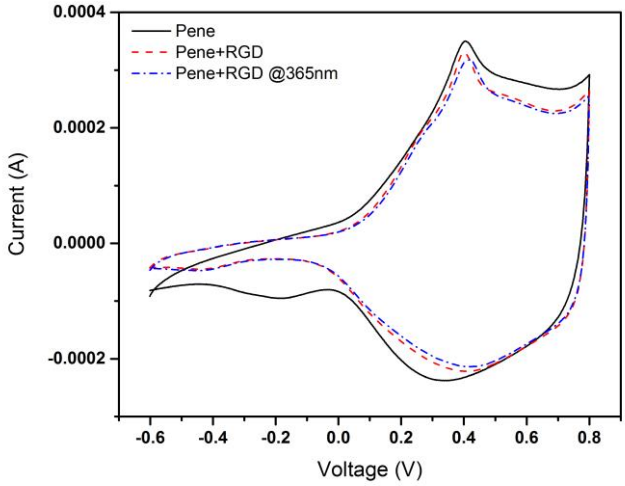


**Figure** 5.4 CV curves for 1st stable cycle for ProDOTene films before and after peptide modification.

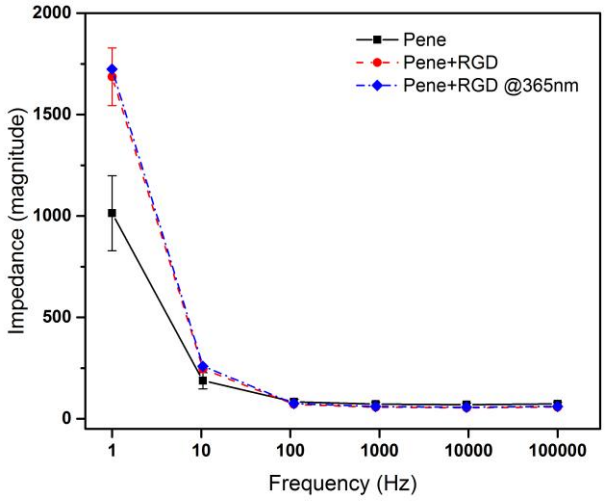


**Figure** 5.5 Impedance magnitude for ProDOTene films before and after peptide modification.

### 5.3.4 Morphology of ProDOTene Films Before and After Peptide Modification

Scanning electron microscopy was conducted on ProDOTene films before and after peptide modification to determine the impact of the RGD peptide on the morphology of the polymer films. Figure 5.6 illustrates the micrographs of the films before and after RGD modification. As demonstrated by Figure 5.6 the surface morphology of the ProDOTene films remains identical after surface modification. All the polymer films demonstrate a rod-like, fibrous morphology with the average diameter of the fibers around 100 nm. Potentiodynamic electrosynthesis methods have been shown to produce different surface morphologies than galvanostatic and potentiostatic synthesis methods.[188] The rod-like, fibrous features observed for ProDOTene films match those of other poly(3,4-alkylenedioxythophene) films deposited via potentiodynamic methods for a high potential range of 0-1.2 V.[60] Similar

to PEDOTacid films modified with YIGSR based peptides, the morphological features of ProDOTene films also remain unaltered after peptide coupling.

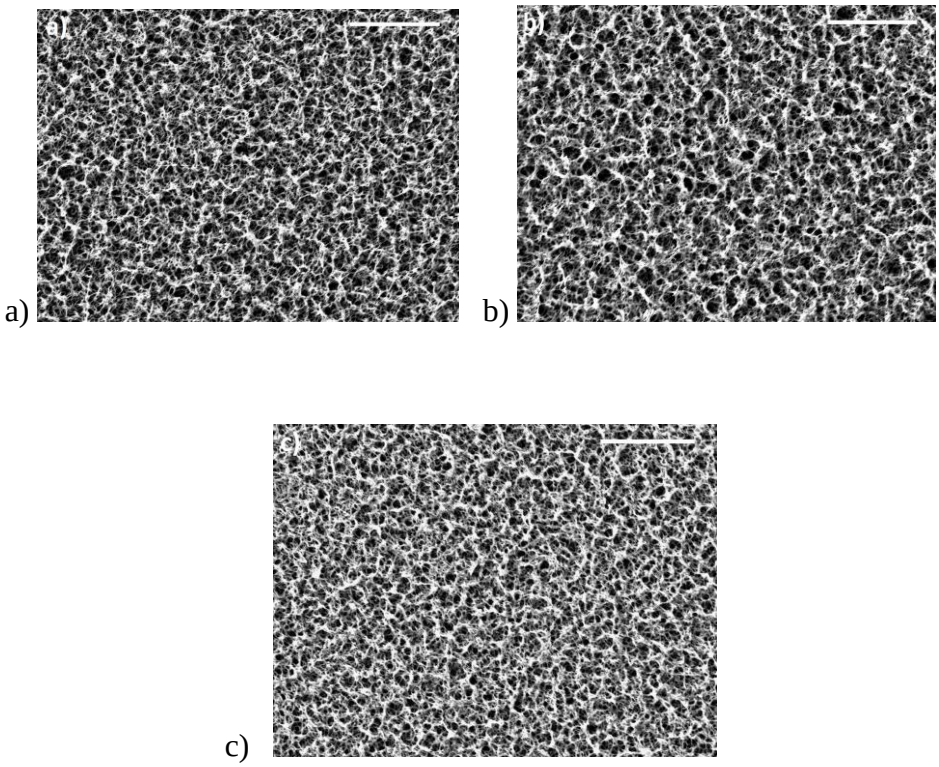


**Figure** 5.6 Morphology of the ProDOTene films before and after peptide modification a) Pene, b) Pene+RGD, and c) Pene+RGD @ 365nm (the scale bar represents 5 µm)

### 5.3.5 In vitro Cell Studies

In vitro cell studies were performed to determine the effect of the attached RGD peptide. 30,000 cells/cm$^2$ were seeded on peptide modified films and dosed with NGF supplemented media. The bioactivity of the RGD peptide was assessed through comparison to negative and positive controls ProDOTene and fibronectin-coated (Fn-coated) ProDOTene polymer films respectively. Along with these controls, one set of

ProDOTene films with RGD peptide were coated with fibronectin protein to test the synergistic effect of the peptide and the whole protein on the PC12 cell attachment. Sample micrographs for ProDOTene films modified with the RGD peptide with and without UV light taken at 72 hours are shown in Figure 5.7 and the number of cells attached to all the surfaces probed in this study are shown in Figure 5.8.

As displayed in Figure 5.7 and Figure 5.8 RGD modification of the films via thiol-ene click chemistry leads to increased PC12 cell attachment. The hydrophobic ProDOTene films (contact angle 95 °) and the fibronectin coated ProDOTene films seem to have no difference in their ability for cell adhesion. Surprisingly, the presence of the RGD peptide on the surface when not treated under UV light leads to reduced cell attachment. The films with chemically conjugated RGD peptide via thiol-ene click chemistry however lead to improved cell attachment (Figure 5.7 (e) and (f)). The Pene+RGD @ 365nm modified films coated with fibronectin protein resulted in statistically significant results ($p \leq 0.05$) compared to Pene films and RGD+Pene films. These results were not significantly different from non-coated Pene+RGD @ 365nm films. RGD peptide has also been used by Lind et al to modify PEDOT-alkyne films with Cu click chemistry and demonstrated specific cell binding to RGD functionalized sample areas. As per our best knowledge, thiol-ene click chemistry has not been utilized so far to display peptide sequences on conducting polymer films of poly(3,4-alkylenedioxythiophene). This can be used as a platform to display different biological molecules which possess a thiol functionality.

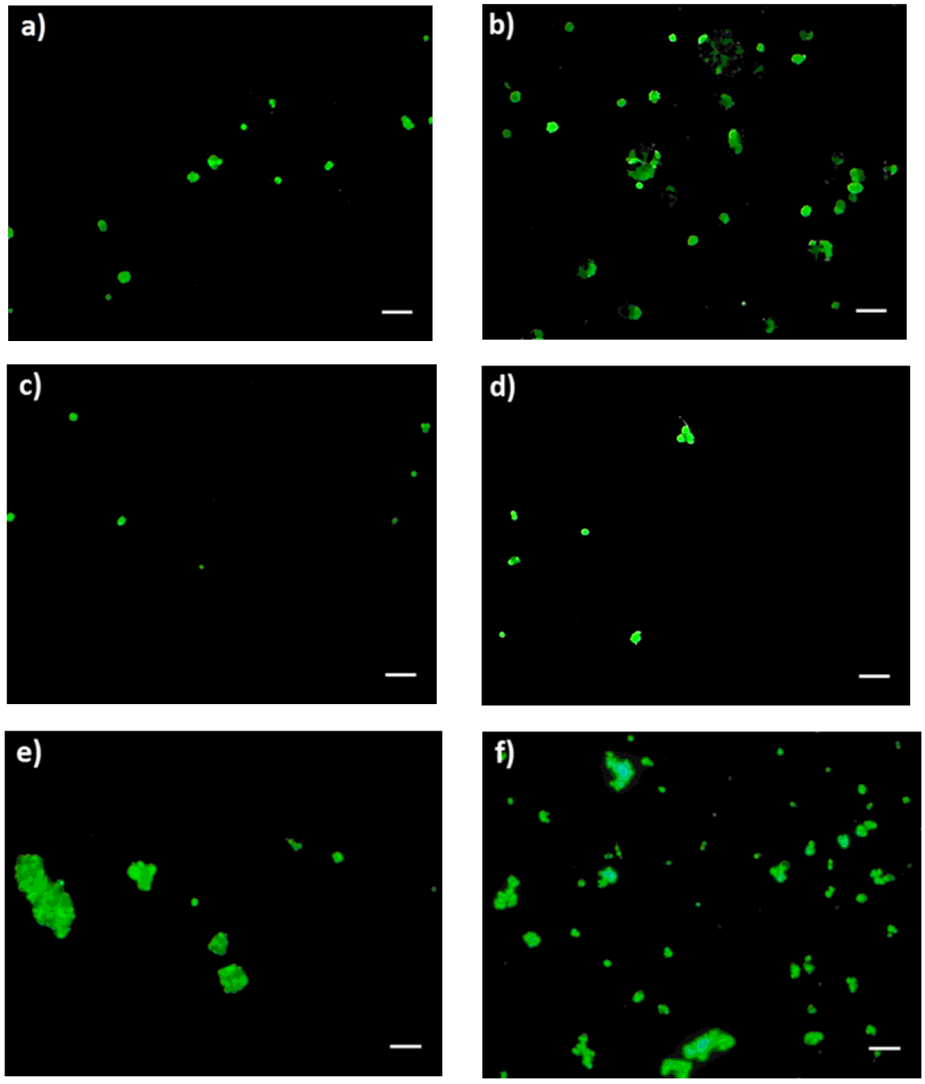


**Figure** 5.7 Sample images of PC12 cell attachment on ProDOTene films before and after RGD modification at 72 h post plating a) Pene, b) Fn-coated Pene, c) Pene+RGD, d) Fn-coated Pene+RGD, e) Pene+RGD @ 365nm, and f) Fn-coated Pene+RGD @ 365nm (the scale bar represents 100 µm)

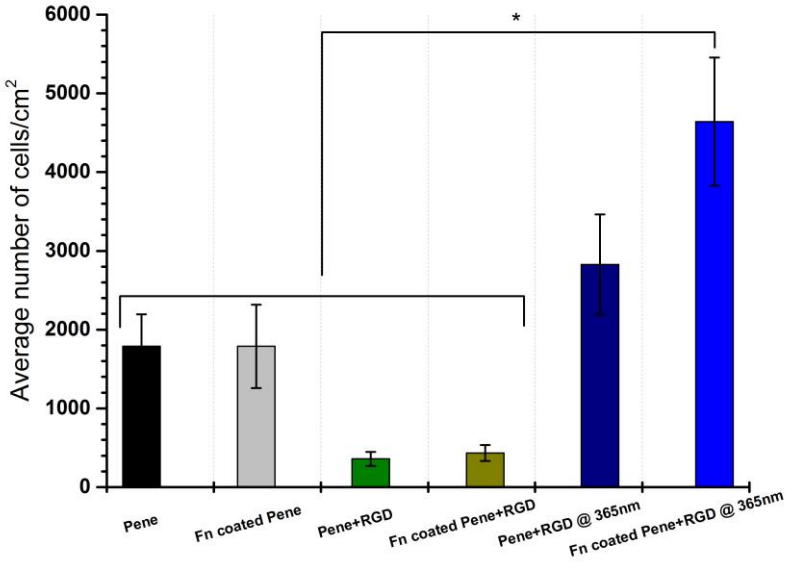


**Figure** 5.8 Average number of cells/cm$^2$ attached to ProDOTene films before and after RGD peptide modification.

## 5.4 Conclusions

Poly(3,4-propylenedioxythiophene) films with an alkene functionality were modified with a RGD peptide via photoinitiated thiol-ene click chemistry. The peptide presence on the films was confirmed via XPS. The peptide functionalized films had comparable electrochemical properties to the unmodified films. The resulting peptide functionalized films were bioactive, as indicated by the increased adhesion of the GFP modified PC12 cells. This method opens up an easy avenue for thiol-functional biological molecules for imparting bioactivity to conducting polymer films.

# Chapter 6

# CONCLUSIONS AND FUTURE WORK

## 6.1 Conclusions

In this thesis we presented the design, synthesis, and characterization of novel hybrid materials based on peptides and conjugated polymeric materials. These unique hybrid systems were developed for two different applications, optoelectronics and neural interfaces.

### 6.1.1 Conclusions for Helical Peptides as Templates Project

To understand the intermolecular spacing effects and their influence on the electronic properties of an organic light emitting diode, α-helical peptides were employed as scaffolds (for oxadiazole containing phenylene vinylene oligomers, Oxa-PPV) owing to their well-understood geometry and structure. Novel PEGylated α-helical peptides were designed and synthesized to strategically place upto three Oxa-PPV chromophores for precisely controlling their spacing and alignment at nano-scale levels. By incorporation of non-natural amino acid, *p*-bromophenylalanine, at specific positions in the helical peptide sequence the same template can be utilized to display chromophores at varying distances (6-17 Å) and orientations. PEGylation of the peptides helped in imparting hydrophilicity and structural stability to the otherwise hydrophobic residue-rich and Oxa-PPV modified peptides. This technique of presenting chromophores presents a means of studying the photophysics of

electroactive species in dilute solutions and emulate the film-like behavior of conjugated polymers in OLEDs with the exception of extrinsic defects.

The Oxa-PPV modified PEGylated α-helical peptides (prepared via Heck coupling strategies) were characterized using a variety of spectroscopic methods. Circular dichroic (CD) spectroscopy showed the helical nature of the scaffolds and the observation of exciton coupled-CD suggested side chain interaction depending on the distance and dihedral angle between chromophores. In particular, it was observed (via steady state PL and time resolved PL) that chromophores prevented from stacking interactions (presented on opposite sides of scaffold, or at longer intermolecular distances of 17 Å) behaved independently and exhibited behavior analogous to single chromophores. The chromophores which did interact with each other either formed excimers when they were separated by smaller distances of 6 Å or formed polaron pairs (which are the major photophysical pathway in polymer films) when they are separated by slightly longer distances of 11 Å. All of these results suggested that PEGylated α-helical peptide system can be effectively used to investigate the poorly understood complex phyotophysical phenomenon.

### 6.1.2 Conclusions for Poly(3,4-alkylenediothiophene) Films as Coatings for Neural Electrodes Project

For bridging the mechanical mismatch and providing long term device performance, poly(3,4-ethylenedioxythiophene) (PEDOT) based coatings are used for interfacing electrodes with biological tissue. Towards these ends, copolymer films of EDOT with carboxylic acid functional EDOT (EDOTacid) were developed for producing functionalized surfaces. By varying the ratio of the monomers in the feed copolymer films with varying carboxylic acid surface concentrations, tunable

hydrophilicities and surface morphologies could be generated. These films provided a means of integration of biological molecules with PEDOT coatings which is a viable strategy to provide biofunctionaliztion. Chemically conjugating the biomolecule to the surface ensures tighter control over immobilization, and minimal biomolecule loss over time. We modified the PEDOTacid copolymer films a laminin derived nonapeptide, CDPGYIGSR which has proven to promote cell attachment and neurite outgrowth. The peptide modified films possessed unaltered electrochemical characteristics and morphologies compared to unmodified films. A PEG spacer molecule, between the polymer film and the peptide sequence, was used to make the peptide more available for cellular interactions. A GFP modified PC12 cell line was used to test the bioactivity of the peptide modified films. We observed that laminin-coated peptide modified films with a longer spacer molecule (3 nm) resulted in superior cell attachment and neurite extensions and also resulted in longer mean neurite lengths. In our attempt to improve the bioactitity of the conjugated polymer films, we also demonstrated the need to use a linker molecule for such rough and porous polymer film surfaces. Preliminary studies on surface modification of vinyl terminated poly(3,4-propylenedioxythiophene) (Pene) films with a thiol functional molecule showed successful incorporation of thiol modified RGD peptide on the films. The fibronectin coated RGD functional films increased adhesion of PC12 cells by around 3 times compared to fibronectin coated Pene films.

## 6.2 Future Work

In this thesis we presented two different peptide-polymer conjugate systems which can be used as platforms to display a variety of molecules ranging from electroactive species to biomolecules.

### 6.2.1 Future Work for Helical Peptides as Templates Project

Identical or similar helical peptide templates can be used to sequester multiple chromophores, structurally similar or dissimilar, at varying distances and in multiple orientations, to permit characterization and control of their spectroscopic properties. The chromophores could be from the PPV family or could be chemically different like thiophene derivatives, benzophenoxazines, perylene derivatives, etc. Using these PEGylated templates multiple hydrophobic molecules could be incorporated with relative ease of synthesis and purification.

For the existing system, Oxa-PPV modified PEGylated helical peptides, detailed transient photophysical characterization experiments should be carried out to probe the decay dynamics of these systems. Preliminary transient photoluminescence studies determined the presence of the different excited state species. This can be further probed by performing transient absorption which can be used to determine the behavior of the chromophores in different orientations after excitation. Experiments can be carefully conducted by preparing solutions that have exactly the same absorbance at the pump wavelength to compare the decay dynamics and can also potentially used to determine the whether the excited species are in the singlet or triplet states.

The helical peptide template can be used to study the intra and intermolecular charge and energy transfer between donor and acceptor pairs for applications in organic photovoltaics. The energy transfer can be radiative (fluorescence or phosphorescence) or non-radiative (inter system crossing). In the case of energy transfer, the exchange mechanism (Dexter) dominates at small chromophore separations and a dipole-induced dipole mechanism (Forster) controls the rate at larger separations (1-10 nm). Since this template has the ability to present chromophores at

large intermolecular distances, these 4 nm long templates can be used to investigate the energy transfer behaviors, assuming there is an offset in the HOMO and LUMO levels, for electroactive species placed at varying distances of upto 2 nm. The choice of donor – acceptor pair, interchromophoric distance, and the nature of the excited species has profound effect on the electron and energy transfer. Formation of excited states such as excimers, exciplexes, or ground state complexes can be explored and the energy transfer between these species can be determined as a function of distance and orientation.

### 6.2.2 Future work for Poly(3,4-alkylenediothiophene) Films as Coatings for Neural Electrodes Project

Carboxylic acid and alkene functional conjugated polymer films present a platform for modifying thiophene based conducting polymer films with biological molecules. Other than laminin and fibronectin derived peptide sequences, other relevant peptide sequences include clot binding peptides[73] and hyaluronic acid binding peptides.[216] This thesis focused on conducting in vitro cell studies using the PC12 cell line. For future in vitro studies cell assays that are representative of the cell type and material likely to be presented around the implanted bioelectrode must be performed. In addition to in vitro studies the ultimate objective must be to conduct in vivo studies to determine the impact of the peptide modified conjugated polymer films can result in sufficient neuron attraction to the implanted site and maintain prolonged electrical connection in spite of possible glial scar formation.

Other than the calorimetric toluidine blue O (TBO) assay, alternate methods can also be employed to determine the grafting density of the peptide molecule. Since the TBO assay is limited to carboxylic acid functional films, the biomolecule surface

density can be determined through radio-labelling. The drawbacks of this method however are that it is expensive and can potentially alter the structure of the biomolecule. Advanced techniques such as Fourier transform infrared microscopy with mapping can also be potentially applied to peptide modified surfaces in vitro or in vivo to gain in depth information regarding the chemical elements present on the surface of the material and their bonding within the desired environment.

Apart from depositing films on metal electrodes, these films could potentially be incorporated in hydrogels to develop materials for neural tissue engineering. The carboxylic acid and vinyl functionality will open up a wide range of chemistries to incorporate biomolecules like peptides, drugs, enzymes, and growth factors in the hydrogels. For instance, the carboxylic acid moiety can also be used to couple hydroxyl terminated drug molecules by an ester functionality. The material can be designed to release the drug molecules on ester hydrolysis. Using hydrogels will lower the mechanical mismatch between the implant and tissue even further thus resulting in a material more suitable for tissue engineering. Finally, growing the biofunctionalized films directly in the brain tissue, or in-situ could also be attempted.

## REFERENCES


1. Xiao, Y.; Hong, H.; Javadi, A.; Engle, J. W.; Xu, W.; Yang, Y.; Zhang, Y.; Barnhart, T. E.; Cai, W.; Gong, S., Multifunctional unimolecular micelles for cancer-targeted drug delivery and positron emission tomography imaging. *Biomaterials* **2012,** 33, (11), 3071-3082.

2. Lu, J.; Shi, M.; Shoichet, M. S., Click Chemistry Functionalized Polymeric Nanoparticles Target Corneal Epithelial Cells through RGD-Cell Surface Receptors. *Bioconjugate Chemistry* **2009,** 20, (1), 87-94.

3. McGann, C. L.; Levenson, E. A.; Kiick, K. L., Resilin-Based Hybrid Hydrogels for Cardiovascular Tissue Engineering. *Macromolecular Chemistry and Physics* **2013,** 214, (2), 203-213.

4. Kakinoki, S.; Yamaoka, T., Stable modification of poly(lactic acid) surface with neurite outgrowth-promoting peptides via hydrophobic collagen-like sequence. *Acta Biomaterialia* **2010,** 6, (6), 1925-1930.

5. Liu, T.-Y.; Hussein, W. M.; Jia, Z.; Ziora, Z. M.; McMillan, N. A. J.; Monteiro, M. J.; Toth, I.; Skwarczynski, M., Self-Adjuvanting Polymer-Peptide Conjugates As Therapeutic Vaccine Candidates against Cervical Cancer. *Biomacromolecules* **2013,** 14, (8), 2798-2806.

6. Hamley, I. W.; Ansari, A.; Castelletto, V.; Nuhn, H.; Rosler, A.; Klok, H. A., Solution self-assembly of hybrid block copolymers containing poly(ethylene glycol) and amphiphilic beta-strand peptide sequences. *Biomacromolecules* **2005,** 6, (3), 1310-1315.

7. Shu, J. Y.; Lund, R.; Xu, T., Solution Structural Characterization of Coiled-Coil Peptide-Polymer Side-Conjugates. *Biomacromolecules* **2012,** 13, (6), 1945-1955.

8. Klok, H. A., Biological-synthetic hybrid block copolymers: Combining the best from two worlds. *Journal of Polymer Science Part a-Polymer Chemistry* **2005,** 43, (1), 1-17.

9. Dehn, S.; Chapman, R.; Jolliffe, K. A.; Perrier, S., Synthetic Strategies for the Design of Peptide/Polymer Conjugates. *Polymer Reviews* **2011,** 51, (2), 214-234.

10. Shu, J. Y.; Panganiban, B.; Xu, T., Peptide-Polymer Conjugates: From Fundamental Science to Application. *Annual Review of Physical Chemistry* **2013,** 64, 631-657.

11. Morell, M.; Puiggali, J., Hybrid Block Copolymers Constituted by Peptides and Synthetic Polymers: An Overview of Synthetic Approaches, Supramolecular Behavior and Potential Applications. *Polymers* **2013,** 5, (1), 188-224.

12. Gauthier, M. A.; Klok, H.-A., Peptide/protein-polymer conjugates: synthetic strategies and design concepts. *Chemical Communications* **2008**, (23), 2591-2611.

13. Cobo, I.; Li, M.; Sumerlin, B. S.; Perrier, S., Smart hybrid materials by conjugation of responsive polymers to biomacromolecules. *Nature Materials* **2015,** 14, (2), 143-159.

14. Ayres, L.; Vos, M. R. J.; Adams, P.; Shklyarevskiy, I. O.; van Hest, J. C. M., Elastin-based side-chain polymers synthesized by ATRP. *Macromolecules* **2003,** 36, (16), 5967-5973.

15. Hentschel, J.; ten Cate, M. G. J.; Boerner, H. G., Peptide-guided organization of peptide-polymer conjugates: Expanding the approach from oligo- to polymers. *Macromolecules* **2007,** 40, (26), 9224-9232.

16. Shu, J. Y.; Huang, Y.-J.; Tan, C.; Presley, A. D.; Chang, J.; Xu, T., Amphiphilic Peptide-Polymer Conjugates Based on the Coiled-Coil Helix Bundle. *Biomacromolecules* **2010,** 11, (6), 1443-1452.

17. Banerjee, S. S.; Aher, N.; Patil, R.; Khandare, J., Poly(ethylene glycol)-Prodrug Conjugates: Concept, Design, and Applications. *Journal of drug delivery* **2012,** 2012, 103973-103973.

18. Pasut, G., Polymers for Protein Conjugation. *Polymers* **2014,** 6, (1), 160-178.

19. Pelegri-O'Day, E. M.; Lin, E.-W.; Maynard, H. D., Therapeutic Protein-Polymer Conjugates: Advancing Beyond PEGylation. *Journal of the American Chemical Society* **2014,** 136, (41), 14323-14332.

20. Krishna, O. D.; Kiick, K. L., Protein- and Peptide-Modified Synthetic Polymeric Biomaterials. *Biopolymers* **2010,** 94, (1), 32-48.

21. Abuchowski, A.; Vanes, T.; Palczuk, N. C.; Davis, F. F., Alteration of immunological properties of bovine serum-albumin by covalent attachment of polyethylene-glycol. *Journal of Biological Chemistry* **1977,** 252, (11), 3578-3581.

22. Castelletto, V.; Hamley, I. W., Self assembly of a model amphiphilic phenylalanine peptide/polyethylene glycol block copolymer in aqueous solution. *Biophysical Chemistry* **2009,** 141, (2-3), 169-174.

23. Vandermeulen, G. W. M.; Tziatzios, C.; Klok, H. A., Reversible self-organization of poly(ethylene glycol)-based hybrid block copolymers mediated by a De Novo four-stranded alpha-helical coiled coil motif. *Macromolecules* **2003,** 36, (11), 4107-4114.

24. Vandermeulen, G. W. M.; Tziatzios, C.; Duncan, R.; Klok, H. A., PEG-based hybrid block copolymers containing alpha-helical coiled coil peptide sequences: Control of self-assembly and preliminary biological evaluation. *Macromolecules* **2005,** 38, (3), 761-769.

25. Choi, Y. Y.; Jang, J. H.; Park, M. H.; Choi, B. G.; Chi, B.; Jeong, B., Block length affects secondary structure, nanoassembly and thermosensitivity of poly(ethylene glycol)-poly(L-alanine) block copolymers. *J. Mater. Chem.* **2010,** 20, (17), 3416-3421.

26. Ragi, C.; Sedaghat-Herati, M. R.; Ouameur, A. A.; Tajmir-Riahi, H. A., The effects of poly(ethylene glycol) on the solution structure of human serum albumin. *Biopolymers* **2005,** 78, (5), 231-236.

27. Pechar, M.; Kopeckova, P.; Joss, L.; Kopecek, J., Associative diblock copolymers of poly(ethylene glycol) and coiled-coil peptides. *Macromol. Biosci.* **2002,** 2, (5), 199-206.

28. Top, A.; Roberts, C. J.; Kiick, K. L., Conformational and Aggregation Properties of a PEGylated Alanine-Rich Polypeptide. *Biomacromolecules* **2011,** 12, (6), 2184-2192.

29. Pasut, G.; Sergi, M.; Veronese, F. M., Anti-cancer PEG-enzymes: 30 years old, but still a current approach. *Advanced Drug Delivery Reviews* **2008,** 60, (1), 69-78.

30. Lu, Y. L.; Harding, S. E.; Turner, A.; Smith, B.; Athwal, D. S.; Grossmann, J. G.; Davis, K. G.; Rowe, A. J., Effect of PEGylation on the solution conformation of antibody fragments. *J. Pharm. Sci.* **2008,** 97, (6), 2062-2079.

31. Gebhardt, K. E.; Ahn, S.; Venkatachalam, G.; Savin, D. A., Rod-sphere transition in polybutadiene-poly(L-lysine) block copolymer assemblies. *Langmuir* **2007,** 23, (5), 2851-2856.

32. Checot, F.; Lecommandoux, S.; Klok, H. A.; Gnanou, Y., From supramolecular polymersomes to stimuli-responsive nano-capsules based on poly(diene-b-peptide) diblock copolymers. *European Physical Journal E* **2003,** 10, (1), 25-35.

33. Krysmann, M. J.; Funari, S. S.; Canetta, E.; Hamley, I. W., The effect of PEG crystallization on the morphology of PEG/peptide block copolymers containing amyloid beta-peptide fragments. *Macromolecular Chemistry and Physics* **2008,** 209, (9), 883-889.

34. Klok, H. A.; Vandermeulen, G. W. M.; Nuhn, H.; Rosler, A.; Hamley, I. W.; Castelletto, V.; Xu, H.; Sheiko, S. S., Peptide mediated formation of hierarchically organized solution and solid state polymer nanostructures. *Faraday Discussions* **2005,** 128, 29-41.

35. Grieshaber, S. E.; Farran, A. J. E.; Lin-Gibson, S.; Kiick, K. L.; Jia, X., Synthesis and Characterization of Elastin-Mimetic Hybrid Polymers with Multiblock, Alternating Molecular Architecture and Elastomeric Properties. *Macromolecules* **2009,** 42, (7), 2532-2541.

36. Marsden, H. R.; Korobko, A. V.; van Leeuwen, E. N. M.; Pouget, E. M.; Veen, S. J.; Sommerdijk, N. A. J. M.; Kros, A., Noncovalent triblock copolymers based on a coiled-coil peptide motif. *Journal of the American Chemical Society* **2008,** 130, (29), 9386-9393.

37. Xiao, Y.; Li, C. M.; Wang, S.; Shi, J.; Ooi, C. P., Incorporation of collagen in poly(3,4-ethylenedioxythiophene) for a bifunctional film with high bio- and electrochemical activity. *Journal of Biomedical Materials Research Part A* **2010,** 92A, (2), 766-772.

38. Pernites, R. B.; Santos, C. M.; Maldonado, M.; Ponnapati, R. R.; Rodrigues, D. F.; Advincula, R. C., Tunable Protein and Bacterial Cell Adsorption on Colloidally Templated Superhydrophobic Polythiophene Films. *Chemistry of Materials* **2012,** 24, (5), 870-880.

39. Green, R. A.; Hassarati, R. T.; Goding, J. A.; Baek, S.; Lovell, N. H.; Martens, P. J.; Poole-Warren, L. A., Conductive Hydrogels: Mechanically Robust Hybrids for Use as Biomaterials. *Macromolecular Bioscience* **2012,** 12, (4), 494-501.

40. Zhang, L.; Stauffer, W. R.; Jane, E. P.; Sammak, P. J.; Cui, X. T., Enhanced Differentiation of Embryonic and Neural Stem Cells to Neuronal Fates on Laminin Peptides Doped Polypyrrole. *Macromolecular Bioscience* **2010,** 10, (12), 1456-1464.

41. De Giglio, E.; Sabbatini, L.; Colucci, S.; Zambonin, G., Synthesis, analytical characterization, and osteoblast adhesion properties on RGD-grafted polypyrrole coatings on titanium substrates. *Journal of Biomaterials Science-Polymer Edition* **2000,** 11, (10), 1073-1083.

42. Lee, J. Y.; Jeong, E. D.; Ahn, C. W.; Lee, J. W., Bioactive conducting scaffolds: Active ester-functionalized polyterthiophene. *Synthetic Metals* **2013,** 185, 66-70.

43. Povlich, L. K.; Cho, J. C.; Leach, M. K.; Corey, J. M.; Kim, J.; Martin, D. C., Synthesis, copolymerization and peptide-modification of carboxylic acid-functionalized 3,4-ethylenedioxythiophene (EDOTacid) for neural electrode interfaces. *Biochim. Biophys. Acta* **2013,** 1830, (9), 4288-4293.

44. Fabregat, G.; Ballano, G.; Armelin, E.; del Valle, L. J.; Cativiela, C.; Aleman, C., An electroactive and biologically responsive hybrid conjugate based on chemical similarity. *Polymer Chemistry* **2013,** 4, (5), 1412-1424.

45. Kas, O. Y.; Charati, M. B.; Rothberg, L. J.; Galvin, M. E.; Kiick, K. L., Regulation of electronic behavior via confinement of PPV-based oligomers on peptide scaffolds. *J. Mater. Chem.* **2008,** 18, (32), 3847-3854.

46. Bong, D. T.; Ghadiri, M. R., Chemoselective Pd(0)-catalyzed peptide coupling in water. *Organic Letters* **2001,** 3, (16), 2509-2511.

47. Ojida, A.; Tsutsumi, H.; Kasagi, N.; Hamachi, I., Suzuki coupling for protein modification. *Tetrahedron Letters* **2005,** 46, (19), 3301-3305.

48. Deiters, A.; Cropp, T. A.; Mukherji, M.; Chin, J. W.; Anderson, J. C.; Schultz, P. G., Adding amino acids with novel reactivity to the genetic code of Saccharomyces cerevisiae. *Journal of the American Chemical Society* **2003,** 125, (39), 11782-11783.

49. Hodgson, D. R. W.; Sanderson, J. M., The synthesis of peptides and proteins containing non-natural amino acids. *Chemical Society Reviews* **2004,** 33, (7), 422-430.

50. Kelley, T. W.; Baude, P. F.; Gerlach, C.; Ender, D. E.; Muyres, D.; Haase, M. A.; Vogel, D. E.; Theiss, S. D., Recent progress in organic electronics: Materials, devices, and processes. *Chemistry of Materials* **2004,** 16, (23), 4413-4422.

51. Hayes, G. R.; Samuel, I. D. W.; Phillips, R. T., Exciton dynamics in electroluminescent polymers studies by femtosecond time-resolved photoluminescence spectroscopy. *Physical Review B* **1995,** 52, (16), 11569-11572.

52. Dyakonov, V.; Frankevich, E., On the role played by polaron pairs in photophysical processes in semiconducting polymers. *Chemical Physics* **1998,** 227, (1-2), 203-217.

53. Frankevich, E. L.; Lymarev, A. A.; Sokolik, I.; Karasz, F. E.; Blumstengel, S.; Baughman, R. H.; Horhold, H. H., Polaron pair generation in poly(phenylene vinylenes). *Physical Review B* **1992,** 46, (15), 9320-9324.

54. Conwell, E. M., Excimers in poly(phenylene vinylene) and its derivatives. *Synthetic Metals* **1997,** 85, (1-3), 995-999.

55. Rothberg, L. J.; Yan, M.; Papadimitrakopoulos, F.; Galvin, M. E.; Kwock, E. W.; Miller, T. M., Photophysics of phenylenevinylene polymers. *Synthetic Metals* **1996,** 80, (1), 41-58.

56. Lowe, C.; Weder, C., Oligo(p-phenylene vinylene) excimers as molecular probes: Deformation-induced color changes in photoluminescent polymer blends. *Advanced Materials* **2002,** 14, (22), 1625-1629.

57. Sirringhaus, H.; Brown, P. J.; Friend, R. H.; Nielsen, M. M.; Bechgaard, K.; Langeveld-Voss, B. M. W.; Spiering, A. J. H.; Janssen, R. A. J.; Meijer, E. W.; Herwig, P.; de Leeuw, D. M., Two-dimensional charge transport in self-organized, high-mobility conjugated polymers. *Nature* **1999,** 401, (6754), 685-688.

58. Kim, D. H.; Richardson-Burns, S. M.; Povlich, L. K.; Abidian, M. R.; Spanninga, S.; Hendricks, J. L.; Martin, D. C., Soft, Fuzzy, and Bioactive Conducting Polymers for Improving the Chronic Performance of Neural Prosthetic Devices. **2007**.

59. Groenendaal, L.; Zotti, G.; Aubert, P. H.; Waybright, S. M.; Reynolds, J. R., Electrochemistry of poly(3,4-alkylenedioxythiophene) derivatives. *Adv. Mater.* **2003,** 15, (11), 855-879.

60. Patra, S.; Barai, K.; Munichandraiah, N., Scanning electron microscopy studies of PEDOT prepared by various electrochemical routes. *Synthetic Metals* **2008,** 158, (10), 430-435.

61. Gomez, N.; Schmidt, C. E., Nerve growth factor-immobilized polypyrrole: Bioactive electrically conducting polymer for enhanced neurite extension. *Journal of Biomedical Materials Research Part A* **2007,** 81A, (1), 135-149.

62. Lee, J. Y.; Schmidt, C. E., Pyrrole-hyaluronic acid conjugates for decreasing cell binding to metals and conducting polymers. *Acta Biomaterialia* **2010,** 6, (11), 4396-4404.

63. Garner, B.; Georgevich, A.; Hodgson, A. J.; Liu, L.; Wallace, G. G., Polypyrrole-heparin composites as stimulus-responsive substrates for endothelial cell growth. *Journal of Biomedical Materials Research* **1999,** 44, (2), 121-129.

64. Lee, J. W.; Serna, F.; Nickels, J.; Schmidt, C. E., Carboxylic acid-functionalized conductive polypyrrole as a bioactive platform for cell adhesion. *Biomacromolecules* **2006,** 7, (6), 1692-1695.

65. Stauffer, W. R.; Cui, X. T., Polypyrrole doped with 2 peptide sequences from laminin. *Biomaterials* **2006,** 27, (11), 2405-2413.

66. Sanghvi, A. B.; Miller, K. P. H.; Belcher, A. M.; Schmidt, C. E., Biomaterials functionalization using a novel peptide that selectively binds to a conducting polymer. *Nature Materials* **2005,** 4, (6), 496-502.

67. Garnier, F.; Youssoufi, H. K.; Srivastava, P.; Yassar, A., Enzyme Recognition by Polypyrrole Functionalized with Bioactive Peptides. *Journal of the American Chemical Society* **1994,** 116, (19), 8813-8814.

68. Cui, X. Y.; Martin, D. C., Electrochemical deposition and characterization of poly(3,4-ethylenedioxythiophene) on neural microelectrode arrays. *Sensors and Actuators B-Chemical* **2003,** 89, (1-2), 92-102.

69. Asplund, M.; von Holst, H.; Inganas, O., Composite biomolecule/PEDOT materials for neural electrodes. *Biointerphases* **2008,** 3, (3), 83-93.

70. Green, R. A.; Lovell, N. H.; Poole-Warren, L. A., Impact of co-incorporating laminin peptide dopants and neurotrophic growth factors on conducting polymer properties. *Acta Biomater.* **2010,** 6, (1), 63-71.

71. Richardson-Burns, S. M.; Hendricks, J. L.; Foster, B.; Povlich, L. K.; Kim, D. H.; Martin, D. C., Polymerization of the conducting polymer poly(3,4-ethylenedioxythiophene) (PEDOT) around living neural cells. *Biomaterials* **2007,** 28, (8), 1539-1552.

72. Green, R. A.; Lovell, N. H.; Poole-Warren, L. A., Cell attachment functionality of bioactive conducting polymers for neural interfaces. *Biomaterials* **2009,** 30, (22), 3637-3644.

73. Fabregat, G.; Teixeira-Dias, B.; del Valle, L. J.; Armelin, E.; Estrany, F.; Aleman, C., Incorporation of a Clot-Binding Peptide into Polythiophene: Properties of Composites for Biomedical Applications. *Acs Applied Materials & Interfaces* **2014,** 6, (15), 11940-11954.

74. Jakubiak, R.; Bao, Z.; Rothberg, L., Dendritic sidegroups as three-dimensional barriers to aggregation quenching of conjugated polymer fluorescence. *Synth. Met.* **2000,** 114, (1), 61-64.

75. Sirringhaus, H.; Brown, P. J.; Friend, R. H.; Nielsen, M. M.; Bechgaard, K.; Langeveld-Voss, B. M. W.; Spiering, A. J. H.; Janssen, R. A. J.; Meijer, E. W., Microstructure-mobility correlation in self-organised, conjugated polymer field-effect transistors. *Synth. Met.* **2000,** 111, 129-132.

76. Nguyen, T. Q.; Martini, I. B.; Liu, J.; Schwartz, B. J., Controlling interchain interactions in conjugated polymers: The effects of chain morphology on exciton-exciton annihilation and aggregation in MEH-PPV films. *J. Phys. Chem. B* **2000,** 104, (2), 237-255.

77. Menon, A.; Dong, H. P.; Niazimbetova, Z. I.; Rothberg, L. J.; Galvin, M. E., Polydispersity effects on conjugated polymer light-emitting diodes. *Chem. Mater.* **2002,** 14, (9), 3668-3675.

78. Sherwood, G. A.; Cheng, R.; Smith, T. M.; Werner, J. H.; Shreve, A. P.; Peteanu, L. A.; Wildeman, J., Aggregation Effects on the Emission Spectra and Dynamics of Model Oligomers of MEH-PPV. *J. Phys. Chem. C* **2009,** 113, (43), 18851-18862.

79. Kas, O. Y.; Charati, M. B.; Kiick, K. L.; Galvin, M. E., Manipulating association of electroactive chromophores via the use of peptidic templates. *Chem. Mater.* **2006,** 18, (18), 4238-4245.

80. Kumar, R. J.; MacDonald, J. M.; Singh, T. B.; Waddington, L. J.; Holmes, A. B., Hierarchical Self-Assembly of Semiconductor Functionalized Peptide alpha-Helices and Optoelectronic Properties. *J. Am. Chem. Soc.* **2011,** 133, (22), 8564-8573.

81. Vadehra, G. S.; Wall, B. D.; Diegelmann, S. R.; Tovar, J. D., On-resin dimerization incorporates a diverse array of pi-conjugated functionality within aqueous self-assembling peptide backbones. *Chem. Commun.* **2010,** 46, (22), 3947-3949.

82. Varghese, R.; Wagenknecht, H.-A., DNA as a supramolecular framework for the helical arrangements of chromophores: towards photoactive DNA-based nanomaterials. *Chem. Commun.* **2009**, (19), 2615-2624.

83. Hariharan, M.; Siegmund, K.; Zheng, Y.; Long, H.; Schatz, G. C.; Lewis, F. D., Perylenediimide-Linked DNA Dumbbells: Long-Distance Electronic Interactions and Hydrophobic Assistance of Base-Pair Melting. *J. Phys. Chem. C* **2010,** 114, (48), 20466-20471.

84. Iwaura, R.; Ohnishi-Kameyama, M.; Iizawa, T., Construction of Helical J-Aggregates Self-Assembled from a Thymidylic Acid Appended Anthracene Dye and DNA as a Template. *Chem. Eur. J.* **2009,** 15, (15), 3729-3735.

85. Schmid, S.; Mena-Osteritz, E.; Kopyshev, A.; Baeuerle, P., Self-Assembling Carbohydrate-Functionalized Oligothiophenes. *Org. Lett.* **2009,** 11, (22), 5098-5101.

86. Matmour, R.; De Cat, I.; George, S. J.; Adriaens, W.; Leclere, P.; Bomans, P. H. H.; Sommerdijk, N.; Gielen, J. C.; Christianen, P. C. M.; Heldens, J. T.; van Hest, J. C. M.; Lowik, D.; De Feyter, S.; Meijer, E. W.; Schenning, A., Oligo(p-phenylenevinylene)-Peptide Conjugates: Synthesis and Self-Assembly in Solution and at the Solid-Liquid Interface. *J. Am. Chem. Soc.* **2008,** 130, (44), 14576-14583.

87. Wigenius, J.; Bjork, P.; Hamedi, M.; Aili, D., Supramolecular Assembly of Designed alpha-Helical Polypeptide-Based Nanostructures and Luminescent Conjugated Polyelectrolytes. *Macromol. Biosci.* **2010,** 10, (8), 836-841.

88. Sinkeldam, R. W.; Hoeben, F. J. M.; Pouderoijen, M. J.; De Cat, I.; Zhang, J.; Furukawa, S.; De Feyter, S.; Vekemans, J.; Meijer, E. W., Chiral alignment of OPV chromophores: Exploitation of the ureidophthalimide-based foldamer. *J. Am. Chem. Soc.* **2006,** 128, (50), 16113-16121.

89. Guryanov, I.; Moretto, A.; Campestrini, S.; Broxterman, Q. B.; Kaptein, B.; Peggion, C.; Formaggio, F.; Toniolo, C., Turn and helical peptide spacers: Combined distance and angular dependencies in the exciton-coupled circular dichroism of intramolecularly interacting bis-porphyrins. *Biopolymers* **2006,** 82, (5), 482-490.

90. McAllister, K. A.; Zou, H.; Cochran, F. V.; Bender, G. M.; Senes, A.; Fry, H. C.; Nanda, V.; Keenan, P. A.; Lear, J. D.; Saven, J. G.; Therien, M. J.; Blasie, J. K.; DeGrado, W. F., Using alpha-helical coiled-coils to design nanostructured metalloporphyrin arrays. *J. Am. Chem. Soc.* **2008,** 130, (36), 11921-11927.

91. Oancea, S.; Formaggio, F.; Campestrini, S.; Broxterman, Q. B.; Kaptein, B.; Toniolo, C., Distance dependency of exciton coupled circular dichroism using turn and helical peptide spacers. *Biopolymers* **2003,** 72, (2), 105-115.

92. Dunetz, J. R.; Sandstrom, C.; Young, E. R.; Baker, P.; Van Name, S. A.; Cathopolous, T.; Fairman, R.; de Paula, J. C.; Akerfeldt, K. S., Self-assembling porphyrin-modified peptides. *Org. Lett.* **2005,** 7, (13), 2559-2561.

93. Pepe-Mooney, B. J.; Kokona, B.; Fairman, R., Characterization of Mesoscale Coiled-Coil Peptide-Porphyrin Complexes. *Biomacromolecules* **2011,** 12, (12), 4196-4203.

94. Janssen, P. G. A.; Meeuwenoord, N.; van der Marel, G.; Jabbari-Farouji, S.; van der Schoot, P.; Surin, M.; Tomovic, Z.; Meijer, E. W.; Schenning, A. P. H. J., ssPNA templated assembly of oligo(p-phenylenevinylene)s. *Chem. Commun.* **2010,** 46, (1), 109-111.

95. Wilson, T. M.; Zeidan, T. A.; Hariharan, M.; Lewis, F. D.; Wasielewski, M. R., Electron Hopping among Cofacially Stacked Perylenediimides Assembled by Using DNA Hairpins. *Angew. Chem., Int. Ed.* **2010,** 49, (13), 2385-2388.

96. Probst, M.; Wenger, D.; Biner, S. M.; Haner, R., The DNA three-way junction as a mould for tripartite chromophore assembly. *Org. Biomol. Chem.* **2012,** 10, (4), 755-759.

97. Coppock, M. B.; Miller, J. R.; Williams, M. E., Assembly of a Trifunctional Artificial Peptide Into an Anti-Parallel Duplex with Three Cu(II) Cross-links. *Inorg. Chem.* **2011,** 50, (3), 949-955.

98. Stevens, A. L.; Janssen, P. G. A.; Ruiz-Carretero, A.; Surin, M.; Schenning, A.; Herz, L. M., Energy Transfer in Single-Stranded DNA-Templated Stacks of Naphthalene Chromophores. *J. Phys. Chem. C* **2011,** 115, (21), 10550-10560.

99. Sisido, M.; Hoshino, S.; Kusano, H.; Kuragaki, M.; Makino, M.; Sasaki, H.; Smith, T. A.; Ghiggino, K. P., Distance dependence of photoinduced electron transfer along alpha-helical polypeptides. *J. Phys. Chem. B* **2001,** 105, (42), 10407-10415.

100. Serron, S. A.; Aldridge, W. S.; Fleming, C. N.; Danell, R. M.; Baik, M. H.; Sykora, M.; Dattelbaum, D. M.; Meyer, T. J., Evidence for through-space electron transfer in the distance dependence of normal and inverted electron transfer in oligoproline arrays. *J. Am. Chem. Soc.* **2004,** 126, (44), 14506-14514.

101. de Graaf, A. J.; Kooijman, M.; Hennink, W. E.; Mastrobattista, E., Nonnatural Amino Acids for Site-Specific Protein Conjugation. *Bioconjugate Chem.* **2009,** 20, (7), 1281-1295.

102. Peng, Z. H.; Bao, Z. N.; Galvin, M. E., Oxadiazole-containing conjugated polymers for light-emitting diodes. *Adv. Mater.* **1998,** 10, (9), 680-684.

103. Buchwald, E.; Meier, M.; Karg, S.; Posch, P.; Schmidt, H. W.; Strohriegl, P.; Riess, W.; Schwoerer, M., Enhanced Efficiency Of Polymer Light-Emitting-Diodes Utilizing Oxadiazole Polymers. *Adv. Mater.* **1995,** 7, (10), 839-842.

104. Niazimbetova, Z. I.; Christian, H. Y.; Bhandari, Y. J.; Beyer, F. L.; Galvin, M. E., Design and development of novel 2-D oligomers for electroactive device application. *J. Phys. Chem. B* **2004,** 108, (25), 8673-8681.

105. Chakrabartty, A.; Kortemme, T.; Baldwin, R. L., Helix Propensities Of The Amino-Acids Measured In Alanine-Based Peptides Without Helix-Stabilizing Side-Chain Interactions. *Prot. Sci.* **1994,** 3, (5), 843-852.

106. De Filippis, V.; De Antoni, F.; Frigo, M.; de Laureto, P. P.; Fontana, A., Enhanced protein thermostability by Ala -> Aib replacement. *Biochemistry* **1998,** 37, (6), 1686-1696.

107. Pomroy, N. C.; Deber, C. M., Conjugation of polyethylene glycol via a disulfide bond confers water solubility upon a peptide model of a protein transmembrane segment. *Anal. Biochem.* **1999,** 275, (2), 224-230.

108. Shu, J. Y.; Tan, C.; DeGrado, W. F.; Xu, T., New design of helix bundle peptide-polymer conjugates. *Biomacromolecules* **2008,** 9, (8), 2111-2117.

109. Bailon, P.; Palleroni, A.; Schaffer, C. A.; Spence, C. L.; Fung, W. J.; Porter, J. E.; Ehrlich, G. K.; Pan, W.; Xu, Z. X.; Modi, M. W.; Farid, A.; Berthold, W., Rational design of a potent, long-lasting form of interferon: A 40 kDa branched polyethylene glycol-conjugated interferon alpha-2a for the treatment of hepatitis C. *Bioconjugate Chem.* **2001,** 12, (2), 195-202.

110. Basu, A.; Yang, K.; Wang, M. L.; Liu, S.; Chintala, R.; Palm, T.; Zhao, H.; Peng, P.; Wu, D. C.; Zhang, Z. F.; Hua, J.; Hsieh, M. C.; Zhou, J.; Petti, G.; Li, X. G.; Janjua, A.; Mendez, M.; Liu, J.; Longley, C.; Zhang, Z.; Mehlig, M.; Borowski, V.; Viswanathan, M.; Filpula, D., Structure-function engineering of interferon-beta-1b for improving stability, solubility, potency, immunogenicity, and pharmacokinetic properties by site-selective mono-PEGylation. *Bioconjugate Chem.* **2006,** 17, (3), 618-630.

111. Russell, R. J.; Pishko, M. V.; Simonian, A. L.; Wild, J. R., Poly(ethylene glycol) hydrogel-encapsulated fluorophore-enzyme conjugates for direct detection of organophosphorus neurotoxins. *Anal. Chem.* **1999,** 71, (21), 4909-4912.

112. Soares, A. L.; Guirmaraes, G. M.; Polakiewicz, B.; Pitombo, R. N. D.; Abrahao-Neto, J., Effects of polyethylene glycol attachment on physicochemical and biological stability of E-coli L-asparaginase. *Int. J. Pharm.* **2002,** 237, (1-2), 163-170.

113. Yang, Z. J.; Wang, J. H.; Yoshioka, T.; Li, B. Q.; Lu, Q.; Li, S. K.; Sun, X. H.; Tan, Y. Y.; Yagi, S. G.; Frenkel, E. P.; Hoffman, R. M., Pharmacokinetics, methionine depletion, and antigenicity of recombinant methioninase in primates. *Clin. Cancer Res.* **2004,** 10, (6), 2131-2138.

114. Harada, A.; Cammas, S.; Kataoka, K., Stabilized alpha-helix structure of poly(L-lysine)-block-poly(ethylene glycol) in aqueous medium through supramolecular assembly. *Macromolecules* **1996,** 29, (19), 6183-6188.

115. Jain, A.; Ashbaugh, H. S., Helix Stabilization of Poly(ethylene glycol)-Peptide Conjugates. *Biomacromolecules* **2011,** 12, (7), 2729-2734.

116. Butterfield, S. M.; Patel, P. R.; Waters, M. L., Contribution of aromatic interactions to alpha-helix stability. *J. Am. Chem. Soc.* **2002,** 124, (33), 9751-9755.

117. Shi, Z. S.; Olson, C. A.; Kallenbach, N. R., Cation-pi interaction in model alpha-helical peptides. *J. Am. Chem. Soc.* **2002,** 124, (13), 3284-3291.

118. Turro, N. J., *Modern Molecular Photochemistry*. University Science Books, Sausalito, CA 1991.

119. Kokona, B.; Kim, A. M.; Roden, R. C.; Daniels, J. P.; Pepe-Mooney, B. J.; Kovaric, B. C.; de Paula, J. C.; Johnson, K. A.; Fairman, R., Self Assembly of Coiled-Coil Peptide-Porphyrin Complexes. *Biomacromolecules* **2009,** 10, (6), 1454-1459.

120. Porzio, W.; Destri, S.; Giovanella, U.; Pasini, M.; Marin, L.; Iosip, M. D.; Campione, M., Solid state properties of oligomers, containing dithienothiophene or fluorene residues suitable for field effect transistor devices. *Thin Solid Films* **2007,** 515, (18), 7318-7323.

121. Friesen, B. A.; Nishida, K. R. A.; McHale, J. L.; Mazur, U., New Nanoscale Insights into the Internal Structure of Tetrakis(4-sulfonatophenyl) Porphyrin Nanorods. *J. Phys. Chem. C* **2009,** 113, (5), 1709-1718.

122. Harada, N.; Nakanishi, K., *Circular Dichroic Spectroscopy – Exciton Coupling in Organic Stereochemistry*. University Science Books, Mill Valley, Ca: 1983.

123. Nakanishi, K.; Berova, N., *Circular Dichroism, Principle and Applications*. Wiley-VCH Publishers Inc: New York, 1994.

124. Lewis, F. D.; Liu, X. Y.; Wu, Y. S.; Zuo, X. B., Stepwise evolution of the structure and electronic properties of DNA. *J. Am. Chem. Soc.* **2003,** 125, (42), 12729-12731.

125. Kuciauskas, D.; Caputo, G. A., Self-Assembly of Peptide-Porphyrin Complexes Leads to pH-dependent Excitonic Coupling. *J. Phys. Chem. B* **2009,** 113, (43), 14439-14447.

126. Norlin, A.; Pan, J.; Leygraf, C., Electrochemical behavior of stimulation/sensing materials for pacemaker electrode applications III. Nanoporous and smooth carbon electrodes. *Journal Of The Electrochemical Society* **2005,** 152, (9), J110-J116.

127. Kringelbach, M. L.; Jenkinson, N.; Owen, S. L. F.; Aziz, T. Z., Translational principles of deep brain stimulation. *Nature Reviews Neuroscience* **2007,** 8, (8), 623-635.

128. Eisen, M. D., Djourno, Eyries, and the first implanted electrical neural stimulator to restore hearing. *Otology & Neurotology* **2003,** 24, (3), 500-506.

129. Weiland, J. D.; Liu, W. T.; Humayun, M. S., Retinal prosthesis. In *Annual Review Of Biomedical Engineering*, **2005**, 7, 361-401.

130. Mercanzini, A.; Renaud, P.; Mercanzini, A., *Microfabricated Cortical Neuroprostheses*. CRC press: **2010**.

131. Forrest, S. R., The path to ubiquitous and low-cost organic electronic appliances on plastic. *Nature* **2004,** 428, (6986), 911-918.

132. Groenendaal, B. L.; Jonas, F.; Freitag, D.; Pielartzik, H.; Reynolds, J. R., Poly(3,4-ethylenedioxythiophene) and its derivatives: Past, present, and future. *Adv. Mater.* **2000,** 12, (7), 481-494.

133. Aasmundtveit, K. E.; Samuelsen, E. J.; Inganas, O.; Pettersson, L. A. A.; Johansson, T.; Ferrer, S., Structural aspects of electrochemical doping and dedoping of poly(3,4-ethylenedioxythiophene). *Synth. Met.* **2000,** 113, (1-2), 93-97.

134. Meskers, S. C. J.; van Duren, J. K. J.; Janssen, R. A. J.; Louwet, F.; Groenendaal, L., Infrared detectors with poly(3,4-ethylenedioxy thiophene)/poly(styrene sulfonic acid) (PEDOT/PSS) as the active material. *Adv. Mater.* **2003,** 15, (7-8), 613-616.

135. Hohnholz, D.; MacDiarmid, A. G.; Sarno, D. M.; Jones, W. E., Uniform thin films of poly-3,4-ethylenedioxythiophene (PEDOT) prepared by in-situ deposition. *Chem. Commun.* **2001**, (23), 2444-2445.

136. Xiao, Y. H.; Cui, X. Y.; Martin, D. C., Electrochemical polymerization and properties of PEDOT/S-EDOT on neural microelectrode arrays. *J. Electroanal. Chem.* **2004,** 573, (1), 43-48.

137. Zhang, Z. Y.; Tao, Y. J.; Xu, X. Q.; Zhou, Y. J.; Cheng, H. F.; Zheng, W. W., Multicolor electrochromism of low-bandgap copolymers based on pyrrole and 3,4-ethylenedioxythiophene: Fine-tuning colors through feed ratio. *J. Appl. Polym. Sci.* **2013,** 129, (3), 1506-1512.

138. Zhang, C.; Xu, Y.; Wang, N. C.; Xu, Y.; Xiang, W. Q.; Ouyang, M.; Ma, C. N., Electrosyntheses and characterizations of novel electrochromic copolymers based on pyrene and 3,4-ethylenedioxythiophene. *Electrochim. Acta* **2009,** 55, (1), 13-18.

139. Akoudad, S.; Roncali, J., Modification of the electrochemical and electronic properties of electrogenerated poly(3,4-ethylenedioxythiophene) by hydroxymethyl and oligo(oxyethylene)substituents. *Electrochem. Commun.* **2000,** 2, (1), 72-76.

140. Ali, E. M.; Kantchev, E. A. B.; Yu, H. H.; Ying, J. Y., Conductivity shift of polyethylenedioxythiophenes in aqueous solutions from side-chain charge perturbation. *Macromolecules* **2007,** 40, (17), 6025-6027.

141. Krishnamoorthy, K.; Kanungo, M.; Contractor, A. Q.; Kumar, A., Electrochromic polymer based on a rigid cyanobiphenyl substituted 3,4-ethylenedioxythiophene. *Synth. Met.* **2001,** 124, (2-3), 471-475.

142. Sarac, A. S.; Sonmez, G.; Cebeci, F. Ã., Electrochemical synthesis and structural studies of polypyrroles, poly(3,4-ethylene-dioxythiophene)s and copolymers of pyrrole and 3,4-ethylenedioxythiophene on carbon fibre microelectrodes. *J. Appl. Electrochem.* **2003,** 33, (3-4), 295-301.

143. Xu, J. K.; Nie, G. M.; Zhang, S. S.; Han, X. J.; Hou, J.; Pu, S. Z., Electrochemical copolymerization of indole and 3,4-ethylenedioxythiophene. *J. Mater. Sci.* **2005,** 40, (11), 2867-2873.

144. Yohannes, T.; Carlberg, J. C.; InganÃ¤s, O.; Solomon, T., Electrochemical and spectroscopic characteristics of copolymers electrochemically synthesized from 3-methylthiophene and 3,4-ethylenedioxy thiophene. *Synth. Met.* **1997,** 88, (1), 15-21.

145. Luo, S. C.; Ali, E. M.; Tansil, N. C.; Yu, H. H.; Gao, S.; Kantchev, E. A. B.; Ying, J. Y., Poly(3,4-ethylenedioxythiophene) (PEDOT) nanobiointerfaces: Thin, ultrasmooth, and functionalized PEDOT films with in vitro and in vivo biocompatibility. *Langmuir* **2008,** 24, (15), 8071-8077.

146. Tiraferri, A.; Elimelech, M., Direct quantification of negatively charged functional groups on membrane surfaces. *J. Membr. Sci.* **2012,** 389, 499-508.

147. Djordjevic, I.; Choudhury, N. R.; Dutta, N. K.; Kumar, S.; Szili, E. J.; Steele, D. A., Polyoctanediol Citrate/Sebacate Bioelastomer Films: Surface Morphology, Chemistry and Functionality. *J. Biomater. Sci., Polym. Ed.* **2010,** 21, (2), 237-251.

148. Jonsson, S. K. M.; Birgerson, J.; Crispin, X.; Greczynski, G.; Osikowicz, W.; Denier van der Gon, A. W.; Salaneck, W. R.; Fahlman, M., The effects of solvents on the morphology and sheet resistance in poly(3,4-ethylenedioxythiophene)-polystyrenesulfonic acid (PEDOT-PSS) films. *Synth. Met.* **2003,** 139, (1), 1-10.

149. Sriprachuabwong, C.; Karuwan, C.; Wisitsorrat, A.; Phokharatkul, D.; Lomas, T.; Sritongkham, P.; Tuantranont, A., Inkjet-printed graphene-PEDOT:PSS modified screen printed carbon electrode for biochemical sensing. *J. Mater. Chem.* **2012,** 22, (12), 5478-5485.

150. Dobbelin, M.; Marcilla, R.; Tollan, C.; Pomposo, J. A.; Sarasua, J. R.; Mecerreyes, D., A new approach to hydrophobic and water-resistant poly(3,4-ethylenedioxythiophene): poly(styrenesulfonate) films using ionic liquids. *J. Mater. Chem.* **2008,** 18, (44), 5354-5358.

151. Drelich, J.; Wilbur, J. L.; Miller, J. D.; Whitesides, G. M., Contact angles for liquid drops at a model heterogeneous surface consisting of alternating and parallel hydrophobic hydrophilic strips. *Langmuir* **1996,** 12, (7), 1913-1922.

152. Kim, D. H.; Richardson-Burns, S. M.; Hendricks, J. L.; Sequera, C.; Martin, D. C., Effect of immobilized nerve growth factor on conductive polymers: Electrical properties and cellular response. *Adv. Funct. Mater.* **2007,** 17, (1), 79-86.

153. Abidian, M. R.; Kim, D. H.; Martin, D. C., Conducting-polymer nanotubes for controlled drug release. *Adv. Mater.* **2006,** 18, (4), 405-409.

154. Luo, S. C.; Sekine, J.; Zhu, B.; Zhao, H. C.; Nakao, A.; Yu, H. H., Polydioxythiophene Nanodots, Nonowires, Nano-Networks, and Tubular Structures: The Effect of Functional Groups and Temperature in Template-Free Electropolymerization. *Acs Nano* **2012,** 6, (4), 3018-3026.

155. Bolognesi, A.; DiGianvincenzo, P.; Giovanella, U.; Mendichi, R.; Schieroni, A. G., Polystyrene functionalized with EDOT oligomers. *Eur. Polym. J.* **2008,** 44, (3), 793-800.

156. Lapkowski, M.; Pron, A., Electrochemical oxidation of poly(3,4-ethylenedioxythiophene) - "in situ" conductivity and spectroscopic investigations. *Synth. Met.* **2000,** 110, (1), 79-83.

157. Hwang, J.; Tanner, D. B.; Schwendeman, I.; Reynolds, J. R., Optical properties of nondegenerate ground-state polymers: Three dioxythiophene-based conjugated polymers. *Phys. Rev. B* **2003,** 67, (11), 115205-10.

158. Blanchard, F.; Carre, B.; Bonhomme, F.; Biensan, P.; Pages, H.; Lemordant, D., Study of poly(3,4-ethylenedioxythiophene) films prepared in propylene carbonate solutions containing different lithium salts. *J. Electroanal. Chem.* **2004,** 569, (2), 203-210.

159. Kiefer, R.; Bowmaker, G. A.; Cooney, R. P.; Kilmartin, P. A.; Travas-Sejdic, J., Cation driven actuation for free standing PEDOT films prepared from propylene carbonate electrolytes containing TBACF3SO3. *Electrochim. Acta* **2008,** 53, (5), 2593-2599.

160. Chang, C. C.; Her, L. J.; Hong, J. L., Copolymer from electropolymerization of thiophene and 3,4-ethylenedioxythiophene and its use as cathode for lithium ion battery. *Electrochim. Acta* **2005,** 50, (22), 4461-4468.

161. Lima, A.; Schottland, P.; Sadki, S.; Chevrot, C., Electropolymerization of 3,4-ethylenedioxythiophene and 3,4-ethylenedioxythiophene methanol in the presence of dodecylbenzenesulfonate. *Synth. Met.* **1998,** 93, (1), 33-41.

162. Hameed, N.; Thomas, S. P.; Abraham, R.; Thomas, S., Morphology and contact angle studies of poly(styrene-co-acrylonitrile) modified epoxy resin blends and their glass fibre reinforced composites. *Express Polym. Lett.* **2007,** 1, (6), 345-355.

163. Feng, L.; Li, S. H.; Li, Y. S.; Li, H. J.; Zhang, L. J.; Zhai, J.; Song, Y. L.; Liu, B. Q.; Jiang, L.; Zhu, D. B., Super-hydrophobic surfaces: From natural to artificial. *Adv. Mater.* **2002,** 14, (24), 1857-1860.

164. Lafuma, A.; Quere, D., Superhydrophobic states. *Nat. Mater.* **2003,** 2, (7), 457-460.

165. Doherty, W. J.; Wysocki, R. J.; Armstrong, N. R.; Saavedra, S. S., Electrochemical copolymerization and spectroelectrochemical characterization of 3,4-ethylenedioxythiophene and 3,4-ethylenedioxythiophene-methanol copolymers on indium-tin oxide. *Macromolecules* **2006,** 39, (13), 4418-4424.

166. Wu, S.; Han, S.; Zheng, Y.; Zheng, H.; Liu, N.; Wang, L.; Cao, Y.; Wang, J., pH-neutral PEDOT:PSS as hole injection layer in polymer light emitting diodes. *Organic Electronics* **2011,** 12, (3), 504-508.

167. Muenzer, A. M.; Melzer, K.; Heimgreiter, M.; Scarpa, G., Random CNT network and regioregular poly(3-hexylthiophen) FETs for pH sensing applications: A comparison. *Biochimica Et Biophysica Acta-General Subjects* **2013,** 1830, (9), 4353-4358.

168. Liu, Z.; Parvez, K.; Li, R.; Dong, R.; Feng, X.; Muellen, K., Transparent Conductive Electrodes from Graphene/PEDOT:PSS Hybrid Inks for Ultrathin Organic Photodetectors. *Advanced Materials* **2015,** 27, (4), 669-675.

169. Bernius, M. T.; Inbasekaran, M.; O'Brien, J.; Wu, W. S., Progress with light-emitting polymers. *Advanced Materials* **2000,** 12, (23), 1737-1750.

170. Nasybulin, E.; Wei, S.; Cox, M.; Kymissis, I.; Levon, K., Morphological and Spectroscopic Studies of Electrochemically Deposited Poly(3,4-ethylenedioxythiophene) (PEDOT) Hole Extraction Layer for Organic Photovoltaic Device (OPVd) Fabrication. *Journal of Physical Chemistry C* **2011,** 115, (10), 4307-4314.

171. Jensen, J.; Dyer, A. L.; Shen, D. E.; Krebs, F. C.; Reynolds, J. R., Direct Photopatterning of Electrochromic Polymers. *Advanced Functional Materials* **2013,** 23, (30), 3728-3737.

172. Green, R. A.; Lovell, N. H.; Wallace, G. G.; Poole-Warren, L. A., Conducting polymers for neural interfaces: Challenges in developing an effective long-term implant. *Biomaterials* **2008,** 29, (24-25), 3393-3399.

173. Ludwig, K. A.; Uram, J. D.; Yang, J.; Martin, D. C.; Kipke, D. R., Chronic neural recordings using silicon microelectrode arrays electrochemically deposited with a poly(3,4-ethylenedioxythiophene) (PEDOT) film. *Journal of Neural Engineering* **2006,** 3, (1), 59-70.

174. Cheong, G. L. M.; Lim, K. S.; Jakubowicz, A.; Martens, P. J.; Poole-Warren, L. A.; Green, R. A., Conductive hydrogels with tailored bioactivity for implantable electrode coatings. *Acta Biomaterialia* **2014,** 10, (3), 1216-1226.

175. Subramanian, A.; Krishnan, U. M.; Sethuraman, S., Development of biomaterial scaffold for nerve tissue engineering: Biomaterial mediated neural regeneration. *Journal of Biomedical Science* **2009,** 16, 108-118.

176. Zhang, M.; Lin, P.; Yang, M.; Yan, F., Fabrication of organic electrochemical transistor arrays for biosensing. *Biochimica Et Biophysica Acta-General Subjects* **2013,** 1830, (9), 4402-4406.

177. Green, R. A.; Williams, C. M.; Lovell, N. H.; Poole-Warren, L. A., Novel neural interface for implant electrodes: improving electroactivity of polypyrrole through MWNT incorporation. *Journal of Materials Science-Materials in Medicine* **2008,** 19, (4), 1625-1629.

178. Cui, X. Y.; Wiler, J.; Dzaman, M.; Altschuler, R. A.; Martin, D. C., In vivo studies of polypyrrole/peptide coated neural probes. *Biomaterials* **2003,** 24, (5), 777-787.

179. Abidian, M. R.; Corey, J. M.; Kipke, D. R.; Martin, D. C., Conducting-Polymer Nanotubes Improve Electrical Properties, Mechanical Adhesion, Neural Attachment, and Neurite Outgrowth of Neural Electrodes. *Small* **2010,** 6, (3), 421-429.

180. Abidian, M. R.; Martin, D. C., Experimental and theoretical characterization of implantable neural microelectrodes modified with conducting polymer nanotubes. *Biomaterials* **2008,** 29, (9), 1273-1283.

181. Karagkiozaki, V.; Karagiannidis, P. G.; Gioti, M.; Kavatzikidou, P.; Georgiou, D.; Georgaraki, E.; Logothetidis, S., Bioelectronics meets nanomedicine for cardiovascular implants: PEDOT-based nanocoatings for tissue regeneration. *Biochimica Et Biophysica Acta-General Subjects* **2013,** 1830, (9), 4294-4304.

182. Mawad, D.; Stewart, E.; Officer, D. L.; Romeo, T.; Wagner, P.; Wagner, K.; Wallace, G. G., A Single Component Conducting Polymer Hydrogel as a Scaffold for Tissue Engineering. *Advanced Functional Materials* **2012,** 22, (13), 2692-2699.

183. Zheng, W.; Razal, J. M.; Whitten, P. G.; Ovalle-Robles, R.; Wallace, G. G.; Baughman, R. H.; Spinks, G. M., Artificial Muscles Based on Polypyrrole/Carbon Nanotube Laminates. *Advanced Materials* **2011,** 23, (26), 2966-2970.

184. Gomez, N.; Lee, J. Y.; Nickels, J. D.; Schmidt, C. E., Micropatterned polypyrrole: A combination of electrical and topographical characteristics for the stimulation of cells. *Advanced Functional Materials* **2007,** 17, (10), 1645-1653.

185. Wang, H.-j.; Ji, L.-w.; Li, D.-f.; Wang, J.-y., Characterization of nanostructure and cell compatibility of polyaniline films with different dopant acids. *Journal of Physical Chemistry B* **2008,** 112, (9), 2671-2677.

186. Stewart, E. M.; Fabretto, M.; Mueller, M.; Molino, P. J.; Griesser, H. J.; Short, R. D.; Wallace, G. G., Cell attachment and proliferation on high conductivity PEDOT-glycol composites produced by vapour phase polymerisation. *Biomaterials Science* **2013,** 1, (4), 368-378.

187. Cen, L.; Neoh, K. G.; Li, Y.; Kang, E. T., Assessment of in vitro bioactivity of hyaluronic acid and sulfated hyaluronic acid functionalized electroactive polymer. *Biomacromolecules* **2004,** 5, (6), 2238-2246.

188. Balint, R.; Cassidy, N. J.; Cartmell, S. H., Conductive polymers: Towards a smart biomaterial for tissue engineering. *Acta Biomaterialia* **2014,** 10, (6), 2341-2353.

189. Ateh, D. D.; Vadgama, P.; Navsaria, H. A., Culture of human keratinocytes on polypyrrole-based conducting polymers. *Tissue Engineering* **2006,** 12, (4), 645-655.

190. Tashiro, K.; Sephel, G. C.; Weeks, B.; Sasaki, M.; Martin, G. R.; Kleinman, H. K.; Yamada, Y., A synthetic peptide containing the IKVAV sequence from the A chain of laminin mediates cell attachment, migration, and neurite outgrowth. *Journal of Biological Chemistry* **1989,** 264, (27), 16174-16182.

191. Hager, G.; Pawelzik, H.; Kreutzberg, G. W.; Zieglgansberger, W., A peptide derived from a neurite outgrowth-promoting domain on the gamma(1) chain of laminin modulates the electrical properties of neocortical neurons. *Neuroscience* **1998,** 86, (4), 1145-1154.

192. Ranieri, J. P.; Bellamkonda, R.; Bekos, E. J.; Gardella, J. A.; Mathieu, H. J.; Ruiz, L.; Aebischer, P., Spatial control of neuronal cell attachment and differentiation on covalently patterned laminin oligopeptide substrates. *International Journal of Developmental Neuroscience* **1994,** 12, (8), 725-735.

193. Bellamkonda, R.; Ranieri, J. P.; Aebischer, P., Laminin oligopeptide derivatized agarose gels allow 3-dimensional neurite extension in-vitro. *Journal of Neuroscience Research* **1995,** 41, (4), 501-509.

194. Borkenhagen, M.; Clemence, J. F.; Sigrist, H.; Aebischer, P., Three-dimensional extracellular matrix engineering in the nervous system. *Journal of Biomedical Materials Research* **1998,** 40, (3), 392-400.

195. Graf, J.; Iwamoto, Y.; Sasaki, M.; Martin, G. R.; Kleinman, H. K.; Robey, F. A.; Yamada, Y., Identification of an amino-acid-sequence in laminin mediating cell attachment, chemotaxis, and receptor-binding. *Cell* **1987,** 48, (6), 989-996.

196. Hersel, U.; Dahmen, C.; Kessler, H., RGD modified polymers: biomaterials for stimulated cell adhesion and beyond. *Biomaterials* **2003,** 24, (24), 4385-4415.

197. Beer, J. H.; Springer, K. T.; Coller, B. S., Immobilized Arg-Gly-Asp (RGD) peptides of varying lengths as structural probes of the platelet glycoprotein IIb/IIIa receptor. *Blood* **1992,** 79, (1), 117-128.

198. Kantlehner, M.; Finsinger, D.; Meyer, J.; Schaffner, P.; Jonczyk, A.; Diefenbach, B.; Nies, B.; Kessler, H., Selective RGD-mediated adhesion of osteoblasts at surfaces of implants. *Angewandte Chemie-International Edition* **1999,** 38, (4), 560-562.

199. Hern, D. L.; Hubbell, J. A., Incorporation of adhesion peptides into nonadhesive hydrogels useful for tissue resurfacing. *Journal of Biomedical Materials Research* **1998,** 39, (2), 266-276.

200. Massia, S. P.; Hubbell, J. A., An Rgd Spacing of 440nm is Sufficient for Integrin Alpha-V-Beta-3-Mediated Fibroblast Spreading and 140nm for Focal Contact and Stress Fiber Formation. *Journal of Cell Biology* **1991,** 114, (5), 1089-1100.

201. Le Saux, G.; Magenau, A.; Gunaratnam, K.; Kilian, K. A.; Boecking, T.; Gooding, J. J.; Gaus, K., Spacing of Integrin Ligands Influences Signal Transduction in Endothelial Cells. *Biophysical Journal* **2011,** 101, (4), 764-773.

202. Chollet, C.; Chanseau, C.; Remy, M.; Guignandon, A.; Bareille, R.; Labrugere, C.; Bordenave, L.; Durrieu, M.-C., The effect of RGD density on osteoblast and endothelial cell behavior on RGD-grafted polyethylene terephthalate surfaces. *Biomaterials* **2009,** 30, (5), 711-720.

203. Lagunas, A.; Comelles, J.; Martinez, E.; Prats-Alfonso, E.; Acosta, G. A.; Albericio, F.; Samitier, J., Cell adhesion and focal contact formation on linear RGD molecular gradients: study of non-linear concentration dependence effects. *Nanomedicine-Nanotechnology Biology and Medicine* **2012,** 8, (4), 432-439.

204. King, Z. A.; Shaw, C. M.; Spanninga, S. A.; Martin, D. C., Structural, chemical and electrochemical characterization of poly(3,4-Ethylenedioxythiophene) (PEDOT) prepared with various counter-ions and heat treatments. *Polymer* **2011,** 52, (5), 1302-1308.

205. Matsuzawa, M.; Weight, F. F.; Potember, R. S.; Liesi, P., Directional neurite outgrowth and axonal differentiation of embryonic hippocampal neurons are promoted by a neurite outgrowth domain of the B2-chain of laminin. *International Journal of Developmental Neuroscience* **1996,** 14, (3), 283-295.

206. Asplund, M.; Nyberg, T.; Inganas, O., Electroactive polymers for neural interfaces. *Polymer Chemistry* **2010,** 1, (9), 1374-1391.

207. Tang, W.; Becker, M. L., "Click" reactions: a versatile toolbox for the synthesis of peptide-conjugates. *Chemical Society Reviews* **2014,** 43, (20), 7013-7039.

208. Azagarsamy, M. A.; Anseth, K. S., Bioorthogonal Click Chemistry: An Indispensable Tool to Create Multifaceted Cell Culture Scaffolds. *Acs Macro Letters* **2013,** 2, (1), 5-9.

209. Fairbanks, B. D.; Schwartz, M. P.; Halevi, A. E.; Nuttelman, C. R.; Bowman, C. N.; Anseth, K. S., A Versatile Synthetic Extracellular Matrix Mimic via Thiol-Norbornene Photopolymerization. *Advanced Materials* **2009,** 21, (48), 5005-5010.

210. McKinnon, D. D.; Kloxin, A. M.; Anseth, K. S., Synthetic hydrogel platform for three-dimensional culture of embryonic stem cell-derived motor neurons. *Biomaterials Science* **2013,** 1, (5), 460-469.

211. Tang, W.; Ma, Y.; Xie, S.; Guo, K.; Katzenmeyer, B.; Wesdemiotis, C.; Becker, M. L., Valency-Dependent Affinity of Bioactive Hydroxyapatite-Binding Dendrons. *Biomacromolecules* **2013,** 14, (9), 3304-3313.

212. Robin, M. P.; Wilson, P.; Mabire, A. B.; Kiviaho, J. K.; Raymond, J. E.; Haddleton, D. M.; O'Reilly, R. K., Conjugation-Induced Fluorescent Labeling of Proteins and Polymers Using Dithiomaleimides. *Journal of the American Chemical Society* **2013,** 135, (8), 2875-2878.

213. Daugaard, A. E.; Hvilsted, S.; Hansen, T. S.; Larsen, N. B., Conductive polymer functionalization by click chemistry. *Macromolecules* **2008,** 41, (12), 4321-4327.

214. Lind, J. U.; Acikgoez, C.; Daugaard, A. E.; Andresen, T. L.; Hvilsted, S.; Textor, M.; Larsen, N. B., Micropatterning of Functional Conductive Polymers with Multiple Surface Chemistries in Register. *Langmuir* **2012,** 28, (15), 6502-6511.

215. Feldman, K. E.; Martin, D. C., Functional Conducting Polymers via Thiol-ene Chemistry. *Biosensors* **2012,** 2, (3), 305-17.

216. Zaleski, K. J.; Kolodka, T.; Cywes-Bentley, C.; McLoughlin, R. M.; Delaney, M. L.; Charlton, B. T.; Johnson, W.; Tzianabos, A. O., Hyaluronic acid binding peptides prevent experimental staphylococcal wound infection. *Antimicrobial Agents and Chemotherapy* **2006,** 50, (11), 3856-3860.

## Appendix A

## PEDOTacid COPOLYMER FILMS MODIFIED WITH YIGSR BASED PEPTIDES – XPS AND SEM FOR LAMININ-COATED PEPTIDE-MODIFIED FILMS, EIS AND IN VITRO CELL STUDIES FOR PEPTIED ONLY MODIFIED FILMS

### A.1 XPS for Laminin-Coated Peptide-Modified PEDOTacid Films

Figure A-1 demonstrates a representative spectra for all the laminin-coated peptide-modified (physically adsorbed or chemically conjugated) PEDOTacid films. The % contribution of nitrogen for these films is ~11%.

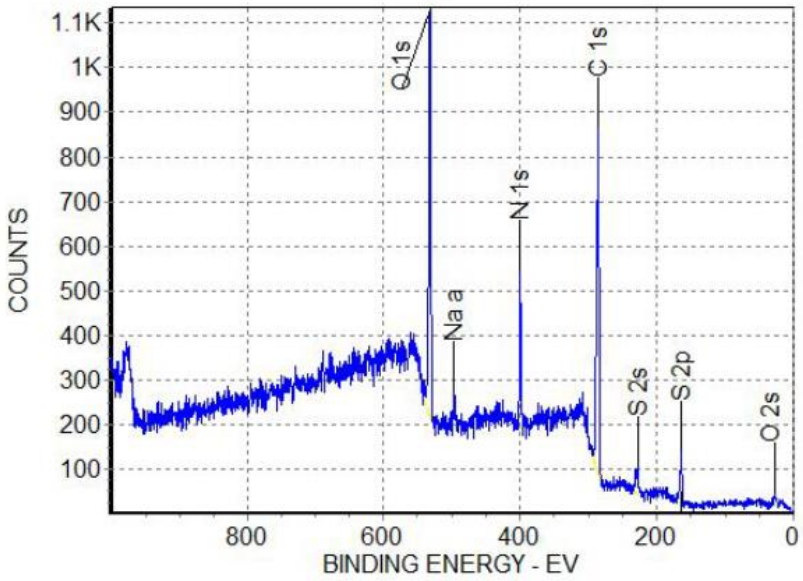


**Figure** A-1 XPS survey spectra for laminin-coated CC $PEG_{10}$-YIGSR.

## A.2 Morphology of Laminin-Coated Peptide-Modified PEDOTacid Films

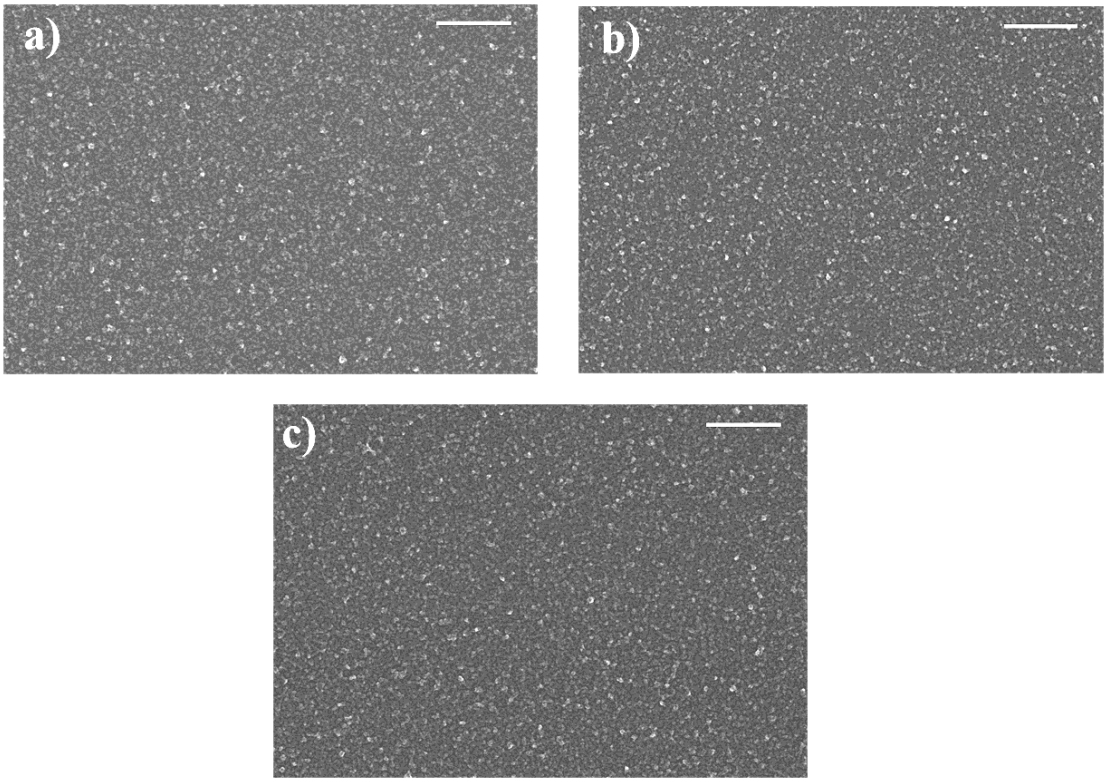


**Figure** A-2 Morphology of laminin-coated peptide-modified PEDOTacid films. a) laminin-coated EA75, b) laminin-coated PA $PEG_{10}$-YIGSR, c) laminin-coated CC-$PEG_{10}$-YIGSR (the scale bar represents 5 µm)

## A.3 Impedance Spectroscopy

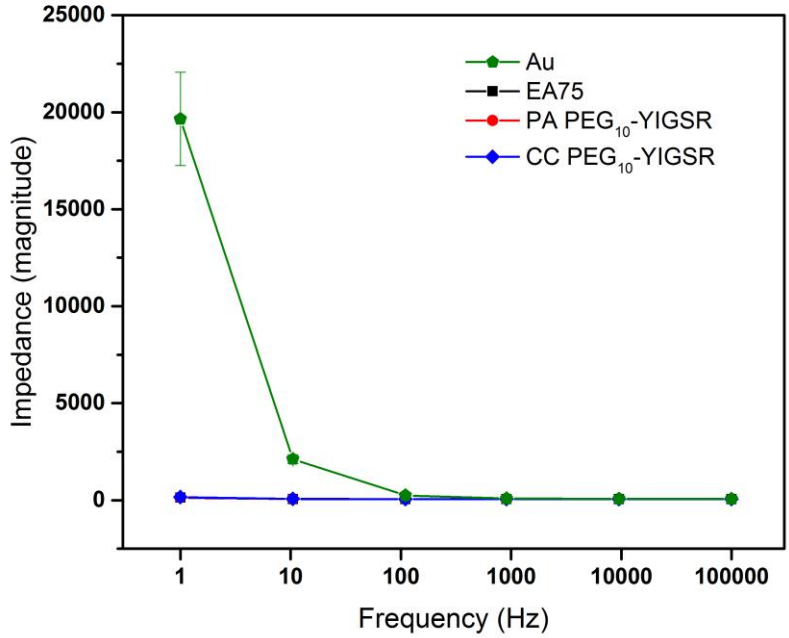


**Figure** A-3 Impedance magnitude comparison for Au electrode with polymer coated films.

## A.4 In-vitro Cell Studies for Peptide-Modified PEDOTacid Films

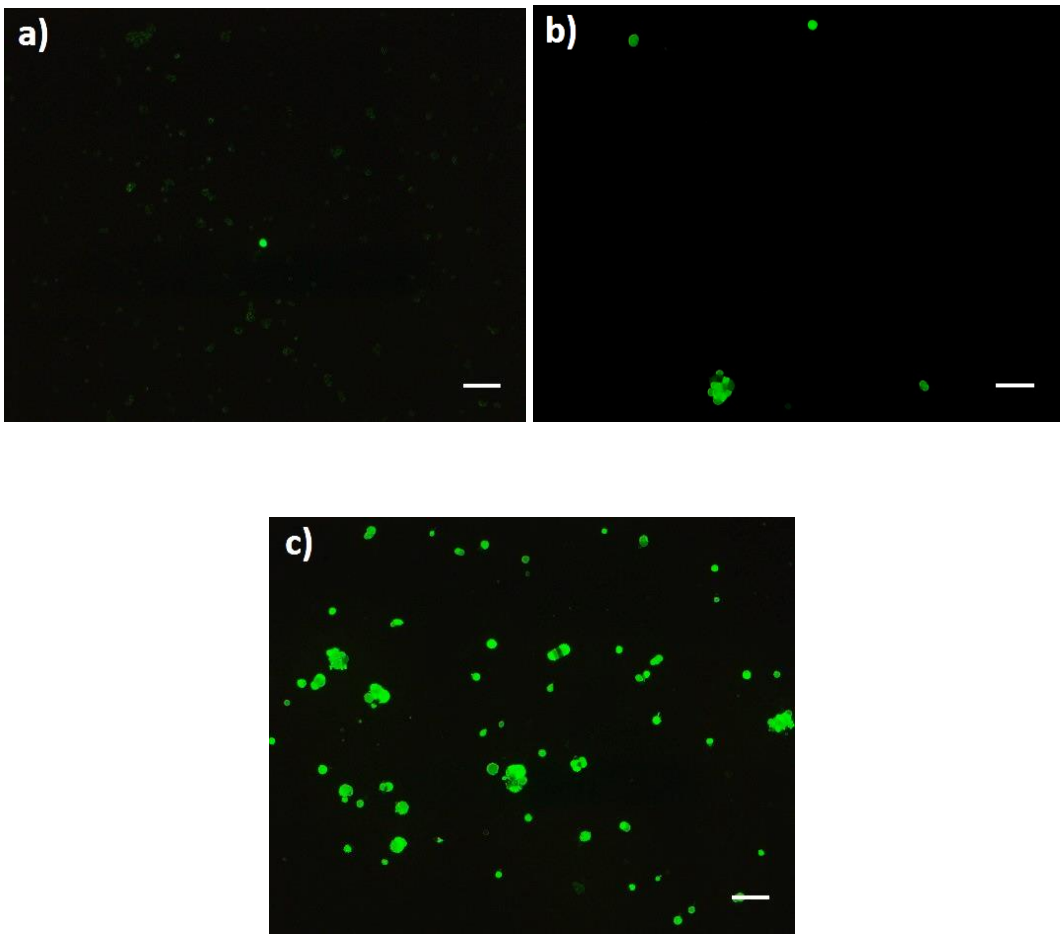


**Figure** A-4 Sample images of PC12 cell attachment on PEDOTacid polymer films before and after peptide modification a) EA75, b) PA $PEG_{10}$-YIGSR, c) CC $PEG_{10}$-YIGSR (the scale bar represents 100 µm)

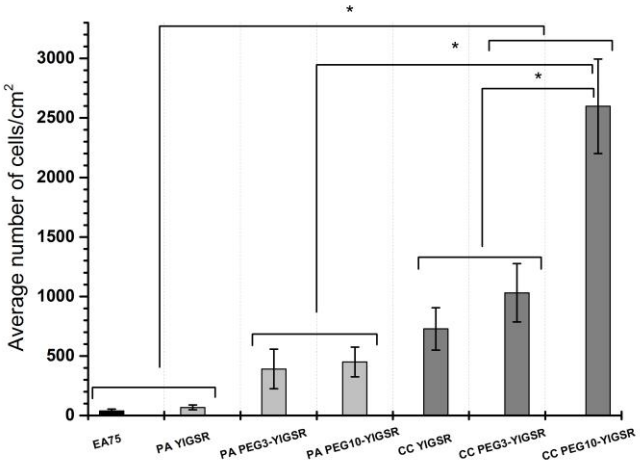


**Figure** A-5 Average number of PC12 cells/cm$^2$ attached to the surface of the PEDOTacid films modified with YIGSR based peptides.

Hydrophilic EA75 films as demonstrated by TBO assay and contact angle measurements (contact angle of 22°) (data not shown) exhibited extremely poor PC12 cell attachment. The carboxylates on the surface also could have led to an overall increase in the negative charge on the surface of the films which could easily have resulted in the cells being repelled by the surface due to the interaction between carboxylates and negatively charged phospholipid cell membrane. This observation is consistent with the behavior of neural cells that are attracted to positively charged surfaces such as poly-L-lysine. When the peptide $PEG_{10}$-YIGSR was physically adsorbed to the surface of the films the number of cells on the surface did increase but this increase was not statistically significant. However, when the peptide $PEG_{10}$-YIGSR was chemically conjugated to the surface of the films, the number of cells attached increased dramatically when compared to EA75 films (Figure A-5). This increase could be attributed to the hydrophilicity of the film decreasing, the increased

concentration of the peptide, and also the reduced number of negative charges on the film as we move from EA75 to PA $PEG_{10}$-YIGSR to CC $PEG_{10}$-YIGSR. Chemically conjugating the YIGSR based nonapeptide to the surface seems to influence the PC12 cells to adhere better to these otherwise hydrophilic surfaces indicating that YIGSR ligand seems to influence cell attachment. Though each of the three peptides chosen, YIGSR (no PEG spacer), $PEG_3$-YIGSR (1 nm PEG spacer) and $PEG_{10}$-YIGSR (3 nm PEG spacer), does have an apparent effect on the cell attachment, $PEG_{10}$-YIGSR is the only peptide that shows statistically significant ($p \leq 0.05$) increase in the number of cells on the surface. Thus chemically conjugating the peptide on the surface yields better activity to the films as compared to the physically adsorbed peptide. The likely improved longevity of the peptide on the surface of the chemically conjugated films results in an increase in cell adhesion, as expected. Since EA75 films coated with whole laminin protein improved cell attachment (Figure 4.10) this condition was used to probe the potential differences in cell differentiation and percent neurite expression of PEDOTacid films modified with YIGSR based peptides.

## Appendix B

## COPYRIGHT PERMISSION LETTERS

### B.1 Permission Letter for Content and Figures in Chapter 2

Acknowledgements to be used by RSC authors

Authors of RSC books and journal articles can reproduce material (for example a figure) from the RSC publication in a non-RSC publication, including theses, without formally requesting permission providing that the correct acknowledgement is given to the RSC publication. This permission extends to reproduction of large portions of text or the whole article or book chapter when being reproduced in a thesis.

The acknowledgement to be used depends on the RSC publication in which the material was published and the form of the acknowledgements is as follows:

• For material being reproduced from an article in *New Journal of Chemistry* the acknowledgement should be in the form:

o [Original citation] - Reproduced by permission of The Royal Society of Chemistry (RSC) on behalf of the Centre National de la Recherche Scientifique (CNRS) and the RSC

• For material being reproduced from an article *Photochemical & Photobiological Sciences* the acknowledgement should be in the form:

o [Original citation] - Reproduced by permission of The Royal Society of Chemistry (RSC) on behalf of the European Society for Photobiology, the European Photochemistry Association, and RSC

• For material being reproduced from an article in *Physical Chemistry Chemical Physics* the acknowledgement should be in the form:

o [Original citation] - Reproduced by permission of the PCCP Owner Societies

• For material reproduced from books and any other journal the acknowledgement should be in the form:

o [Original citation] - Reproduced by permission of The Royal Society of Chemistry

The acknowledgement should also include a hyperlink to the article on the RSC website.

The form of the acknowledgement is also specified in the RSC agreement/licence signed by the corresponding author.

Except in cases of republication in a thesis, this express permission does not cover the reproduction of large portions of text from the RSC publication or reproduction of the whole article or book chapter.

A publisher of a non-RSC publication can use this document as proof that permission is granted to use the material in the non-RSC publication.

## B.2 Permission Email from Adam Hischberg for Content and Figures in Chapter 3

Date: April 23rd 2015

From: “Adam Hischberg” ahirschberg@cambridge.org

Subject: Re: Permission Request

To: <nandita@udel.edu>

Reference

Journal of Materials Research / Volume 29 / Issue 23 / 2014, pp 2835 - 2844

Electrochemical deposition and characterization of carboxylic acid functionalized PEDOT copolymers

by Nandita Bhagwat, Kristi L. Kiick and David C. Martin

Copyright © 2014 Materials Research Society.

Dissertation

Title: Novel conjugates of peptides and conjugated polymers for optoelectronics and neural interfaces

Institution: University of Delaware

Rights/Acknowledgement

Permission is granted for nonexclusive rights to reprint the Cambridge journal article of which you are a co-author in your forthcoming dissertation/thesis as described above. This permission requires full acknowledgement,

This permission is subject to the following conditions:

a.) the material to be reprinted must be original to the Cambridge University Press journal article and author and must not involve material obtained from a third party; any material copyrighted by or credited in the Cambridge publication to another source may require further clearance by you from the original source, and Cambridge University Press is not liable for the use of third party material

b.) you must forward or refer to Cambridge University Press all reprint/republication permission requests that you may receive involving the material published by Cambridge University Press

c.) please inform your co-authors and ensure that they do not object to your use of the article

Sincerely,

Adam Hirschberg
Senior Permissions Associate
Cambridge University Press
32 Avenue of the Americas
New York, NY 10013-2473